EVALUATION AND REMOVAL OF FORMATION DAMAGE CAUSED BY OIL-BASED DRILLING FLUIDS WEIGHTED WITH MICRONIZED ILMENITE

A Dissertation

by

MANAYER Q A A AL-MUJALHEM

Submitted to the Office of Graduate and Professional Studies of
Texas A&M University
in partial fulfillment of the requirements for the degree of

DOCTOR OF PHILOSOPHY

Chair of Committee,	Hadi Nasrabadi
Committee Members,	Jerome J. Schubert
	Ibere Nascentes Alves
	Mahmoud M. El-Halwagi
Head of Department,	Jeff Spath

May 2021

Major Subject: Petroleum Engineering

ABSTRACT

Solids found in drilling fluids, particularly weighting materials, can cause significant formation damage due to plugging of pores. This study investigates formation damage caused by using an oil-based drilling fluid system weighted with micronized ilmenite. It also evaluates the solubility efficiency of different acid systems to determine a feasible method for filter cake removal to enhance production from drilled wells.

Oil-based drilling fluid systems were prepared, and rheological properties of the fluids were measured. High Pressure/High Temperature (HP/HT) filtration experiments were conducted to investigate filtration behavior and filter cake formation. A coreflood system was used to simulate field-comparable dynamic fluid circulation, measuring permeability damage after fluid filtration for 30 minutes. Varying permeability sandstone cores were used for filtration studies. CT scan analysis was used to investigate the formation damage and quantify the depth of solids invasion.

An HP/HT reactor was used to measure the solubility efficiency of micronized ilmenite in different acid systems. ICP-OES, XRF, and XRD techniques were used to describe the solubility reactions.

Ilmenite-based and barite-based drilling fluids with a specific gravity of 2.0 were compared during performance evaluation. The PV and YP were measured to be 55 cp and 16 lb/100 ft^2 for ilmenite, and 64 cp and 11 lb/100 ft^2 for barite, respectively. Static filtration experiments for an ilmenite-based OBM showed a leak-off volume of 1.2 cm^3. Formation damage evaluation for a barite-based drilling fluid showed an 11% reduction

in a low permeability core, increasing to 40% permeability reduction in a medium permeability core. Ilmenite-based fluids showed no reduction of permeability in both. Overall, micronized ilmenite-based fluids showed better performance compared to micronized barite-based fluids, with less formation damage.

Of the acid systems tested, regular mud acid had the highest filter cake solubility of 80% at 200˚F and a 10:1 acid to solids ratio, while a mixture of glycolic and citric acids dissolved 30% of the ilmenite-based filter cake.

Increased fluid performance compared to micronized barite-weighted fluids suggests particle size is not the only factor causing enhancement and damage reduction. Furthermore, determining the efficacy of solubility of ilmenite-weighted OBM filter cake in organic acids translates to establishing safer, more cost-effective field practices.

DEDICATION

To the late Dr. Hisham A. Nasr-El-Din, may his soul rest in peace.

ACKNOWLEDGEMENTS

I would like to thank my committee chair, Dr. Hadi Nasrabadi, and my committee members, Dr. Jerome Schubert, Dr. Mahmoud El-Halwagi, and Dr. Ibere Alves, for their valuable guidance and support throughout the course of this research. I would also like to recognize Ms. Gia Alexander for proofreading and editing all written work pertaining to my research.

To Dr. Hisham Nasr-El-Din, my original committee chair, may he rest in peace: Thank you for your treasured advice, involvement, and dedication to this project and to my success throughout the past few years.

To my fellow colleagues: I truly value the advice and knowledge sharing that transpired over the years.

To my friends: Thank you for your endless moral support. More importantly, thank you for making my time at Texas A&M University a truly great experience.

Finally, to my family: I express my utmost love and gratitude for your endless encouragement and support. Thank you for being patient and believing in me, and for always being there for me, not matter how far away I am.

CONTRIBUTORS AND FUNDING SOURCES

Contributors

This work was supervised by a dissertation committee consisting of Professors Hisham A. Nasr-El-Din and Hadi Nasrabadi, committee co-advisors, Professors Jerome J. Schubert and Ibere Nascentes Alves of the Harold Vance Department of Petroleum Engineering, and Professor Mahmoud M. El-Halwagi of the Artie McFerrin Department of Chemical Engineering at Texas A&M University.

Initial research detailed in Chapter III was performed in collaboration with Dr. Ahmed Ibrahim of the Department of Petroleum Engineering and was published in 2020. All other work conducted for this dissertation was completed by the student independently.

Funding Sources

Graduate study was supported in part by various teaching and research assistantships from the Texas A&M University College of Engineering and the Harold Vance Department of Petroleum Engineering.

This work was also made possible in part by funding provided by the Kuwait Foundation for the Advancement of Sciences (KFAS) under the Program for Scientific Excellence Scholarship. Its contents are solely the responsibility of the authors and do not necessarily represent the official views of the KFAS.

NOMENCLATURE

API	American Petroleum Institute
CT	Computed Tomography
DF	Drilling Fluid
DI	Deionized
DTPA	Diethylenetriaminepentaacetic Acid
ECD	Equivalent Circulating Density
ERD	Extended Reach Drilling
ICP-OES	Inductively Coupled Plasma-Optical Emission Spectrometry
IEM/IEDF	Invert Emulsion Mud/Drilling Fluid
HCl	Hydrochloric Acid
HF	Hydrofluoric Acid
HEDTA	Hydroxyethylethylenediaminetriacetic Acid
HP/HT	High Pressure/High Temperature
HU	Hounsfield Units
KFAS	Kuwait Foundation for the Advancement of Sciences
NADF	Non-Aqueous Drilling Fluid
NPT	Non-Productive Time
OBM	Oil-Based Mud
ppg	Pounds per gallon
PSD	Particle Size Distribution

PV	Plastic Viscosity
ROP	Rate of Penetration
SG	Specific Gravity
WBM	Water-Based Mud
YP	Yield Point
XRD	X-Ray Diffraction
XRF	X-Ray Fluorescence

TABLE OF CONTENTS

Page

ABSTRACT ii

DEDICATION iv

ACKNOWLEDGEMENTS v

CONTRIBUTORS AND FUNDING SOURCES vi

NOMENCLATURE vii

TABLE OF CONTENTS ix

LIST OF FIGURES xi

LIST OF TABLES xvi

CHAPTER I INTRODUCTION 1

- Drilling Fluids 1
  - Drilling Fluid Functions 1
  - Drilling Fluid Formulation 2
- Formation Damage 5
  - Filter Cake 6
- Weighting Materials 9
  - Barite 9
  - Manganese Tetroxide 11
  - Ilmenite 12
- Filter Cake Removal 14
  - Ilmenite Solubility 15
- Research Objectives 17

CHAPTER II EXPERIMENTAL METHODS AND MATERIALS 19

- Materials 19
  - Micronized Ilmenite 19
  - Drilling Fluid Systems 21
  - Cores 23
  - Crude Oil 23

Acid Systems 23
Experimental Methods 25
Drilling Fluid Performance 25
Formation Damage Evaluation 27
Solubility Testing 33

CHAPTER III EVALUATION OF MICRONIZED ILMENITE AS A WEIGHTING AGENT IN OIL-BASED DRILLING FLUIDS 39

Background 39
Formation Damage Evaluation Methods 41
Results and Discussion 42
Rheological Parameters 42
Filter Press 44
Mudloop 45

CHAPTER IV REMOVAL OF MICRONIZED ILMENITE-WEIGHTED OIL-BASED FILTER CAKE 62

Background 62
Organic Acids 63
Results and Discussion 65
Micronized Ilmenite 65
Micronized Ilmenite-Based Drilling Fluid Filter Cake 82

CHAPTER V CONCLUSIONS 86

Field Cases 86
Performance Evaluation 87
Damage Removal 88
Recommendations 89

REFERENCES 92

APPENDIX A CORE PERMEABILITY MEASUREMENTS 106

APPENDIX B ADDITIONAL SOLUBILITY DATA 112

Micronized Ilmenite Solubility Testing 112
Initial Organic Acid Systems 113
Secondary Organic Acid Systems 118
Micronized Ilmenite-Weighted Filter Cake Solubility Testing 122

LIST OF FIGURES

Page

Figure I-1 A schematic of filter cake formation during dynamic conditions. Reprinted from (Calçada et al. 2011). 7

Figure II-1 XRD analysis of micronized ilmenite powder. 20

Figure II-2 OFITE drilling fluids mixer. 21

Figure II-3 OFITE aging cell and Teflon liner. 26

Figure II-4 OFITE 4-roller oven. 26

Figure II-5 Grace M3600 Automatic Viscometer. 27

Figure II-6 OFITE HP/HT Filter Press. 29

Figure II-7 Mud loop schematic. Reprinted with permission from (Ibrahim et al. 2020). 31

Figure II-8 Drilling fluid circulation inside the core holder. Reprinted with permission from (Ibrahim et al. 2020). 31

Figure II-9 Parr Bench Top Reactor. 35

Figure II-10 Optima 7000 DV ICP-OES. 36

Figure II-11 Bruker D8 ADVANCE Eco XRD System. 37

Figure II-12 Bruker S2 Ranger XRF Spectrometer. 38

Figure III-1 Filtrate volume collected during a 30-minute dynamic filtration test and the created filter cake. Reprinted with permission from (Ibrahim et al. 2020). 44

Figure III-2 Dynamic filtration results of Experiment 2 (5 µm barite-based drilling fluid/Bandera sandstone) at a 400 psi overbalance. Reprinted with permission from (Ibrahim et al. 2020). 48

Figure III-3 Dynamic filtration results of Experiment 3 (5 µm ilmenite-based drilling fluid/Bandera sandstone) at a 400 psi overbalance. Reprinted with permission from (Ibrahim et al. 2020). 48

Figure III-4 CT scan analysis for Experiment 2 before and after filter cake formation. Reprinted with permission from (Ibrahim et al. 2020). 49

Figure III-5 Dynamic filtration results of Experiment 4 at a 400-psi overbalance. Images show the core surface after initial filter cake formation (left) and after flowback and final permeability measurements (right). Reprinted with permission from (Ibrahim et al. 2020). 52

Figure III-6 Dynamic filtration results of Experiment 5 at a 400-psi overbalance and an image of the filter cake formed on the core surface. Reprinted with permission from (Ibrahim et al. 2020)..... 53

Figure III-7 Dynamic filtration results of Experiment 6 at a 400-psi overbalance and an image of the filter cake formed on the core surface. Reprinted with permission from (Ibrahim et al. 2020)..... 54

Figure III-8 CT-scan analysis for Experiment 5 before and after filter cake formation. Reprinted with permission from (Ibrahim et al. 2020). 55

Figure III-9 A Berea sandstone core surface (left) after initial filter cake formation (Experiment 7) and (right) after flowback and final permeability measurements. Reprinted with permission from (Ibrahim et al. 2020). 57

Figure III-10 CT-scan analysis for Experiment 8 before and after filter cake formation. Reprinted with permission from (Ibrahim et al. 2020). 58

Figure III-11 CT-scan analysis for Experiment 9 before and after filter cake formation. Reprinted with permission from (Ibrahim et al. 2020). 59

Figure III-12 Percentage of permeability reduction as a function of pore throat diameter/barite size ratio for barite-based drilling fluids. Reprinted with permission from (Ibrahim et al. 2020)..... 60

Figure IV-1 ICP analysis for effluent samples collected from ilmenite solubility testing with 15 wt% HCl + 8 wt% HEDTA. 67

Figure IV-2 XRD analysis of a micronized ilmenite sample before and after exposure to a 7.5 wt% oxalic and 1 wt% HCl acid system for 24 hours. 71

Figure IV-3 XRD analysis of a micronized ilmenite sample after exposure to a 7.5 wt% oxalic and 1 wt% HCl acid system for 24 hours. 71

Figure IV-4 ICP analysis for effluent samples collected from ilmenite solubility testing with 7.5 wt% Oxalic + 1 wt% HCl acids. 72

Figure IV-5 ICP analysis for effluent samples collected from ilmenite solubility testing with 7 wt% glycolic + 1 wt% HCl acids. 73

Figure IV-6 ICP analysis for effluent samples collected from ilmenite solubility testing with 13 wt% lactic + 1 wt% HCl acids. 74

Figure IV-7 ICP analysis for effluent samples collected from ilmenite solubility testing with 11.6 wt% Citric + 1 wt% HCl acids. 75

Figure IV-8 ICP analysis of iron concentrations in effluent samples collected from ilmenite solubility testing with organic acid systems. 75

Figure IV-9 ICP analysis of titanium concentrations in effluent samples collected from ilmenite solubility testing with organic acid systems. 76

Figure IV-10 ICP analysis for effluent samples collected from ilmenite solubility testing with 20 wt% Oxalic + 10 wt% HCl acids. 78

Figure IV-11 Residual solids filtered and dried after exposure to 20 wt% Oxalic + 10 wt% HCl acids for 24 hours exhibited a color change due to solids precipitation. 78

Figure IV-12 XRD analysis of the first micronized ilmenite sample after exposure to a 20 wt% oxalic and 10 wt% HCl acid system for 24 hours. 79

Figure IV-13 XRD analysis of the second micronized ilmenite sample after exposure to a 20 wt% oxalic and 10 wt% HCl acid system for 24 hours. 79

Figure IV-14 ICP analysis for effluent samples collected from ilmenite solubility testing with 20 wt% oxalic + 10 wt% glycolic acids. 80

Figure IV-15 XRD analysis of a micronized ilmenite sample after exposure to a 20 wt% oxalic and 10 wt% glycolic acid system for 24 hours. 81

Figure IV-16 ICP analysis for effluent samples collected from ilmenite solubility testing with 10 wt% glycolic + 11.6 wt% citric acids. 82

Figure IV-17 The filter cake used in the solubility test with regular mud acid (left) and the residue after the 4-hour solubility test collected on 5 μm filter paper (right). Reprinted with permission from (Ibrahim et al. 2020). 83

Figure IV-18 The filter cake used in the solubility test with the 10 wt% glycolic and 11.6 wt% citric acid system. 84

Figure A-1 Pressure drop across the core for Experiment 1 at an injection rate of 1 cm^3/min at 250˚F. 106

Figure A-2 Pressure drop across the core for Experiment 2 at an injection rate of 1 cm^3/min at 250˚F. 107

Figure A-3 Pressure drop across the core for Experiment 3 at an injection rate of 1 cm^3/min at 250˚F. 107

Figure A-4 Pressure drop across the core for Experiment 4 at an injection rate of 0.5 cm^3/min (initial) and 2 cm^3/min (both) at 250˚F. 108

Figure A-5 Pressure drop across the core for Experiment 5 at an injection rate of 0.5 cm^3/min at room temperature (RT) and 250˚F (HT). 108

Figure A-6 Pressure drop across the core for Experiment 6 at an injection rate of 0.5 cm^3/min at room temperature (RT) and 250˚F (HT). 109

Figure A-7 Pressure drop across the core for Experiment 7 at 250˚F. 109

Figure A-8 Pressure drop across the core for Experiment 8 at an injection rate of 1 cm^3/min at 250˚F. 110

Figure A-9 Pressure drop across the core for Experiment 9 at an injection rate of 5 cm^3/min at 250˚F. 110

Figure A-10 Pressure drop across the core for Experiment 10 at an injection rate of 5 cm^3/min at 250˚F. 111

Figure B-1 XRD analysis of three ilmenite samples (original, after regular mud acid, and after HCl + HEDTA). 112

Figure B-2 Effluent samples collected from solubility testing of micronized ilmenite with a 7.5 wt% oxalic and 1 wt% HCl acid system at (left to right) 1, 3, 6, 14, 17.5, 20, and 24 hours. 113

Figure B-3 XRD analysis of a micronized ilmenite sample after exposure to a 7 wt% glycolic and 1 wt% HCl acid system for 24 hours. 113

Figure B-4 Effluent samples collected from solubility testing of micronized ilmenite with a 7 wt% glycolic and 1 wt% HCl acid system at (left to right) 1, 4, 12, 14, 16, 18, 20, and 24 hours. 114

Figure B-5 XRD analysis of a micronized ilmenite sample after exposure to a 13 wt% lactic and 1 wt% HCl acid system for 24 hours. 114

Figure B-6 Effluent samples collected from solubility testing of micronized ilmenite with a 13 wt% lactic and 1 wt% HCl acid system at (left to right) 2, 4, 6.5, 9.5, 20, and 24 hours. 115

Figure B-7 Effluent samples collected from solubility testing of micronized ilmenite with a 11.6 wt% citric and 1 wt% HCl acid system at (left to right) 2, 6, 9, 12.5, 20.5, and 24 hours. 115

Figure B-8 XRD analysis of a micronized ilmenite sample after exposure to a 11.6 wt% citric and 1 wt% HCl acid system for 24 hours. 116

Figure B-9 Effluent spent acid samples collected after initial organic acid solubility tests. The samples from left to right are oxalic, glycolic, lactic, and citric.... 117

Figure B-10 Effluent samples collected from solubility testing of micronized ilmenite with a 20 wt% oxalic and 10 wt% HCl acid system at (left to right) 1.5, 3, 9, 11, 15, and 18.5 hours. 118

Figure B-11 Effluent samples collected from solubility testing of micronized ilmenite with a 20 wt% oxalic and 10 wt% glycolic acid system at (left to right) 0.5, 6, 10, 13, 17, 20.5, and 24 hours. 118

Figure B-12 XRD analysis of a micronized ilmenite sample after exposure to a 10% glycolic and 11.6 wt% citric acid system for 24 hours. 119

Figure B-13 Effluent samples collected from solubility testing of micronized ilmenite with a 10 wt% glycolic and 11.6 wt% citric acid system at (left to right) 2, 4, 10, 13, 17, 20.5, and 24 hours. 119

Figure B-14 Effluent spent acid samples collected after secondary organic acid solubility tests. The samples from left to right are oxalic/HCl, oxalic/glycolic, and citric/glycolic. 120

Figure B-15 ICP analysis for effluent samples collected from filter cake solubility testing with 10 wt% glycolic + 11.6 wt% citric acids. 123

Figure B-16 XRD analysis of a micronized ilmenite-weighted drilling fluid filter cake after exposure to a 10% glycolic and 11.6 wt% citric acid system for 24 hours. 124

Figure B-17 Effluent samples collected from solubility testing of micronized ilmenite-weighted drilling fluid filter cake with a 10 wt% glycolic and 11.6 wt% citric acid system at (left to right) 1, 4.5, 15, 17.5, 19.5, 22, and 24 hours. 124

LIST OF TABLES

Page

Table I-1 Summary of weighting material properties. 14

Table II-1 XRF analysis of micronized ilmenite. 20

Table II-2 PSD of micronized ilmenite. 20

Table II-3 Composition of the oil-based drilling fluid systems with ilmenite and barite as weighting materials. Reprinted with permission from (Ibrahim et al. 2020). 22

Table II-4 Viscosity and density of crude oil as a function of temperature. Reprinted with permission from (Ibrahim et al. 2020). 23

Table II-5 Summary of acid formulations for acid testing. 25

Table III-1 Rheological properties of oil-based drilling fluid systems with a density of 2.0 SG at 125˚F. Reprinted with permission from (Ibrahim et al. 2020). 43

Table III-2 Rheological properties of oil-based drilling fluid systems with a density of 1.5 SG at 125˚F. Reprinted with permission from (Ibrahim et al. 2020). 43

Table III-3 Experimental design for formation damage assessment of several oil-based drilling fluid systems and formation permeabilities. Reprinted with permission from (Ibrahim et al. 2020) 46

Table III-4 Formation damage analysis for Experiments 1-6 with a drilling fluid density of 2.0 SG. Reprinted with permission from (Ibrahim et al. 2020) 47

Table III-5 Formation damage analysis for Experiments 7-10 with a drilling fluid density of 1.5 SG. Reprinted with permission from (Ibrahim et al. 2020) 56

Table III-6 Particle size distribution of the weighting materials. Reprinted with permission from (Ibrahim et al. 2020) 61

Table IV-1 XRF analysis of oxides in original ilmenite, compared with residual ilmenite after a 10 hour solubility test with 15 wt% HCl + 8 wt% HEDTA. Reprinted with permission from (Ibrahim et al. 2020). 66

Table IV-2 XRF analysis of oxides in the residual ilmenite after a 4-hour solubility test with regular mud acid. Reprinted with permission from (Ibrahim et al. 2020). 68

Table IV-3 A summary of solubility efficiency for conventional acid systems tested. Reprinted with permission from (Ibrahim et al. 2020). 69

Table IV-4 A summary of solubility efficiencies for initial organic acid systems tested. 77

Table IV-5 A summary of solubility efficiencies for secondary organic acid systems tested. 82

Table B-1 Summary of XRD results for residual solids after exposure to initial organic acid systems. 116

Table B-2 Summary of XRD results for residual solids after exposure to secondary organic acid systems. 120

Table B-3 Measured pH values for organic acid systems before and after solubility testing. 121

Table B-4 Composition of the 1.9 SG micronized ilmenite-weighted oil-based drilling fluid system used to create the filter cake for solubility tests. 122

Table B-5 XRD results for filter cake residual solids after exposure to a 10% glycolic and 11.6 wt% citric acid system for 24 hours. 125

CHAPTER I

INTRODUCTION

Drilling Fluids

Drilling fluids (DF), also referred to as drilling muds, are a mixture of chemicals and additives that serve as the circulating fluid used during the drilling process for oil and gas-related activities. Fluids flow in a closed system from the mud pits on the surface, downhole through the drillstring, the bottomhole assembly (BHA), drill bit nozzles, and back up the annulus of the drilled well to the surface. Drilling fluids are necessary for successful drilling operations as they serve a number of functions that are vital to the drilling of a well.

Drilling Fluid Functions

Arguably, the most important function of a drilling fluid is its ability to control formation pressures. This is achieved by maintaining a specific fluid density translating to a hydrostatic pressure previously determined to be safe, that falls within the drilling window, typically lying between formation pore pressure and formation rock fracture pressure. The most common drilling method, known as overbalanced drilling, is to maintain a drilling fluid density, both static and dynamic, that lies within a safe margin (around 300 psi) above the formation pore pressure. Depending on how narrow a drilling window is, this method may risk fracturing the formation or cause fluid to flow from the well to the near-wellbore region, possibly inducing losses. In many cases, this risk outweighs its contrary counterpart, which would drill using a density at or below the pore

pressure, risking reservoir fluids entering the well and migrating up to the surface, a phenomenon known as a kick, which is potentially disastrous.

Another important function of a drilling fluid system is its ability to carry drilled cuttings away from the bit and either transport them to the surface while drilling or suspend them during brief static periods to the avoid accumulation of solids at the bottom of the well. Such deposits could lead to slowing down drilling operations, known as a decrease in the rate of penetration (ROP), or result in the bit getting stuck and requiring suspending drilling altogether, thus increasing non-productive time (NPT) and/or downtime on the rig site. The rheological properties of a fluid, including measured parameters such as true and effective viscosities, as well as gel strengths, allow researchers to quantify the carrying capacity of the fluid system in static and dynamic conditions.

Circulation of a drilling fluid also helps cool and lubricate the bit and BHA, while also promoting chemical and mechanical wellbore stability. Factors such as fluid composition and density, downhole temperature, formation lithology, and drilling conditions must be selected to work cohesively. Otherwise, formations may collapse due to a number of reasons. For example, the chemical compatibility of a fluid with the formation is of utmost importance. Clays prone to swelling may be hydrated by drilling fluid, causing instability or the possibility of stick-slip while drilling due to tight hole complications.

Drilling Fluid Formulation

In order to avoid drilling complications and achieve the above functions, muds are made up of different components or chemical additives. A combination of any or all

additives can make a system. The base fluid, defining the type of system used, may be freshwater, brine, diesel, mineral oil, or synthetic oil. A weighting material is typically an inert solid added to provide additional density to the fluid. A viscosifier, typically a polymer or organophilic clay, adds viscosity to the fluid, enhancing its rheological properties. A fluid loss additive or filtration control agent is used to minimize the amount of fluid that may seep into formation pores during circulation. In addition to that, a bridging agent, such as calcium carbonate, may be used to further consolidate the fluid and prevent filtrate invasion into the reservoir.

A lubricant may be necessary to reduce torque and drag during drilling, especially in deviated wells. A pH control agent is necessary to activate certain additives, such as emulsifiers, which are needed in oil-based systems, to keep water emulsified and maintain the fluid system's structure. A surface-wetting agent is also commonly used to oil-wet solids in an oil-based formulation, dispersing in the system to maintain stability. Depending on specific drilling needs, other additives include corrosion inhibitors, rheology enhancers, and suspending agents.

Each well, or section of a well, drilled will require a subset of these components specifically customized to meet drilling needs. The fluid formulation to be used depends on many factors, some of which include well depth, well trajectory, formations to be drilled, bottomhole temperature and pressure, availability of rig equipment, cost, environmental regulations, drilling schedule, and offset well history (Bleier 1990; Alkhalaf 2019).

Based on drilling requirements, two general classifications of drilling fluids exist, water-based mud (WBM) and oil-based mud (OBM). The terms non-aqueous drilling fluid (NADF) or invert emulsion drilling fluid (IEM/IEDF) may also be used in place of the latter. These classifications categorize the main component that makes up the continuous or external phase of the fluid; whereas water, or brine, constitutes the external phase of a WBM, while oil or a synthetic fluid serves as the external phase of an OBM. Sub-classifications exist for each of the categories based on variations of other components of the drilling fluid. This work focuses on the composition and applications of oil-based drilling fluids.

Oil-Based Drilling Fluids

OBM is often preferred in drilling because it exhibits certain superior performance-related capabilities, including lubricity, thermal stability, clay/shale inhibition, resistance to chemical contamination, solids tolerance, increased ROP, and corrosion reduction (Alkhalaf et al. 2019). OBM may also be recycled, conditioned, and used multiple times, which can be more economical. However, invert emulsions can also be problematic for several reasons. Diesel and other oil base fluids are not considered environmentally friendly, especially when drilling offshore (Khodja et al. 2010). Environmental regulations are based on the possibility of fluid leakage, loss of circulation incidents, and discharge of fluids and contaminated drilled solids. Mineral oils and synthetic fluids are replacing the conventional base oils as a result (Bennett 1984). OBM is also non-conductive, prohibiting logging equipment from being operational. Furthermore, OBM does contain water/brine emulsified as droplets that make up the

internal, discontinuous phase. An adequate supply of emulsifiers and proper mechanical shearing are both necessary to ensure maximum fluid performance and avoid further drilling issues.

Formation Damage

The reduction of permeability in a reservoir or formation surrounding a drilled wellbore, the near-wellbore region, is known as formation damage. Several mechanisms have been identified that promote formation damage caused by drilling fluids. Primary mechanisms can be categorized as either mechanical, chemical, biological, or thermal (Bennion 1999). The mechanisms (Bishop 1997) include:

- incompatibilities between different fluids
- incompatibilities between fluids and the rock/formation
- solids invasion
- phase trapping/blocking
- chemical adsorption or wettability alteration
- fines migration
- biological activity

With respect to drilling fluid circulation, multiple mechanisms may be at work. Depending on the wettability of the formation being drilled, its lithology, and the composition of reservoir fluids existing in the near-wellbore region, a drilling fluid coming in contact with the formation will, due to overbalanced drilling, flow into the formation pores. Also, chemical incompatibilities with fluids may cause emulsion blockages or

solids precipitation. Additionally, improper or inadequate inhibition in drilling fluids may cause swelling of clays in the formation, also resulting in pore blockage.

Solid particles existing in a drilling fluid formulation may be small enough to flow into pores, thereby plugging them (Fisk and Jamison 1989). Likewise, flow from a fluid will cause fine solids already in the formation rock to migrate, also plugging pores. Moreover, emulsifiers within the fluid may adhere to formation surfaces, altering the wettability of and plugging the pore throats. Lastly, bacterial agents existing within drilling fluid additives may generate slimes within the pore spaces, further plugging pores and reducing permeability. According to Reed (1989), the most significant drilling fluid-related formation damage mechanism is the filtrate-rock interaction, which causes fines migration to plug pores. Another significant factor impacting the extent of damage to the formation is the magnitude of the overbalance pressure (Ismail and Murugesu 2005). The larger the differential pressure, the further solids and filtrate will attempt to flow.

Filter Cake

Because a drilling fluid is made up of both liquids and solids, it will tend to flow into the permeable formation and continue to do so until different sizes of the solid particles have plugged the face of the well and a minimal amount of the liquid phase, known as filtrate, is able to flow through the solids (Patton and Phelan 1985). The initial filtrate is known as spurt loss. At this point, which takes place shortly after initial circulation, a thin film of DF solids will form along the wellbore surface; this layer is known as the filter cake. More precisely, the visible film forming on the exterior of the formation wall, or rather, the well surface, is known as the external filter cake. Before this

layer forms, filtrate and solid particles flow into the near-wellbore region, completely plugging the pores and form another layer, known as the internal filter cake (Liu and Civan 1995).

Depending on circulation conditions, or lack thereof due to the interruption of pumping, one of two filtration mechanisms may be at play, affecting the process of filter cake formation (Scheid et al. 2010). When static conditions occur, solid particle size is the main determinant of thickness and filtrate flow. When dynamic conditions take place, the equilibrium between erosion rate of solids due to drag forces during flow and deposition rate of solids determines thickness (Liu and Civan 1996). **Figure I-1** illustrates the process of filter cake formation.

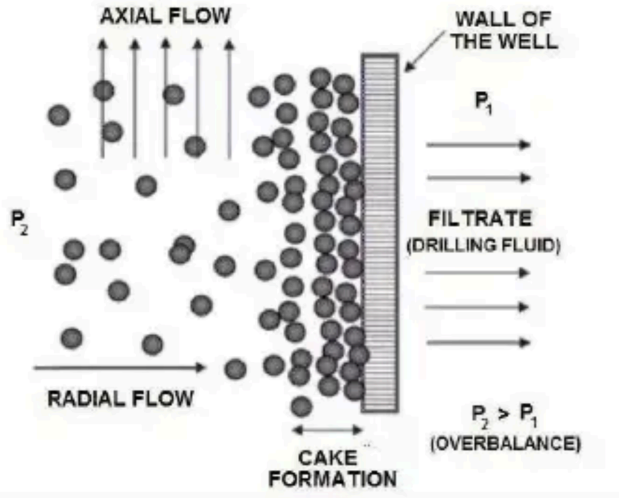

Figure I-1 A schematic of filter cake formation during dynamic conditions. Reprinted from (Calçada et al. 2011).

Filter cake quality depends on thickness, heterogeneity, and formation speed. The incidence of differential sticking, the entrapment of a section of the drillstring in the filter cake, will increase with filter cake thickness, adding to NPT (Amanullah and Tan 2000). As such, a filter cake must not only be relatively impermeable; it should also be uniformly thin and have the ability to form rapidly (Salehi et al. 2015).

A delay in filter cake formation or lack of bridging capabilities will allow for increased filtrate invasion into the rock formation, which, in turn, increases the intensity of formation damage caused by the drilling fluids. One important factor affecting filter cake quality is the particle size distribution of solids making up the filter cake (Al-Yami et al. 2010; Fleming et al. 2020). According to Herzig et al. (1970), mobilization and retention forces between particles differ based on their size. In larger particles more than 30 μm in size, friction and hydrodynamic drag forces are dominant. However, for smaller particles closer to 1 μm in size, surface forces, such as electrical and van der Waals forces take over. Furthermore, particle size physically determines whether a particle will flow into a pore space and whether particles bridging together will allow fluid to pass through them. Typically, when varying particle sizes exist in a drilling fluid system, larger particles "form the skeleton of the filter cake" first (Elkatatny et al. 2012a). After that, smaller particles settle in the porous spaces between the larger particles.

Moreover, an additional consideration that must be made when formulating a drilling fluid is the selection of proper additives that will form a high-quality filter cake and prevent further formation damage. Fluid loss additives have a significant effect; however, careful selection of all solid particles in a formulation is of great importance as

well. Seeing as weighting materials are the largest contributor of solid particles to a formulation, especially with high-density fluids, which are increasingly becoming required in HP/HT applications for deeper, more complex wells, the scope of this research will include the evaluation of formation damage specifically caused by weighting material selection.

Weighting Materials

Numerous weighting materials have been used in drilling fluid formulations. Water-soluble salts, including chlorides, bromides, and formates are commonly used to maintain fluid density when required hydrostatic pressures are relatively low. Other weighting materials used in industry are typically inert solids, such as barite, hematite, manganese tetroxide, and ilmenite. Weighting material selection for a particular drilling fluid formulation is based on several factors (Al-Bagoury and Steele 2012). A weighting agent must be able to deliver the required density for safe drilling, provide an adequate rheological profile to carry and suspend cuttings, be hard enough not to break down, but not too hard that abrasion is problematic for equipment wear, and flow back or be readily soluble to avoid propagating formation damage.

Barite

Barium sulfate ($BaSO_4$), or barite, is the most commonly used weighting agent in both oil and water-based drilling fluids (Tehrani et al. 2014). API barite is a tan powder and has an average density of 4.2 SG. Its inert quality has made it versatile and applicable in different systems.

Although it is essentially the "go-to" weighting material, many issues exist with the use and performance of barite in drilling. Barite is known to have increased sag tendencies, more so in OBM than WBM. This sag can be dangerous while drilling, as sagging may change the density profile of the column of fluid, triggering underbalanced drilling conditions in parts of the well (Aldea et al. 2001). In some instances, drilling fluid densities were measured to have deviated up to 7 ppg from the original formulation (Hanson 1990). As a result, sag may also lead to well control situations, loss of circulation, and stuck pipe instances (Massam et al. 2004).

Barite is also not acid-soluble and is thus difficult to flow back, meaning that pores plugged with barite solids will likely not flow out of the reservoir once a well starts producing. Removal methods are limited due to weak solubility. Dissolution rates improved in certain chelating agents; however, the use of chelates can be cost inhibitive (Putnis et al. 1995; Lakatos et al. 2002; Nasr-El-Din et al. 2004; Bageri et al. 2017).

Moreover, barite has been identified as having higher than recommended concentrations of heavy metals, including manganese, copper, zinc, cadmium, and lead, making barite-coated cuttings and used drilling fluids difficult to dispose of (Fjogstad et al. 2000). The presence of barite in a well has also been known to interfere with gamma-ray logs, causing a misrepresentation in measured reservoir properties (Fattah and Lashin 2016).

Furthermore, extensive use has led to a shortage in global supply of barite, causing a surge in price (Blomberg and Melberg 1984; Tehrani et al. 2014). In fact, API standards

have been lowered to allow API barite with a density of 4.1 SG to be used in drilling applications to address the decrease in supply (Al-Bagoury and Steele 2012).

Recently, extensive exploration within the oil and gas industry has identified potential prospects that are deeper, are located amid harsher conditions, and that require more advanced methods and trajectories for extraction. In terms of drilling, this creates a need for fluid systems that are denser and have higher temperature and solids-loading tolerances. As such, research has shifted towards identifying and enhancing alternatives to API barite. Focusing on the particle size distributions of barite and other weighting materials was identified as a potential route towards enhanced performance (Taugbøl et al. 2005; Al-Bagoury 2014). Milling of barite into an ultrafine material using special treatment technologies proved effective, with stable properties and a lower dilution rates due to an increase in solids removal efficiency. Mohamed et al. (2017) also reported improved removal efficiency using diethylenetriaminepentaacetic acid (DTPA), a chelating agent.

Manganese Tetroxide

Manganese tetroxide (Mn_3O_4) was identified as an alternative micronized solid weighting material that has been used in field applications more recently. With hard, spherical particles, and a density of 4.8 SG, it is able to provide a more preferable rheological profile. Manganese tetroxide is also acid-soluble, making it easier to remove compared to barite (Al Moajil et al. 2008). This research was extended to develop drilling fluid formulations weighted with a mixture of manganese tetroxide and barite, which

showed good rheology and filtration, reduced sag, and somewhat increased filter cake solubility (Wagle et al. 2017).

Ilmenite

Ilmenite ($FeTiO_3$) is another weighting agent also used in both WBM and OBM (Haaland et al. 1976). It is a black powder with a density, higher than that of barite, of about 4.6 SG, which is beneficial because using higher density weighting materials decreases solids loading of a fluid formulation. Reduced solids content translates to enhanced rheological properties and an increase in ROP, lowering the overall cost of drilling (Saasen et al. 2001; Blattel and Rupert 1982). A decrease in the solids concentration of a fluid has also been proven to reduce formation damage (Ismail et al. 1994). Furthermore, ilmenite was found to have significantly decreased concentrations of heavy metals compared to barite (Rae et al. 2001).

Additionally, ilmenite is widely used in other industries such as paints and coating, cosmetics, and fabrics, as it is a good source of titanium dioxide, or rutile (Elkatatny et al. 2013b). Accordingly, and due the to acid solubility of ilmenite, the solubilization or extraction of rutile is an industrial process that is routinely done.

After field trials, some disadvantages to using ilmenite became apparent. Ilmenite particles have increased hardness, which means they are less likely to be ground to finer particles during circulation. This reduces the need for dilution, which is advantageous; however, the increased hardness causes particles to be especially abrasive, damaging downhole and surface equipment and tools as fluid is circulated through them. Recommendations were made to decrease the particle size of ilmenite solids in order to

reduce the abrasion. Furthermore, as an iron oxide, ilmenite has magnetic properties that may potentially affect the performance of downhole tools (Tehrani et al. 2014).

Micronized Ilmenite

Following problematic field tests, recommendations, and extensive testing, several versions of micronized ilmenite were developed (Fjogstad et al. 2002). The current, treated, and adjusted version of the weighting material, which is the subject of this study, has an average particle size of 5 μm and a sphericity of 0.85 (Xiao et al. 2015). Particle hardness was greatly maintained, while abrasive tendencies were resolved the by removal of coarse particles. Finally, the magnetite content was decreased as well (Al-Bagoury and Steele 2012).

Laboratory testing detailed by Elkatatny (2012) and Al-Bagoury (2014) shows a decrease in sag tendency in fluids weighted by micronized ilmenite. The formulations for WBM and OBM systems weighted with micronized ilmenite have been optimized and tested as well (Elkatatny et al. 2013a; Xiao et al. 2013). Conventional filtration through limestone cores has been deemed acceptable at HP/HT conditions, ilmenite dispersion was stable, and rheological properties were determined to be adequate.

The economic factors surrounding the choice of weighting materials used are crucial when exploring them as options for drilling fluid systems. According to Al-Bagoury (2014), micronized ilmenite serves as an intermediary between conventional barite and “high-end specialty” weighting materials in terms of price point. However, cost per volume of material is not the only aspect that should be studied.

Additional considerations that need to be taken into account include many factors, some of which are summarized in **Table I-1**. For example, the volume of material needed differs for each weighting material due to density differences. Additionally, the hardness of solid particles, which decreases the need for dilution, also decreases the constant need to replenish other additives lost due to degradation and filtering. Increased solids loading leads to an increase in plastic viscosity of a system, which, in turn, decreases the concentration of viscosifiers required to maintain rheological stability. Accordingly, the enhancement of rheological properties aid in decreasing equivalent circulating density (ECD), which allows for increased ROP while drilling. Furthermore, reduced sag tendencies and improved filtration help decrease the incidence of drilling interruptions, thereby decreasing NPT, number of drilling days, and overall rig cost.

Weighting Material	**Density** *SG*	**D50** *μm*	**Moh's Hardness**	**Acid Soluble?**
API Barite	4.2	15-20	2.5-3.5	✗
Micronized Barite	4.2	1-10	2.5-3.5	✗
Ilmenite	4.6	30-45	5-6	✓
Micronized Ilmenite	4.6	5	5-6	✓
Manganese Tetroxide	4.8	1	5.5	✓

Table I-1 Summary of weighting material properties.

Filter Cake Removal

The process of dissolving a filter cake is crucial to damage remediation and the productivity of wells. Chemical treatments include different types of organic and inorganic

acids, as well as several chelating agents. The composition of a filter cake is the main determinant when selecting a treatment method, and, as the main contributor to filter cake solid particles is the weighting material, understanding the solubility of the weighting agent being used is key. Chemical reactions and temperature limitations must also be understood in order to identify proper damage remediation techniques. It is also beneficial to determine the optimal acid-to-filter-cake-solids ratio at which dissolution is more effective.

Ilmenite Solubility

The solubility of ilmenite has been studied for the extent of its use in other industries. Hydrochloric acid is widely used to solubilize ilmenite and obtain rutile. The mechanism behind this chemical reaction was detailed by van Dyk et al. (2002). Several factors were hypothesized to have an impact on dissolution, including particle size, acid concentration, temperature, stirring speed, acid-to-ilmenite ratio, and the inclusion of additives. The basic chemical reaction between ilmenite and HCl is:

$$FeTiO_3 + 2HCl \rightarrow Fe^{2+} + TiO^{2+} + 2Cl^- + 2OH^-$$

The mechanism suggested by Van Dyk et al. (2002) considers this chemical reaction as the controlling factor in the initial stages of contact between ilmenite and HCl, in which both iron and titanium go into solution. Next, however, the concentration of titanium in solution may cause Ti(IV) to polymerize. This process occurs when concentrations of titanium and hydrogen in solution are greater than 10-3 M and 0.5 M, respectively (Nabivanets and Kudritskaya 1967). Beyond this point, diffusion of the

polymer becomes the rate-limiting step in the reaction, indicating that the initial acid-to-ilmenite ratio must be high enough to avoid polymerization.

Olanipekun (1999) found that particle size influences the rate at which this reaction takes place. Al-Bagoury and Steele (2012) confirmed that micronized ilmenite, with an average particle size of 5 μm, had a higher dissolution rate compared to ilmenite with larger particle sizes. As for acid concentration, HCl is typically used at a maximum concentration of 15 wt% in the oil and gas industry due to tubing/pipe corrosion concerns and limitations to the effectiveness of corrosion inhibitors at increased concentrations.

Sinha (1984) performed acid leaching of ilmenite testing at temperatures ranging from 80 to 108˚C (176 to 226.4˚F) and found that increasing temperature increased the rate of dissolution. At an initial acid-to-ilmenite ratio of 1:1, only iron was dissolved.

Elkatatny et al. (2013b) reported partial solubility of iron and titanium in micronized ilmenite in 10 and 15 wt% HCl after 10 hours at 180˚F and complete removal of micronized ilmenite-weighted WBM filter cake formed on Indiana limestone after soaking in 5 wt% HCl for 16 hours at 250˚F. Al-Bagoury (2014) also reported partial solubility of iron and titanium in micronized ilmenite in 15 wt% HCl after 10 hours at 180˚F and complete removal of OBM filter cake formed on Berea sandstone after soaking in a mutual solvent, then 5 wt% HCl for 4 hours at 300˚F. In addition, Xiao et al. (2015) examined the solubility of damage created by a micronized ilmenite-weighted OBM internal filter cake using a coreflood system. In this case, 5 wt% HCl was not sufficient to remove all damage. Instead, 10-15 wt% was deemed more reasonable.

Sulfuric acid is also used extensively to produce titanium dioxide from ilmenite (Fouda et al. 2010). Maximum solubility, determined by Han et al. (1987), resulted from 14 M sulfuric acid, with the reaction taking place within a temperature range of 88-115˚C. The chemical reactions governing ilmenite dissolution in sulfuric are as follows (Jonglertjunya and Rubcumintara 2012):

$$H_2SO_4 + H_2O \rightarrow 2H_3O^+ + SO_4^{2-}$$

$$FeTiO_3 + 4H_3O^+ \rightarrow TiO_2^+ + Fe^{2+} + 6H_2O$$

Other solvents that have been used in the ilmenite dissolution process include ethanol, m-cresol, sodium phosphate, sodium hydroxide, ammonium hydroxide, phosphoric acid, and oxalic acid.

Research Objectives

This study focuses on the experimental evaluation of micronized ilmenite, with an average particle size (D_{50}) of 5 μm, as a weighting agent in oil-based drilling fluid systems. The main objectives of this research are:

1. To quantify and understand the extent and depth of formation damage resulting from the use of oil-based drilling fluid systems weighted with micronized ilmenite in sandstone reservoirs at HP/HT conditions. A comparison will be conducted with fluid systems weighted with micronized barite to avoid conclusions based solely on the effect of particle size.
2. To determine and evaluate alternative methods of formation damage removal and remediation by measuring the solubility of micronized

ilmenite and filter cakes created by micronized ilmenite-weighted oil-based drilling fluids in different acid systems.

CHAPTER II

EXPERIMENTAL METHODS AND MATERIALS*

In this chapter, experimental materials used in this study, including weighting materials, cores, drilling fluid systems, and acids, are introduced. The experimental approach taken in all steps of this research, including evaluating the effect of micronized ilmenite on OBM performance, understanding its potential in creating formation damage, and examining remediation efficiency after damage, have also been described. Equipment necessary for this approach has be discussed as well.

Materials

Micronized Ilmenite

The micronized ilmenite, also known as Microdense®, was provided by Elkem Silicon Products. This weighting material has a specific gravity of 4.6, is black in color, and is in powder form. X-ray diffraction (XRD) analysis of micronized ilmenite, shown in **Figure II-1**, indicated that its mineralogy is composed of approximately 88.12% ilmenite ($FeTiO_3$), 9.42% hematite (Fe_2O_3), and trace amounts of anorthite ($CaAl_2Si_2O_8$), a feldspar mineral. X-ray fluorescence (XRF) analysis specified that the elemental composition of micronized ilmenite includes iron, titanium, aluminum, magnesium, and silicon oxides, as is shown in **Table II-1**. This suggests that the feldspar material identified

* Part of this chapter is reprinted with permission from "Evaluation of Formation Damage of Oil-Based Drilling Fluids Weighted with Micronized Ilmenite or Micronized Barite" by Ibrahim, A. F., Al-Mujalhem, M. Q., Nasr-El-Din, H. A., and Al-Bagoury, M., 2020, *SPE Drilling & Completion*, Copyright 2020 by Society of Petroleum Engineers.

by XRD may be magnesium-based, rather than calcium-based, as the two elements have similar chemical properties. Additionally, the particle size distribution of micronized ilmenite (**Table II-2**), shows a D_{50} particle size of approximately 5µm.

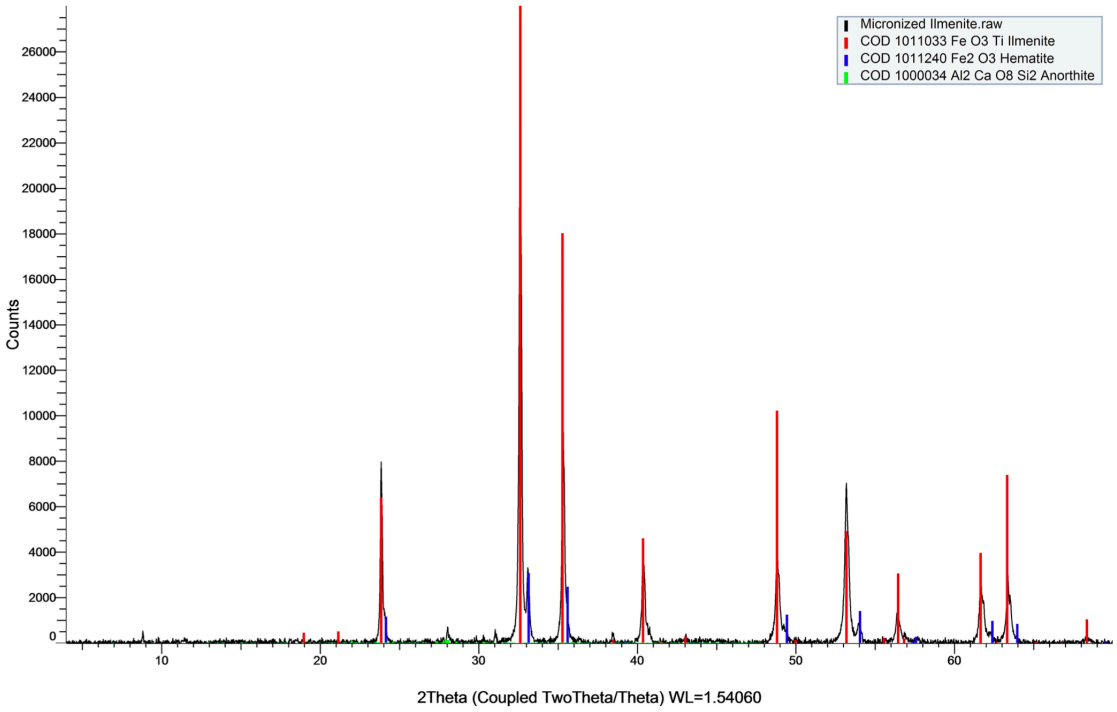

Figure II-1 XRD analysis of micronized ilmenite powder.

Oxides	Fe_2O_3	TiO_2	Al_2O_3	MgO	SiO_2
Concentration (wt%)	51	43.1	2.4	0.54	2.97

Table II-1 XRF analysis of micronized ilmenite.

Particle Size (µm)	D_{10}	D_{50}	D_{90}
	2.0	5.5	12.2

Table II-2 PSD of micronized ilmenite.

Drilling Fluid Systems

Three different oil-based drilling fluids were prepared with barite (2.7 and 5 μm) and ilmenite (5 μm) as weighting materials. **Table II-3** shows the composition of each system with a density of 2.0 SG and the mixing time for each component using a drilling fluid multimixer, shown in **Figure II-2**, at a speed of 11,500 rev/min. Two additional OBM fluid samples were prepared using a similar formulation and weighted up to a density of 1.5 SG using micronized ilmenite and barite (5 μm). Aminated lignite of 10 ppb was used as a fluid loss control additive for the latter samples. Water used to formulate the $CaCl_2$ brine, as well as that needed for all other experimental procedures, and sample preparation in this study, was deionized water acquired at room temperature from a water purification system with a measured resistivity of 18.2 MΩ•cm.

Figure II-2 OFITE drilling fluids mixer.

MATERIAL	MIXING TIME	5 µm ILMENITE	5 µm BARITE	2.7 µm BARITE
	min	*g*	*g*	*g*
Mineral Oil	-	406.3	386.9	386.9
HT Primary Emulsifier	5	30.0	28.6	32.6
Secondary Emulsifier	5	20.0	19.1	19.1
Organophilic Clay	10	10.5	10.0	7.0
Lime	5	24.3	23.2	23.2
Fluid Loss Additive (Polymer)	5	7.7	7.3	7.3
Fluid Loss Additive (Lignite)	5	40.9	39.0	39.0
$CaCl_2$ Brine (21 g $CaCl_2$, 79 g Water)	5	157.9	150.4	150.4
Wetting Agent	5	4.2	4.0	4.6
Barite	15	0.0	1400.0	1400.0
Ilmenite	15	1401.9	0.0	0.0
Simulated Drill Solids (Hymod Prima Clay)	5	42.0	40.0	40.0

Table II-3 Composition of the oil-based drilling fluid systems with ilmenite and barite as weighting materials. Reprinted with permission from (Ibrahim et al. 2020).

Cores

Bandera, Berea, and Boise sandstone cores were used in this study to simulate reservoir formations with varying permeabilities: low, medium, and high. The average measured permeabilities of the cores are 7, 80, and 600 md, respectively. Core blocks were cut into cylindrical plugs with dimensions of 1.5-in. diameter and 6-in. length, and of 2.5-in. diameter and 1-in. length, for use in the mud loop and filter press, respectively.

Crude Oil

A dead crude oil from Texas was used to measure initial and final core permeability to assess formation damage caused by each drilling fluid. **Table II-4** shows the viscosity and the density of the crude oil.

Temperature *°C*	**Viscosity** *cP*	**Density** g/cm^3
25	3.03	0.82
30	2.44	0.81
40	2.04	0.81
50	1.71	0.80
60	1.88	0.79
70	1.61	0.78

Table II-4 Viscosity and density of crude oil as a function of temperature. Reprinted with permission from (Ibrahim et al. 2020).

Acid Systems

Each of the following aqueous acid systems used in solubility testing was prepared to maintain an acid to solids ratio of 10:1:

A. 15 wt% Hydrochloric Acid (HCl)

B. 15 wt% HCl and 8 wt% Hydroxyethylethylenediaminetriacetic Acid (HEDTA)

C. Regular Mud Acid [12 wt% HCl and 3 wt% Hydrofluoric Acid (HF)]

D. Organic Mud Acid (9 wt% Formic and 1 wt% HF)

E. Organic Mud Acid (9 wt% Lactic and 1 wt% HF)

F. 7.5 wt% Oxalic Acid and 1 wt% HCl

G. 7 wt% Glycolic Acid and 1 wt% HCl

H. 13 wt% Lactic Acid and 1 wt% HCl

I. 11.6 wt% Citric Acid and 1 wt% HCl

J. 20 wt% Oxalic Acid and 10 wt% HCl

K. 20 wt% Oxalic Acid and 10 wt% Glycolic Acid

L. 11.6 wt% Citric Acid and 10 wt% Glycolic Acid

Table II-5 specifies the amount of each acid added to DI water to create the acid systems listed above. An exception is the use of ammonium bifluoride salt to generate HF through hydrolyzation reactions with HCl, formic, and lactic acids. For the purpose of consistency, 20 g of solids were used in all tests, necessitating the preparation of acids with a mass of 200 g.

ACID SYSTEM	Mass Added (g)		
	ACID 1	ACID 2	WATER
A	82.19	-	117.81
B	82.19	16.33	101.48
C	80.73	8.56	110.71
D	18.95	2.85	178.2
E	21.18	2.85	175.97
F	15.15	5.48	179.37
G	20	5.48	174.52
H	30.59	5.48	163.93
I	23.32	5.48	171.2
J	40.4	54.8	104.8
K	40.4	28.57	131.03
L	23.32	28.57	148.11

Table II-5 Summary of acid formulations for acid testing.

Experimental Methods

Drilling Fluid Performance

Fluid Aging

Simulating exposure of a drilling fluid to downhole HP/HT conditions during circulation, rather than using a freshly mixed drilling fluid sample, provides a more accurate representation of the expected performance of a drilling fluid system in the field. This was accomplished by aging, or hot rolling, all fluid samples before testing. A volume of approximately 300 cm^3 of each drilling fluid was poured into a Teflon liner, secured with a piston lid, and placed inside a 500 cm^3 stainless steel aging cell (**Figure II-3**). The cell was secured with an inner cap, O-ring, and outer cap that were held in place by set screws. Nitrogen was used to pressurize the cell to 50 psi through a valve stem. The aging cell was then placed on its side in a 4-roller oven (**Figure II-4**) at a temperature of 250˚F,

rolling at a speed of 25 rev/min, to simulate dynamic circulating conditions and avoid any settling or separation of the fluid. Each fluid was rolled under these conditions for 16 hours.

Figure II-3 OFITE aging cell and Teflon liner.

Figure II-4 OFITE 4-roller oven.

Rheological Measurements

A Grace M3600 automatic viscometer (**Figure II-5**) was used to measure rheological parameters of the drilling fluid systems. This type of viscometer uses a typical arrangement of two concentric cylinders; one rotates while the movement of the fluid

between them generates torque on the other, known as a bob. Displacement of the bob translates to a viscosity dial reading. True viscosity values were measured at 150˚F at set rotational speeds of 600, 300, 200, 100, 6, and 3 rev/min, corresponding to shear rates of 1021, 511, 340. 170, 10,2, and 5.1 sec^{-1}, respectively. Gel strengths (10 second and 10 minute) were also measured in accordance with API recommended practices.

Figure II-5 Grace M3600 Automatic Viscometer.

Formation Damage Evaluation

This section describes the steps taken to understand the potential that micronized ilmenite-weighted oil-based drilling fluid systems have with respect to internal and external filter cake formation, solids and filtrate invasion, and ease of filter cake flowback. Procedures for HP/HT fluid filtration and computed tomography techniques used as part of this study are detailed.

Fluid Filtration

Multiple methods were used to evaluate the filtration capabilities of a micronized ilmenite-weighted OBM. Measuring fluid filtrate invasion through a core or simulated reservoir rock and observing formed filter cake thickness and texture are performed using a conventional filter press. A modified coreflood simulated a more accurate representation of drilling fluid flow in a well, while quantifying damage through permeability measurements. Both techniques require similar core and fluid preparation.

Core Preparation

Sandstone cores were cut to the size required by each apparatus. The cores were dried at 150˚F overnight, and the dry weight was recorded. In conventional testing, cores were saturated with a 10 wt% potassium chloride (KCl) brine to inhibit swelling of clays contained within the sandstone. Wet weight was recorded, and cores were wrapped with Teflon tape to prevent fluid flow around the core. For mud loop testing, dry cores were scanned using computed tomography (CT) imaging. The cores were then saturated with dead crude oil under a vacuum for 4 hours. The saturated weight was then recorded, and the cores were CT scanned in the saturated state.

Conventional Filtration

HP/HT filtration experiments were conducted using an OFITE Static/Dynamic Filter Press (**Figure II-6**) at 250˚F and 500 psi overbalance. The filter press was modified to investigate filtration and drilling fluid filter cake formation capabilities on Berea sandstone cores (2.5-in. diameter and 1-in. thickness), rather than on filter paper. Following API experimental testing standards, a conventional dynamic filter press

procedure was used to perform the filtration, which includes a 500-cm^3 stainless steel cell with caps, valve stems, O-rings, a heating element, a propeller, and a nitrogen gas line. The fluid samples were poured into the cell. The cell caps were secured with locking screws and valve stems on both ends. After that, the cell was placed in its designated heating jacket. A differential pressure of 500 psi and a temperature of 250°F were applied to the cell. The mixing speed was set to 150 rev/min. The lower valve of the cell was opened, and the drilling fluid filtrate passing through the core was collected in a graduated cylinder. Collected filtrate volume was recorded as a function of time for 30 minutes. Following the test, the filter cake-topped core was removed from the cell for observation and analysis.

Figure II-6 OFITE HP/HT Filter Press.

To test the solubility of the micronized ilmenite-weighted filter cake (described below), following the conventional filtration test, cores were soaked in a hydrocarbon

solvent, xylene, for two hours to remove any organic materials, allowing a larger surface area of the filter cake to be exposed to the acid system. After that, cores were dried for 4 hours, and the filter cake was scraped off and weighed to confirm the correct amount of filter cake required to maintain the desired acid to solids ratio.

Mud Loop Testing

Apparatus

A conventional dynamic filter press places the drilling fluid vertically above the core. Although a propeller provides the fluid with shear, having the same small volume of drilling fluid in a confined space is not an accurate simulation of downhole drilling fluid circulation, especially as gravity is the main driving force for fluid flow and particle settling. As such, the coreflood setup used in this study (**Figure II-7**) was adjusted, with some likeness to the flow loop introduced by Ibrahim et al. (2018), to perform dynamic filtration testing that more closely resembles actual circulation. The schematic labels in the figure point out the (1) oven, (2) core holder, (3) core, (4) spacer, (5) syringe pump, (6-8) fluid accumulators, (9) pressure transducer, (10) hydraulic hand pump, (11, 12) backpressure regulators, (13) data acquisition and recording system, and (14) compressed gas supply.

In the coreflood setup, a two-liter accumulator was used to store the crude oil and was connected to the inlet of the core holder for initial and final permeability measurements. Two other accumulators were connected to the outlet to create a drilling fluid circulation loop. Pressure regulators maintained the correct pressure, while a syringe pump was used to inject the fluids, and a hydraulic hand pump was used to control the

overburden pressure. A pressure transducer was used to measure the pressure differential between the core inlet and outlet during the permeability measurements, and the data was recorded using LabVIEW software. **Figure II-8** shows the use of a hollow, 1-inch long spacer at the core outlet interface, which allowed the necessary space for filter cake formation and drilling fluid circulation.

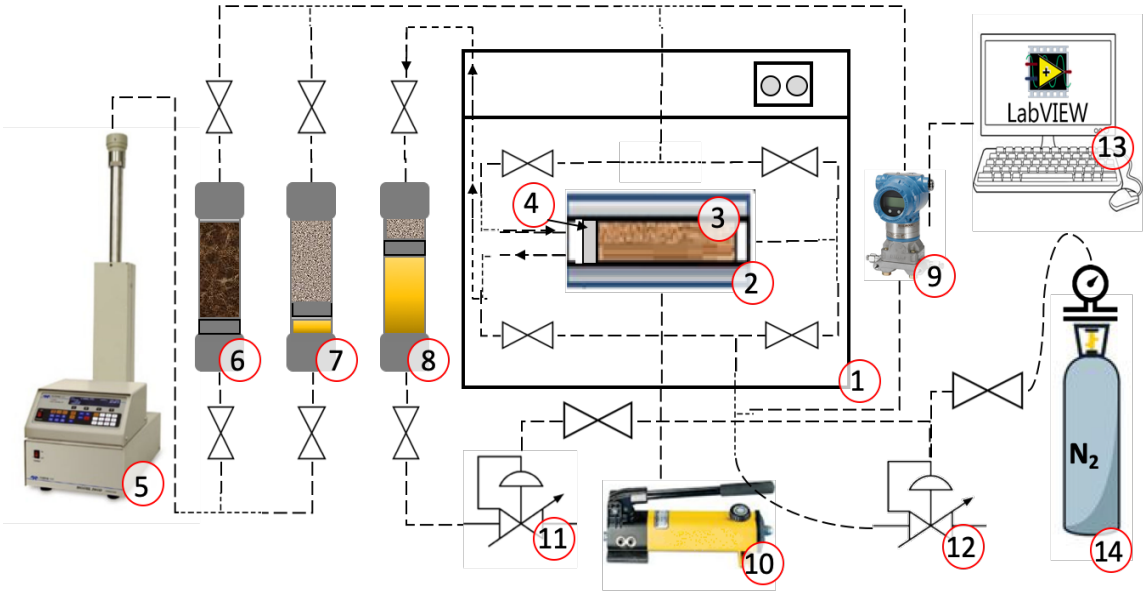

Figure II-7 Mud loop schematic. Reprinted with permission from (Ibrahim et al. 2020).

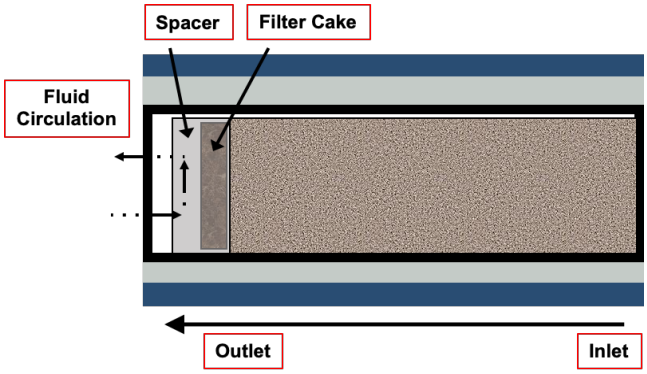

Figure II-8 Drilling fluid circulation inside the core holder. Reprinted with permission from (Ibrahim et al. 2020).

Filtration Procedure

After preparation of fluids, cores, and accumulators, the core was inserted into the core holder, and the spacer was inserted from the outlet direction. The backpressure regulator, labeled (12) in **Figure II-7**, was set to 100 psi to avoid the unintentional reverse flow of fluids. Crude oil was then injected at a constant flow rate from the inlet direction for permeability measurements. The pressure drop across the core was recorded continuously until stabilization. This process was repeated multiple times at different flow rates. Pressure drop values were used with Darcy's Law to calculate the permeability of the core. After that, the oven temperature was set to 250˚F, and crude oil was injected continuously for 3 hours. Permeability measurements were repeated at high-temperature conditions.

Subsequently, the inlet lines were closed, fluid flow was reversed, and the drilling fluid was circulated in the drilling fluid loop at a flow rate of 1 cm^3/min. The pressure in the loop increased up to a set point of 500 psi applied to the second backpressure regulator [labeled (11) in **Figure II-7**]. The 500-psi set point was selected to allow for a gap between injection pressure and overburden, creating an overbalance pressure of 400 psi in the spacer region of the core holder.

Once the pressure set point was reached, the lines on the side opposite to the drilling fluid circulation (inlet) were opened and connected to the backpressure regulator (11). Similar to a conventional filter press test, drilling fluid circulation continued for 30 minutes from that point, and the filtrate was collected and measured. Upon test completion, the system was returned to direct flow for final permeability measurements

with crude oil using a procedure similar to the one described above. After experiment completion, the core was removed and CT scanned to evaluate particle invasion after drilling fluid circulation and flowback.

Computed Tomography (CT)

A Toshiba Aquilion RXL CT Scanner was used to scan cores before and after mud loop testing in conjunction with ImageJ, an image processing computer program for scientific images. CT scans were analyzed and the pixels from images of horizontal slices across the length of a core were translated into an average value, the average CT number, measured in Hounsfield Units (HU). This value describes radiodensity of each slice of the core, allowing for a qualitative analysis of a change of distribution of matter within the pore spaces of the core. A significant change in CT number of a particular slice after mud loop testing, typically an increase, indicates the presence of a denser material, drilling fluid filter cake components, occupying the pores at that location, rather than the lighter crude oil that saturated the core during the previous scan. This testing approach provides a quantitative sense of the depth of invasion of the solids into the core, or the size of the internal filter cake.

Solubility Testing

Solubility tests were conducted on both 5µm ilmenite powder and the filter cake resulting from an OBM weighted with micronized ilmenite to evaluate the cleaning efficiency of different solvents.

Parr Reactor

Solubility tests were conducted at HP/HT conditions using a Parr Bench Top Reactor, shown in **Figure II-9**. For each test, the acid system was prepared and poured into the vessel. A known mass of solids being tested, either micronized ilmenite powder or filter cake solids, were added to the vessel. The vessel was closed and secured with a gasket and screws. After that, the system was pressurized using compressed nitrogen gas. The outlet line was opened to purge the vessel of any excess oxygen. After one minute, the outlet line was closed, and the system was stabilized at a pressure of 800 psi, lower than the desired test pressure of 1000 psi, to allow for pressure increases in the system as a result of heating. The heating jacket was connected to the vessel and set to heat the vessel to a temperature of 200˚F. A magnetic stirrer drive was used to stir the solution at 500 rev/min for the duration of the test. A sampling line was opened momentarily at specified time intervals to collect several 1 cm^3 samples of the solution for ion concentration analysis.

Figure II-9 Parr Bench Top Reactor.

After each test had concluded, the heating jacket was disconnected, and the reactor was depressurized and disassembled once it had cooled down. The solution was then filtered using 5 μm filter paper. Filtered solids were dried overnight, collected, weighed to determine solubility efficiency of the solvent, and stored for mineralogical composition analysis.

Inductively Coupled Plasma-Optical Emission Spectroscopy (ICP-OES)

ICP-OES is a technique used to detect the presence and concentration of specific elements or ions. An Optima 700 DV system, shown in **Figure II-10**, utilizes a pump to transport desired testing samples to a high-temperature plasma, which is created using a connected argon gas source. The collision of the sample with plasma will cause it to split into the charged ions it is composed of. Charged ions emit electromagnetic radiation at known wavelengths that are characteristic to specific elements. Wavelengths are detected, identified, and recorded on the accompanying computer software.

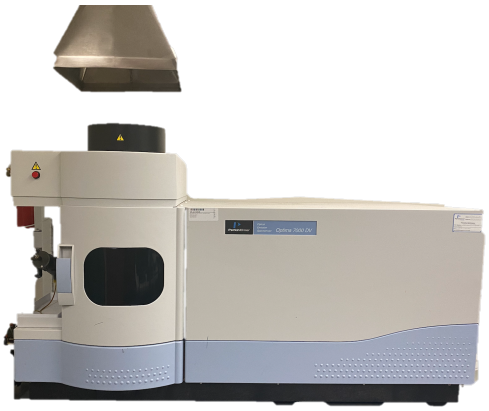

Figure II-10 Optima 7000 DV ICP-OES.

During solubility testing using the Parr reactor, 1 cm^3 effluent samples were collected at varying time intervals. These samples were diluted using DI water, a pipette, and a volumetric flask to fall within an acceptable concentration range limitation defined by the equipment. Diluted samples were then analyzed by the ICP-OES for ions of interest, mainly iron and titanium.

X-Ray Diffraction (XRD)

XRD is another technique to identify sample composition. This technique directs x-rays towards the powder sample being tested. The sample is rotated until peak intensity in diffracted rays occurs. An x-ray collector counts the signal from the diffracted rays at different angles to account for all possible directions. It then translates the resulting peaks into d-spacing values, which are unique to a specific mineral.

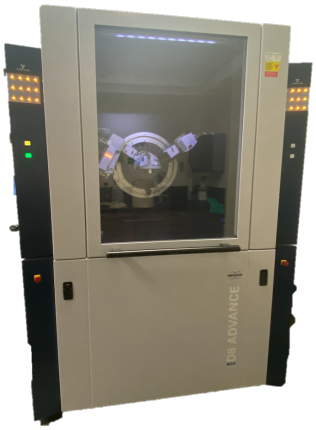

Figure II-11 Bruker D8 ADVANCE Eco XRD System.

After each of the solubility tests, solids remaining out of solution after reaction with the acid system were filtered, dried, and collected, then subjected to non-destructive mineralogical analysis using the Bruker D8 ADVANCE Eco XRD System (**Figure II-11**). The solid samples must be in powder form, and only a small amount (a few grams) is spread flat into its designated space in a sample holder, to be placed in the XRD machine for testing.

X-Ray Fluorescence (XRF)

While XRD measures minerology, XRF identifies the elemental composition of a solid sample. X-rays are directed towards and absorbed by the solids sample, causing it to become excited. Energy is released in the form of radiation, with wavelengths that are characteristic of the different elements present in the sample.

Similar to XRD, a few grams of filtered solids from the solubility tests were analyzed in powder form using the Bruker S2 Ranger XRF Spectrometer (**Figure II-12**). This non-destructive technique revealed that the elemental composition of micronized

ilmenite included iron, titanium, magnesium, and silicon oxides. After establishing the baseline concentrations, the same oxides were investigated in filtered ilmenite samples after acid system exposure. Changes in oxide concentrations provided qualitative characterization data for each solubility reaction.

Figure II-12 Bruker S2 Ranger XRF Spectrometer.

CHAPTER III

EVALUATION OF MICRONIZED ILMENITE AS A WEIGHTING AGENT IN OIL-BASED DRILLING FLUIDS[*]

Background

In the field of drilling, overbalanced drilling is the process by which pressure in the wellbore exceeds that of surrounding formation fluids by a safe margin. This process is more commonly used and allows for faster drilling while maintaining a lower risk of blowout. This is because the difference between drilling fluid pressure and formation pressure during overbalanced drilling causes invasion of drilling fluid filtrate from the annulus into the formation (Hoberock and Bratcher 1998). Underbalanced drilling, on the other hand, is more expensive and does not eliminate all types of damage in all reservoirs (Bennion and Thomas 1994).

Formation damage is defined here as the reduction in permeability in the near-wellbore region due to a number of reasons, one of which is drilling activities. Loss of fluids and small particles while drilling may result in chemical incompatibility with the formation and plugging of the pores, and is considered one of the most common causes of formation damage, leading to decreased productivity in a well (Amaefule et al. 1988). Minimizing formation damage using appropriate drilling fluid additives that can generate

---

[*] Part of this chapter is reprinted with permission from "Evaluation of Formation Damage of Oil-Based Drilling Fluids Weighted with Micronized Ilmenite or Micronized Barite" by Ibrahim, A. F., Al-Mujalhem, M. Q., Nasr-El-Din, H. A., and Al-Bagoury, M., 2020, *SPE Drilling & Completion*, Copyright 2020 by Society of Petroleum Engineers.

a filter cake that is thin with decreased permeability is one of the key elements necessary for the success of drilling operations (Mahmoud and Nasr-El-Din 2018).

A weighting agent is a high-density and fine, particulate solid material used to increase the density of drilling fluids. It is also the main contributing component of solid particles in a filter cake. American Petroleum Institute (API) barite is the most commonly used weighting material (Bruton et al. 2006). However, it has some disadvantages, such as sagging, removal difficulty, and associated formation damage (Nasr-El-Din et al. 2004). Furthermore, there has been a noticeable supply shortage of high-quality barite and a significant increase in the price of barite over the past decade, causing the need to consider alternative materials (Tehrani et al. 2014). Alkhalaf et al. (2019) studied the effect of replacing barite with potassium formate or manganese tetroxide.

The use of micronized weighting agents, such as manganese tetroxide, micronized ilmenite, or micronized barite, improves the overall fluid performance, reducing the plastic viscosity (PV) and minimizing the tendency to sag. Micronized ilmenite ($FeTiO_3$) was introduced as a weighting material to avoid the shortcomings of barite (Al-Bagoury and Steele 2012). The higher density of ilmenite [4.6 specific gravity (SG)] compared to barite (4.2 SG) allows for decreasing overall solids content of the fluid. The use of micronized ilmenite caused improvement in ROP, along with the enhancement of rheological properties. Under similar conditions, the micronized ilmenite showed low sag tendency, low PV, and increased acid solubility compared to API barite. Particle hardness also indicates that degradation in size will not occur during drilling, reducing the need for fluid maintenance and allowing for larger volumes to be recycled (Ivan et al. 2018).

Furthermore, micronized ilmenite has finer particles and decreased magnetite content, causing abrasiveness and magnetic issues known with conventional ilmenite to be eliminated (Al-Bagoury 2014). These desirable features can be applied in challenging drilling operations such as horizontal drilling, deepwater drilling, and slimhole applications.

Elkatatny et al. (2012b) reported the evaluation of an ilmenite-based drilling fluid and its filter cake in HP/HT conditions. A minimal amount of $CaCO_3$ particles could decrease the filtrate volume because of its benefits in particle packing. Moreover, Ivan et al. (2018) reported using micronized ilmenite in oil-based fluids used to drill extended-reach drilling (ERD) wells in offshore Abu Dhabi. Lower PV values, compared with those of traditional fluids, resulted in a lower ECD, which allowed successful drilling of longer horizontal sections.

Formation Damage Evaluation Methods

A conventional filter press is a popular evaluation method for formation damage caused by drilling fluids. Conventional filtration allows for multiple consecutive tests to be conducted on a single core: permeability measurements, filter cake formation, fluid loss assessment, filter cake solubility, and return permeability calculations. Dynamic testing combats the gravitational settling and sag tendencies of drilling fluids, causing results to be closer to those occurring in the field. However, limitations include the inability to mimic reverse fluid flow of produced fluids, along with the lack of fresh fluid supply introduction to simulate circulation. These limitations potentially underestimate the actual damage caused by drilling fluid systems in the field.

The use of a coreflood system to more closely simulate field conditions and tackle the above limitations has been addressed in this research. Both filtration methods were used, with a focus on mud loop testing, which took reverse fluid flowback into account, focusing on damage remaining in the simulated reservoir formation after production or flowback has occurred. Results from the conducted coreflood/mud loop experiments, along with conventional filtration and analysis using CT images, are presented in this chapter.

Results and Discussion

Rheological Parameters

The viscosity data for the drilling fluids with a density of 2.0 and 1.5 SG are shown in **Table III-1** and **Table III-2**, respectively. Measured viscosity and gel strength values for the different fluid formulations at shear rates ranging from 5.1 to 1021 s^{-1} (3-600 rev/min) are shown. Overall rheological parameters at all shear rates are fairly similar for both barite-based fluids. Decreased values at all shear rates for the ilmenite-based fluid indicate an overall improvement in performance, allowing for a reduction in pump pressure and enhancement of ROP while drilling.

PARAMETER		5 µm Ilmenite-Based Fluid	5 µm Barite-Based Fluid	2.7 µm Barite-Based Fluid
600 rpm	*cP*	126	155	155
300 rpm		71	89	90
200 rpm		52	65	65
100 rpm		32	39	40
6 rpm		7	9	10
3 rpm		6	7	9
Gels - 10 min	*lb/100 ft²*	7	8	11
Gels – 10 s		9	12	12
Plastic Viscosity	*cP*	55	66	65
Yield Point	*lb/100 ft²*	16	23	25

Table III-1 Rheological properties of oil-based drilling fluid systems with a density of 2.0 SG at 125˚F. Reprinted with permission from (Ibrahim et al. 2020).

PARAMETER		5 µm Ilmenite-Based Fluid	5 µm Barite-Based Fluid
600 rpm	*cP*	56	61
300 rpm		32	36
200 rpm		24	27
100 rpm		15	17
6 rpm		5	6
3 rpm		4	6
Gels - 10 min	*lb/100 ft²*	6	6
Gels – 10 s		10	8
Plastic Viscosity	*cP*	24	25
Yield Point	*lb/100 ft²*	8	11

Table III-2 Rheological properties of oil-based drilling fluid systems with a density of 1.5 SG at 125˚F. Reprinted with permission from (Ibrahim et al. 2020).

Filter Press

A standard dynamic filter press experiment was conducted using a Berea sandstone core with the micronized ilmenite-based drilling fluid. The experiment was conducted at an overbalance pressure of 500 psi, 250˚F, and rotation speed of 150 rev/min. **Figure III-1** shows filtrate accumulation for the duration of the 30-minute test, with a spurt loss of approximately 0.06 cm^3 and an indicated filter cake formation time of approximately 8 minutes. The total filtrate volume was 1.8 cm^3, and the filter cake formed with a thickness of $3/32^{nd}$ in.

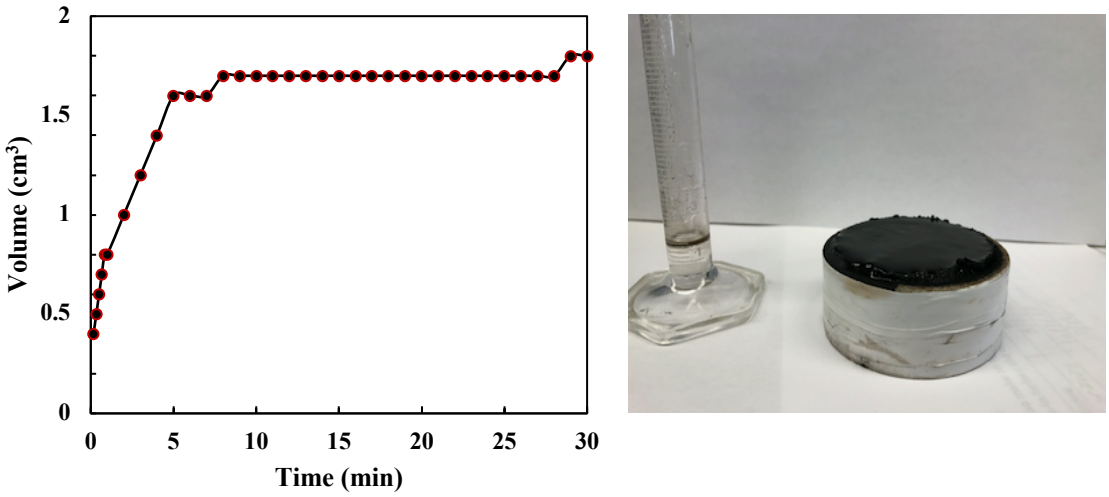

Figure III-1 Filtrate volume collected during a 30-minute dynamic filtration test and the created filter cake. Reprinted with permission from (Ibrahim et al. 2020).

As for the low SG fluids, static filtration experiments at 500 psi and 150˚F resulted in a total filtrate volume of 7 cm^3 for the ilmenite-based drilling fluid and 4 cm^3 for the barite-based drilling fluid. Both fluids formed filter cakes with a thickness of $2/32^{nd}$ in.

Mudloop

The aim of this work was to evaluate formation damage caused by oil-based drilling fluids that use ilmenite as the weighting material in different formations with different permeabilities. Ten coreflood experiments were conducted to test several OBM fluid systems against different permeabilities and to compare performance to barite-weighted drilling fluids. A summary of all coreflood experiments is shown in **Table III-3**. The first three experiments were designed to evaluate formation damage from the three fluid systems in low-permeability sandstone cores. Formation damage in medium-permeability sandstone was then evaluated by conducting Experiments 4-6. Low-specific gravity fluids were then used to investigate the damage in high- and medium-permeability sandstone cores in Experiments 7-10.

EXP.	FLUID	DRILLING FLUID DENSITY	CORE	PERMEABILITY
1	2.7 µm Barite	2.0 SG	Bandera Sandstone	Low Permeability
2	5 µm Barite			
3	5 µm Ilmenite			
4	2.7 µm Barite		Berea Sandstone	Medium Permeability
5	5 µm Barite			
6	5 µm Ilmenite			
7	5 µm Barite	1.5 SG	Berea Sandstone	Medium Permeability
8	5 µm Ilmenite			
9	5 µm Barite		Boise Sandstone	High Permeability
10	5 µm Ilmenite			

Table III-3 Experimental design for formation damage assessment of several oil-based drilling fluid systems and formation permeabilities. Reprinted with permission from (Ibrahim et al. 2020).

Formation Damage in Low-Permeability Sandstone

As described above, coreflood experiments were conducted to determine the initial and final permeabilities of the cores while examining filtration properties, filter cake formation, and overall damage created by the formed filter cake through solids invasion. This subsection focuses on the first three experiments, which evaluate the performance and damage caused by the three OBM systems with regard to a low-permeability Bandera sandstone core, with an average measured absolute permeability of 7.2 md and an average porosity of 15.4%. The results obtained for coreflood Experiments 1-3 are summarized in **Table III-4**.

EXP.	ABSOLUTE PERMEABILITY	POROSITY	FILTRATE VOLUME	RETURN PERMEABILITY
	md	vol%	cm^3	%
1	7.66	15	4.4	83.7
2	8.4	13.3	2	90.7
3	5.64	18	2.4	96.5
4	33.6	19	5.6	71
5	69.1	19.5	3	60
6	60	19.6	2.6	98.3

Table III-4 Formation damage analysis for Experiments 1-6 with a drilling fluid density of 2.0 SG. Reprinted with permission from (Ibrahim et al. 2020).

Collected fluid filtrates from each dynamic filtration experiment may be an indicator of damage, with a higher volume indicating greater damage. The measured volumes were 4.4, 2, and 2.4 cm^3, respectively, for the three experiments. A visual representation of the filtrate volume as a function of time appears in **Figure III-2,** representing the test progression for Experiment 2; **Figure III-3** represents the same for Experiment 3.

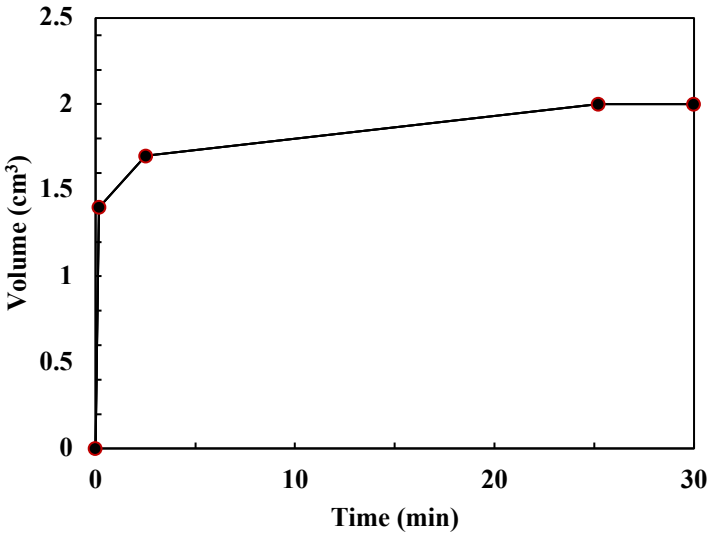

Figure III-2 Dynamic filtration results of Experiment 2 (5 µm barite-based drilling fluid/Bandera sandstone) at a 400 psi overbalance. Reprinted with permission from (Ibrahim et al. 2020).

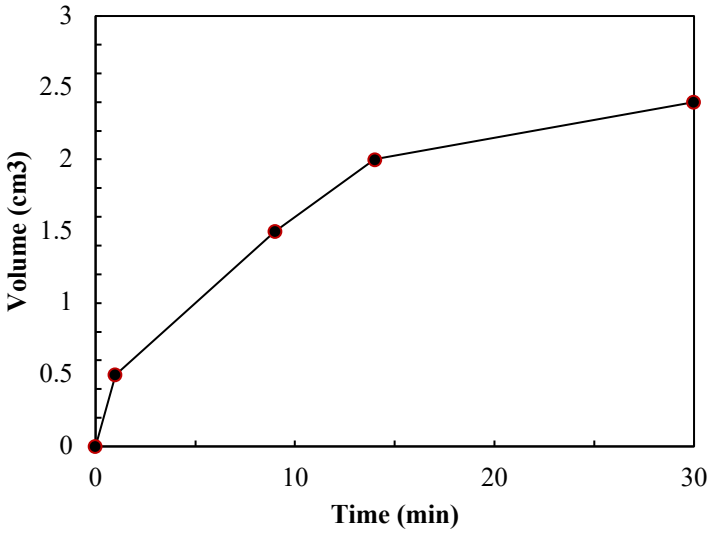

Figure III-3 Dynamic filtration results of Experiment 3 (5 µm ilmenite-based drilling fluid/Bandera sandstone) at a 400 psi overbalance. Reprinted with permission from (Ibrahim et al. 2020).

Another indicator to observe in conjunction with these experiments is a comparison of CT images on the cores before and after drilling fluid circulation during coreflood experiments. A CT number generated for each thin cross-section along the core before and after exposure to a drilling fluid suggests the depth of invasion of solids into the core. **Figure III-4** visually depicts the damage formed through exposure during Experiment 2, and a large difference between corresponding values before and after treatment indicates formation damage by solid invasion in the first inch of the core.

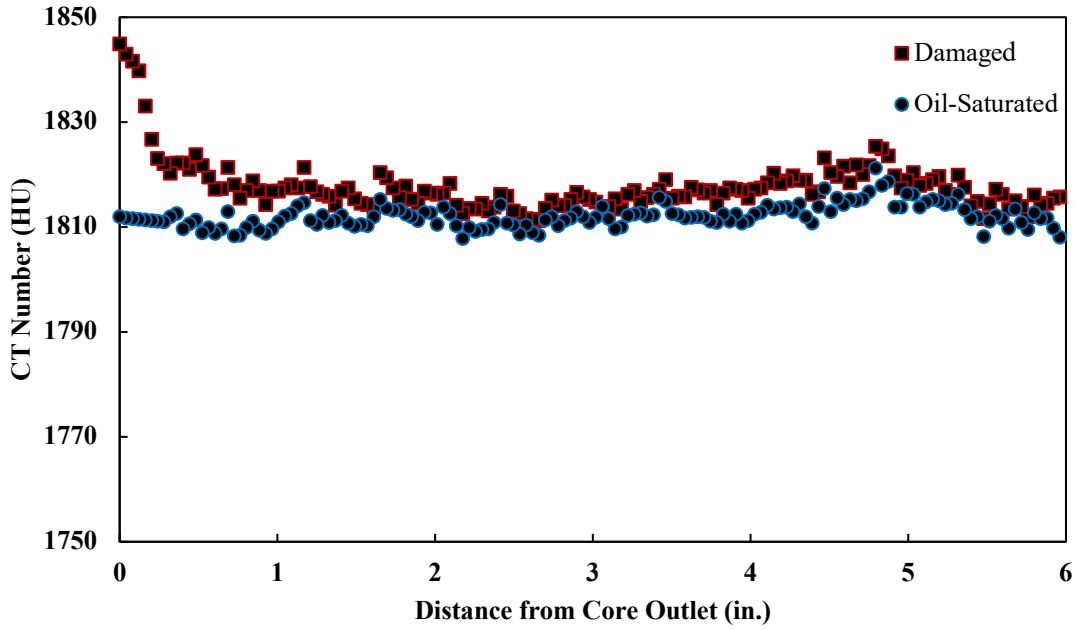

Figure III-4 CT scan analysis for Experiment 2 before and after filter cake formation. Reprinted with permission from (Ibrahim et al. 2020).

Solids plugging the pores in the core will result in varying pressure drops when measuring initial and final permeability, further quantifying the damage caused by exposure to the OBM systems being evaluated. Formation damage was calculated as follows:

$$\text{Damage}, \% = \frac{k_i - k_f}{k_i} = \frac{\Delta p_f - \Delta p_i}{\Delta p_f}, \quad \ldots\ldots(1)$$

where k is the absolute core permeability (md), and Δp is the stabilized pressure drop across the core (psi). The subscripts i and f stand for the initial and final permeability, respectively. With this, the barite-weighted fluid systems used in the first two experiments exhibited a reduction in permeability of 16.3 and 9.3%, respectively. The core used in Experiment 3, however, did not show a variance in pressure drop, suggesting that the micronized ilmenite-weighted fluid did not cause a reduction in permeability, with a return permeability of 96.5%.

Formation Damage in Medium-Permeability Sandstone

This subsection focuses on Experiments 4-6, which evaluate the performance and damage caused by the three OBM systems with regard to a medium-permeability Berea sandstone core, with an average measured absolute permeability of 54.2 md and an average porosity of 19.4%. The results obtained for coreflood Experiments 4-6 are also summarized in **Table III-4.**

The measured fluid filtrate volumes for the three HP/HT dynamic filtration tests were 5.6, 3, and 2.6 cm^3 in 30 minutes, respectively, which also indicates less damage

caused by the ilmenite-weighted fluid. Visual representation for the three experiments is shown in **Figure III-5, Figure III-6,** and **Figure III-7,** along with images of the filter cake formed on the surface of the cores. Furthermore, CT-scan analysis for the core used in Experiment 5, shown in **Figure III-8,** suggests more extensive damage in the medium permeability core, reaching a depth of two inches.

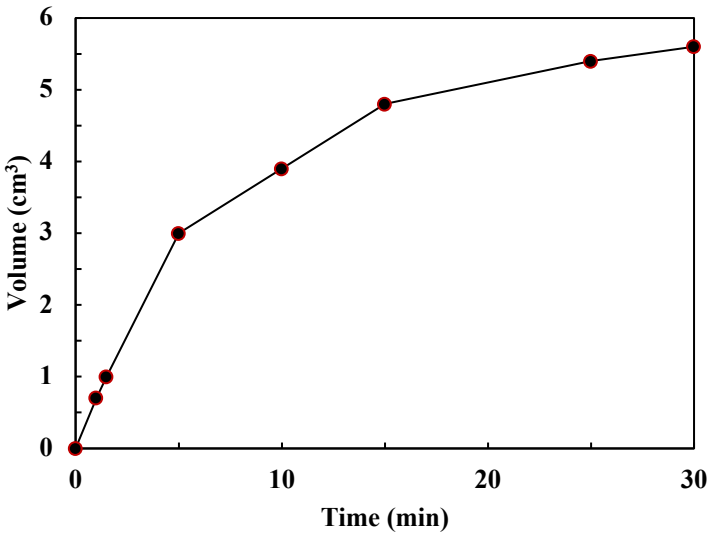

Figure III-5 Dynamic filtration results of Experiment 4 at a 400-psi overbalance. Images show the core surface after initial filter cake formation (left) and after flowback and final permeability measurements (right). Reprinted with permission from (Ibrahim et al. 2020).

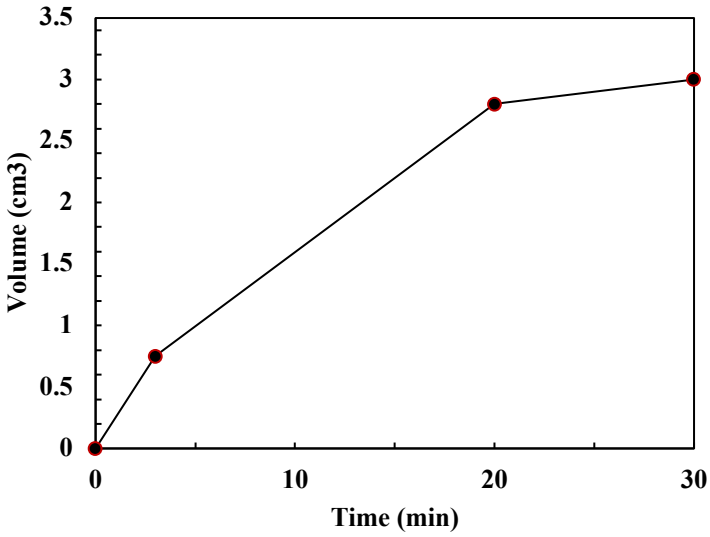

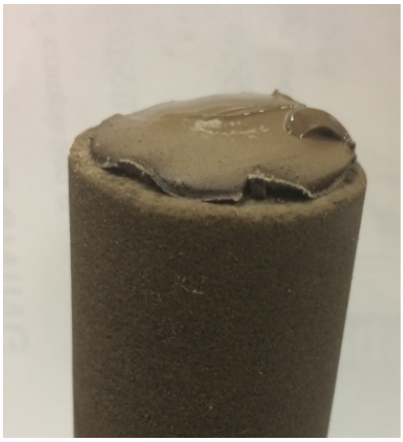

Figure III-6 Dynamic filtration results of Experiment 5 at a 400-psi overbalance and an image of the filter cake formed on the core surface. Reprinted with permission from (Ibrahim et al. 2020).

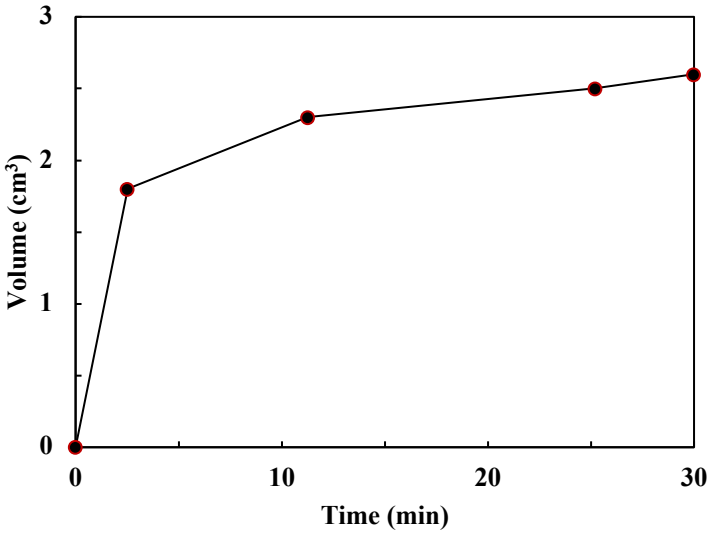

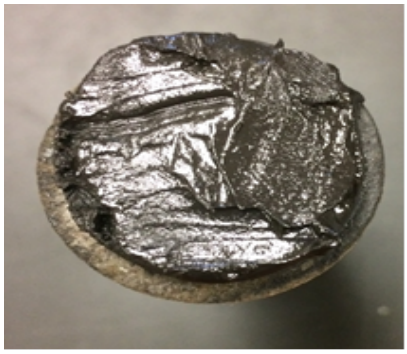

Figure III-7 Dynamic filtration results of Experiment 6 at a 400-psi overbalance and an image of the filter cake formed on the core surface. Reprinted with permission from (Ibrahim et al. 2020).

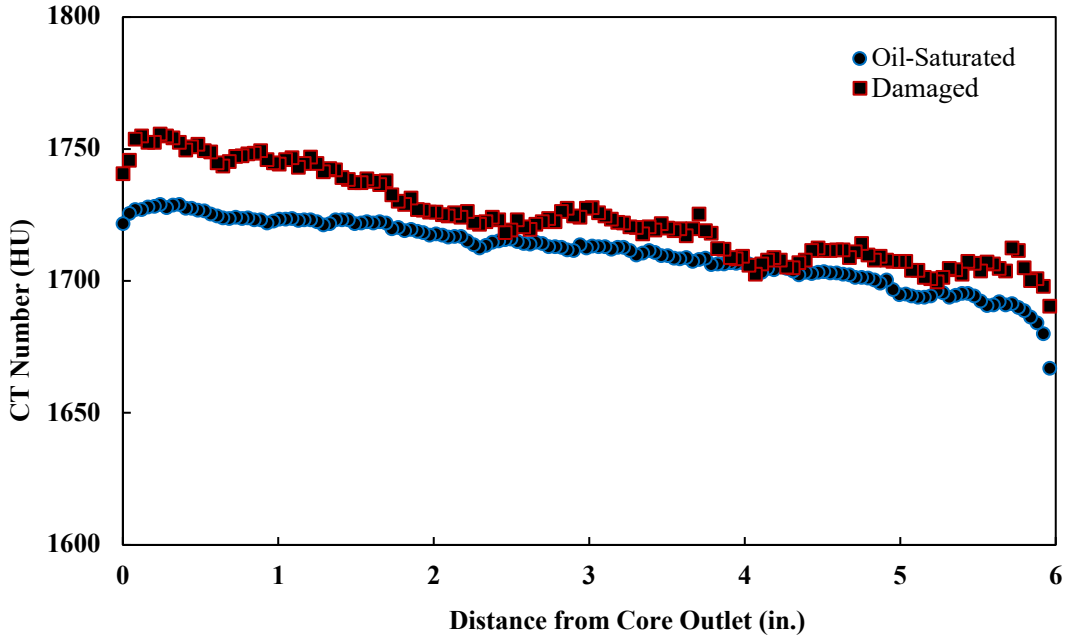

Figure III-8 CT-scan analysis for Experiment 5 before and after filter cake formation. Reprinted with permission from (Ibrahim et al. 2020).

Permeability measurements during coreflood tests resulted in larger reductions in permeability for cores used with barite-weighted fluids, 29 and 40%, respectively. However, similar to the low-permeability core, the ilmenite-weighted drilling fluid system caused no permeability reduction, as was measured during Experiment 6. The results of the experiments in this section are generally in agreement with each other, with filtrate volumes complementing damage quantified and viewed through imaging. Medium-permeability cores exhibited more damage in general, but ilmenite-weighted fluids were nondamaging in both cases.

Formation Damage in Medium-Permeability Sandstone with Low SG Fluid

In order to induce formation damage from an ilmenite-based drilling fluid specifically, a 1.5 SG drilling fluid was prepared with a relaxed fluid loss of 7 cm^3, and medium- to high-permeability cores were used. This set of experiments focused on comparing only ilmenite and barite-weighted fluids with the same average particle size (5 μm). Experiments 7 and 8 used Berea sandstone cores with an average measured absolute permeability of 51 md and an average porosity of 18.3%. The results obtained from this section of the study are summarized in **Table III-5**.

EXP.	ABSOLUTE PERMEABILITY	POROSITY	RETURN PERMEABILITY
	md	vol%	%
7	60	19.6	60
8	42	17	89
9	400	25	60
10	490	25.6	70

Table III-5 Formation damage analysis for Experiments 7-10 with a drilling fluid density of 1.5 SG. Reprinted with permission from (Ibrahim et al. 2020).

The barite-based fluid showed damage to permeability similar to that of a fluid with 2.0 SG density; even the static fluid loss was only 4 cm^3. The filter cake formed on the face of the core is shown in **Figure III-9.** The deliberately high fluid loss for the 1.5 SG ilmenite-based fluid caused some damage to the core permeability in this case, with a permeability reduction of 11% and solid invasion to a depth of nearly two inches from the

core outlet, as is shown in **Figure III-10.** It is also important to note that dynamic filtration of these fluids resulted in a fluid volume greater than 15 cm^3 in both cases. These results again show the importance of controlling the fluid loss to minimize resulting formation damage.

Figure III-9 A Berea sandstone core surface (left) after initial filter cake formation (Experiment 7) and (right) after flowback and final permeability measurements. Reprinted with permission from (Ibrahim et al. 2020).

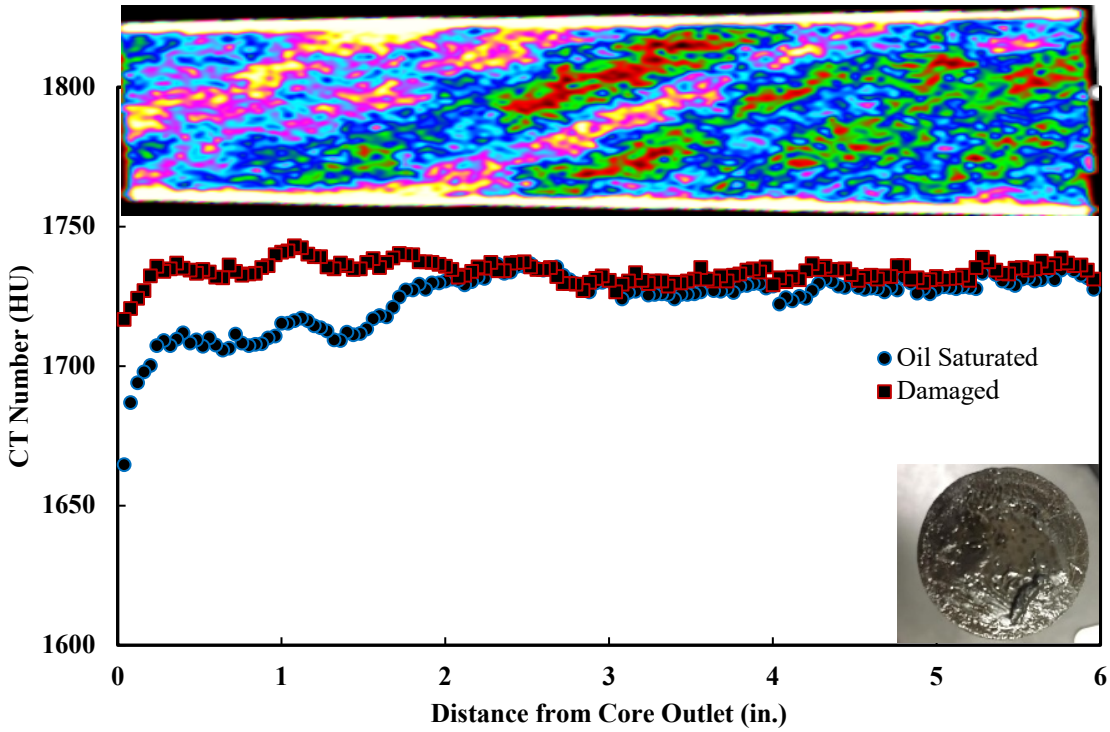

Figure III-10 CT-scan analysis for Experiment 8 before and after filter cake formation. Reprinted with permission from (Ibrahim et al. 2020).

Formation Damage in High-Permeability Sandstone with Low SG Fluid

Experiments 9 and 10 used Boise sandstone cores with an average measured absolute permeability of 445 md and an average porosity of 25.3%. The results obtained from this section of the study are also summarized in **Table III-5**.

The barite-based fluid continued to create formation damage, with a 40% reduction in permeability. CT imaging indicates solids invasion of up to one inch, as shown in **Figure III-11.** The ilmenite-based fluid used in Experiment 10 created more significant damage to permeability in this case, with a reduction of 30%.

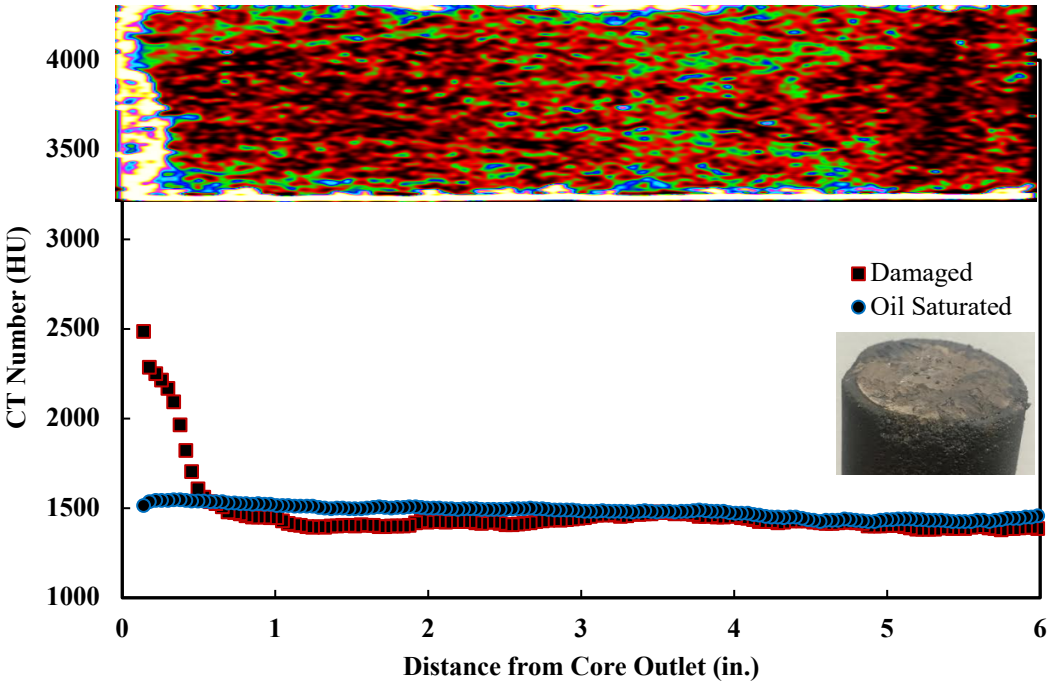

Figure III-11 CT-scan analysis for Experiment 9 before and after filter cake formation. Reprinted with permission from (Ibrahim et al. 2020).

Barite-based drilling fluids caused formation damage to the different sandstone formations. The percentage of permeability reduction was a function of the barite size and the pore throat size. The average pore throat (in μm) of the core can be calculated as the square root of the permeability (in md). **Figure III-12** shows a direct correlation between the formation damage and logarithmic scale of the pore throat diameter/barite size ratio.

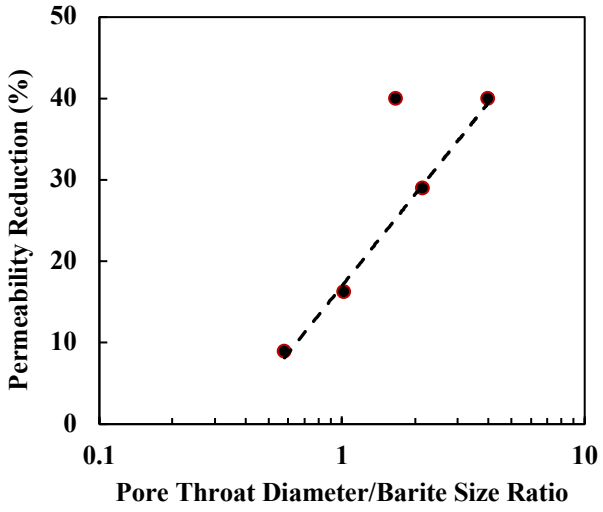

Figure III-12 Percentage of permeability reduction as a function of pore throat diameter/barite size ratio for barite-based drilling fluids. Reprinted with permission from (Ibrahim et al. 2020).

As shown in **Table III-6**, the particle size distributions of 5 µm ilmenite and 5 µm barite are almost identical. Aside from particle size and morphology of both materials, an explanation for the high damage caused by barite compared to ilmenite stems from the fact that the surface chemistries of barite and ilmenite are different. Ilmenite is a mixed metal oxide mineral ($FeTiO_3$) with a hydroxyl group on the surface, while barite has low solubility in water with high surface activity, particularly the colloidal and micronized materials. The particle invasion of barite and the difficulty to flow back indicates the bridging of barite particles inside the core.

WEIGHTING AGENT	5 µm Ilmenite	5 µm Barite	2.7 µm Barite
D_{10} (µm)	2.0	2.0	1.3
D_{50} (µm)	5.5	5.4	2.7
D_{90} (µm)	12.2	11.3	5.6
Density (SG)	4.6	4.4	4.3
BET (m^2/g)	1.6	1.2	2.5

Table III-6 Particle size distribution of the weighting materials. Reprinted with permission from (Ibrahim et al. 2020).

CHAPTER IV

REMOVAL OF MICRONIZED ILMENITE-WEIGHTED OIL-BASED FILTER CAKE*

Background

The drilling process is the most harmful to the reservoir, mainly due to drilling fluid filtrate invasion into the near-wellbore region. Drilling fluid systems are carefully formulated, and additives are chosen at optimal concentrations to create a high quality, impermeable filter cake that will minimize formation damage. Unfortunately, however, due to chemical incompatibilities and the need to include dense solid particles to maintain hydrostatic pressures while drilling, some physical damage to the reservoir is unavoidable. As such, it is vital to understand possible mechanisms for damage removal for a particular fluid system. Accordingly, this portion of the study aims to investigate the solubility of iron and titanium ions in micronized ilmenite.

Typical filter cake removal methods include mechanical techniques, such as scraping or jetting, and chemical dissolution using a number of solvents. A specific method is chosen based on the cause of damage, availability of chemicals and equipment, and economic feasibility. Solvents may include cheap, strong acids, or more costly organic acids, chelating agents, and premium chemical treatments. Common acids used to remove

---

* Part of this chapter is reprinted with permission from "Evaluation of Formation Damage of Oil-Based Drilling Fluids Weighted with Micronized Ilmenite or Micronized Barite" by Ibrahim, A. F., Al-Mujalhem, M. Q., Nasr-El-Din, H. A., and Al-Bagoury, M., 2020, *SPE Drilling & Completion*, Copyright 2020 by Society of Petroleum Engineers.

drilling fluid filter cake include HCl and regular mud acid, a mixture of HCl and HF, used in sandstone reservoirs, where a lack of calcite renders HCl unreactive (Smith and Hendrickson 1965).

Different combinations and mixtures of solvents may help limit, retard, or solubilize certain ions, allowing for improved reaction rates and removal efficiencies. For example, Su (2016) found that combining HCl with a chelating agent, HEDTA, is a good method to prevent the precipitation of iron into solution, but at a concentration of 7.5 wt% HCl and 7.5 wt% HEDTA, this system was not able to completely remove a micronized ilmenite-weighted WBM filter cake.

Organic Acids

Organic acids may be preferred for remediation treatments to avoid using high concentrations of strong, corrosive acids. However, organic acids are known to have weaker reactions and maximum concentration limitations due to the low solubility of produced calcium salts in the reservoir (Mohamed et al. 2015). Organic acids commonly used in the oil and gas industry include acetic, citric, formic, and lactic acids. Moreover, combining a small concentration of HCl with an organic acid provides a safer, more cost-effective method to investigate formation damage removal (Dill and Keeney 1978; Al Moajil and Nasr-El-Din 2014).

Contrary to this, however, alternative organic acids have been used to replace HCl in regular mud acid due to its high corrosivity and high spending rate (Al-Harbi et al. 2013). Formic and lactic acids have been used in conjunction with HF to form organic mud acids, functioning to retard HF and act as a chelating agent.

Although the solubility of an ilmenite-weighted drilling fluid filter cake in organic acids has not been extensively reported in the literature, the solubility of ilmenite has been researched in other industries. Omidi et al. (2018) specified oxalic acid as a good chelating agent with a strong acidic effect. The chemical reactions taking place between oxalic acid and ilmenite are described as follows (Omidi et al. 2018):

$$H_2C_2O_4 \leftrightarrow H^+ + HC_2O_4^-,\ K_{a1} = 5.378*10^{-2}$$

$$HC_2O_4 \leftrightarrow H^+ + C_2O_4^{2-},\ K_{a2} = 5.42*10^{-5}$$

Optimized results of ilmenite dissolution in an HCl/oxalic acid system were presented by the authors. They found that optimal dissolution occurs at 4 hours using a 2:1 oxalic acid to HCl ratio, 30 wt% total acid concentration, and 10:1 acid to ilmenite ratio at 320˚F.

Moreover, Jonglertjunya and Rubcumintara (2012) investigated several different organic acids, including oxalic and citric acids. The chemical reaction governing iron and titanium dissolution in citric acid was identified as:

$$C_6H_8O_7 + H_2O \rightarrow H_3O^+ + C_6H_7O_7^-$$

$$FeTiO_3 + 4H_3O^+ \rightarrow TiO^{2+} + Fe^{2+} + 6H_2O$$

Optimal conditions for ilmenite dissolution by citric acid were identified as an acid concentration of 1M and a stirring speed of 750 rpm for 20 hours.

The use of organic acids to address formation damage caused by drilling fluids both in the field and the lab is well-documented in the literature. Al Moajil (2010) reported testing lactic, glycolic, formic, malonic, and acetic acids with manganese tetroxide. Elkatatny et al. (2013c) used an HCl/glycolic acid system to successfully remove manganese tetroxide-weighted filter cake.

Results and Discussion

Micronized Ilmenite

Ilmenite is an acid-soluble weighting agent, which is a preferable property for filter cake removal in reservoir fluids. The solubility of ilmenite in HCl depends on the reaction conditions, such as the HCl / ilmenite ratio, temperature, acid concentration, and reaction time. The solubility of ilmenite in 15% HCl for 16 hours is >40%. The incomplete solubility is related to the reverse reaction of titanium oxychloride (TiOCl).

In this part of the study, different solubility tests were conducted for micronized ilmenite powder (D_{50} = 5 µm) with different acid systems. The solubility experiments were conducted using an HP/HT reactor at 1,000 psi and 200˚F. The acid-to-ilmenite ratio was 10:1, and the solution was mixed at 500 rpm. XRF and XRD analyses were conducted on the ilmenite powder before and after the solubility tests. ICP-OES testing was conducted on the effluent samples to measure the dissolved ion concentrations.

15 wt% HCl + 8 wt% HEDTA Acid System

Maintaining the acid-to-solids ratio of 10:1, 200 g of the acid system were added to 20 g of ilmenite. The residual solids remaining after a 10-hour solubility test weighed 14 g, resulting in a solubility efficiency of approximately 30%. **Table IV-1** shows the XRF analysis for the residual ilmenite after solubility testing, compared to the original sample. **Figure IV-1** shows the increase in the concentration of different ions dissolved in the liquid phase, measured by ICP-OES, as the reaction time progressed.

	ORIGINAL SAMPLE		AFTER SOLUBILITY		
OXIDES	**Concentration** *wt%*	**Weight** *g*	**Concentration** *wt%*	**Weight** *g*	**Solubility Efficiency** *%*
Fe_2O_3	51.00	10.20	43.90	6.15	39.75
TiO_2	43.10	8.62	52.56	7.36	14.64
Al_2O_3	2.40	0.48	1.14	0.16	66.75
MgO	0.54	0.11	0.36	0.05	53.33
SiO_2	2.97	0.59	1.43	0.20	66.30

Table IV-1 XRF analysis of oxides in original ilmenite, compared with residual ilmenite after a 10 hour solubility test with 15 wt% HCl + 8 wt% HEDTA. Reprinted with permission from (Ibrahim et al. 2020).

Of the ions of interest, this acid system showed the ability to solubilize iron with more ease, compared to titanium. Iron oxides were solubilized at a 40% efficiency, while titanium oxides showed an efficiency of 15%. The reaction with titanium also reached an equilibrium faster, stabilizing after 2 hours, while the reaction with iron continued to about 4 hours.

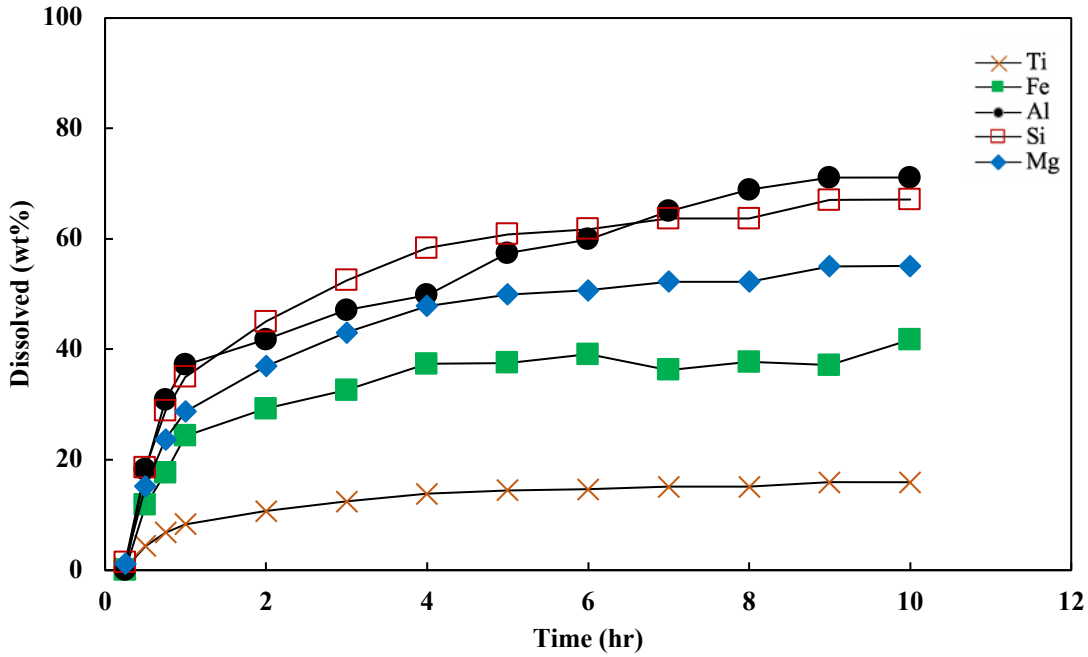

Figure IV-1 ICP analysis for effluent samples collected from ilmenite solubility testing with 15 wt% HCl + 8 wt% HEDTA.

Regular Mud Acid (12 wt% HCl + 3 wt% HF) System

The solubility test was repeated using a regular mud acid system. After reacting for 4 hours at 200 ˚F, the ilmenite sample weighed 4.13 g. The measured efficiency of dissolved ilmenite was 79.35%. **Table IV-2** shows the XRF analysis for the residual solids after the solubility test, where the mud acid dissolved 84% of the iron oxide and 77% of the titanium oxide.

	AFTER SOLUBILITY		
OXIDES	**Concentration** *wt%*	**Weight** *g*	**Solubility Efficiency** *%*
Fe_2O_3	45.92	1.90	81.41
TiO_2	52.97	2.19	74.62
Al_2O_3	0.00	0.00	100.00
MgO	0.41	0.02	84.32
SiO_2	0.70	0.03	95.13

Table IV-2 XRF analysis of oxides in the residual ilmenite after a 4-hour solubility test with regular mud acid. Reprinted with permission from (Ibrahim et al. 2020).

The solubility test with mud acid was repeated for a longer time period. Increasing the reaction time to 6 hours resulted only in a slight increase in the solubility of the ilmenite to 83.3%.

Organic Mud Acid Systems

Formic and lactic mud acid systems were also used to dissolve ilmenite. 200 g of a 9 wt% formic and 1 wt% HF acid system were added to 20 g of ilmenite for 6 hrs at 200°F. The total weight loss was equal to 2.06 g, and the solubility efficiency was calculated to be 10.3%. Similarly, 200 g of 9 wt% lactic and 1 wt% HF acids were added to 20 g ilmenite. The total weight loss in this case was 5.9 g, resulting in a solubility efficiency of 29.5%.

The presence of the fluoride ion (F^{-1}) provided by the mud acid improves the solubility of titanium and enhances the overall ilmenite solubility. As shown in **Table IV-3**, solubility increased from 40.1% to > 80% by the use of 3 wt% HF with 12 wt% HCl

compared to 15 wt% HCl alone. Technically, for field applications, 15 wt% HCl should be enough to break down the filter cake and provide easy flowback for the small-sized micronized ilmenite particles.

ACID SYSTEM	INITIAL SAMPLE	RESIDUAL SOLIDS	SOLUBILITY EFFICIENCY
	g	*g*	*%*
15 wt% HCl	20	11.9	40.1
15 wt% HCl + 8 wt% HEDTA	20	14	30
12 wt% HCl + 3 wt% HF *REGULAR MUD ACID*	20	4.13	79.35
9 wt% Formic Acid + 1 wt% HF *ORGANIC MUD ACID*	20	17.94	10.3
9 wt% Lactic Acid + 1 wt% HF *ORGANIC MUD ACID*	20	14.1	29.5

Table IV-3 A summary of solubility efficiency for conventional acid systems tested. Reprinted with permission from (Ibrahim et al. 2020).

Exploring Organic Acids

However, as mentioned above, the use of HCl in the field presents risk in terms of transportation and handling, corrosion of the tubulars, and precipitation of solids in the reservoir that may introduce more damage. As such, oxalic, glycolic, lactic, and citric acids were selected to evaluate solubility performance with micronized ilmenite. 1 wt% HCl was added to each system to aid the reactions and decrease the pH of the acid systems.

Due to uncertainty in reaction times between micronized ilmenite and organic acids, the following set of solubility tests were run for 24 hours each, while ICP-EOS was used to examine the concentration of titanium and iron ions dissolved in the acid systems and provide a better understanding of the reaction timeframes. All other parameters, including a temperature of 200˚F, a pressure of 1000 psi, and a stirring speed of 500 rpm, were held constant.

7.5 wt% Oxalic + 1 wt% Hydrochloric Acid System

After the 24-hour solubility test, filtered residual solids weighed 24.83 g. An increase in solid mass post-reaction indicates precipitation of an unknown compound. XRD results comparing the solid sample before and after solubility testing, shown in **Figure IV-2**, identifies some original peaks that disappear with acid exposure, while others emerge. Disappearing peaks are consistent with hematite, which exists at a concentration of 9.4% in the original micronized ilmenite sample. New peaks (**Figure IV-3**) were identified as ferrous oxalate, an inorganic compound with low water solubility. Nevertheless, the concentration of ilmenite identified in the original sample decreased by 18%. ICP-OES analysis, shown in **Figure IV-4**, reiterated this narrative, as the reaction showed a large concentration of iron in solution during the first couple of hours, which continued to decrease until the reaction equilibrated at around 17 hours.

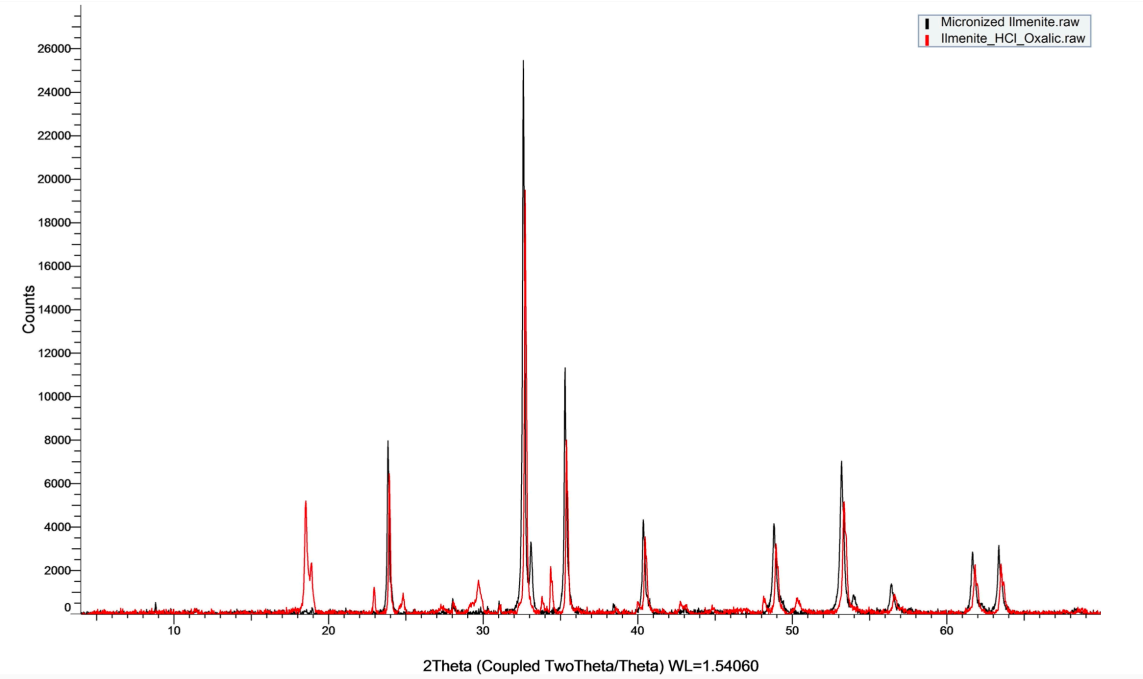

Figure IV-2 XRD analysis of a micronized ilmenite sample before and after exposure to a 7.5 wt% oxalic and 1 wt% HCl acid system for 24 hours.

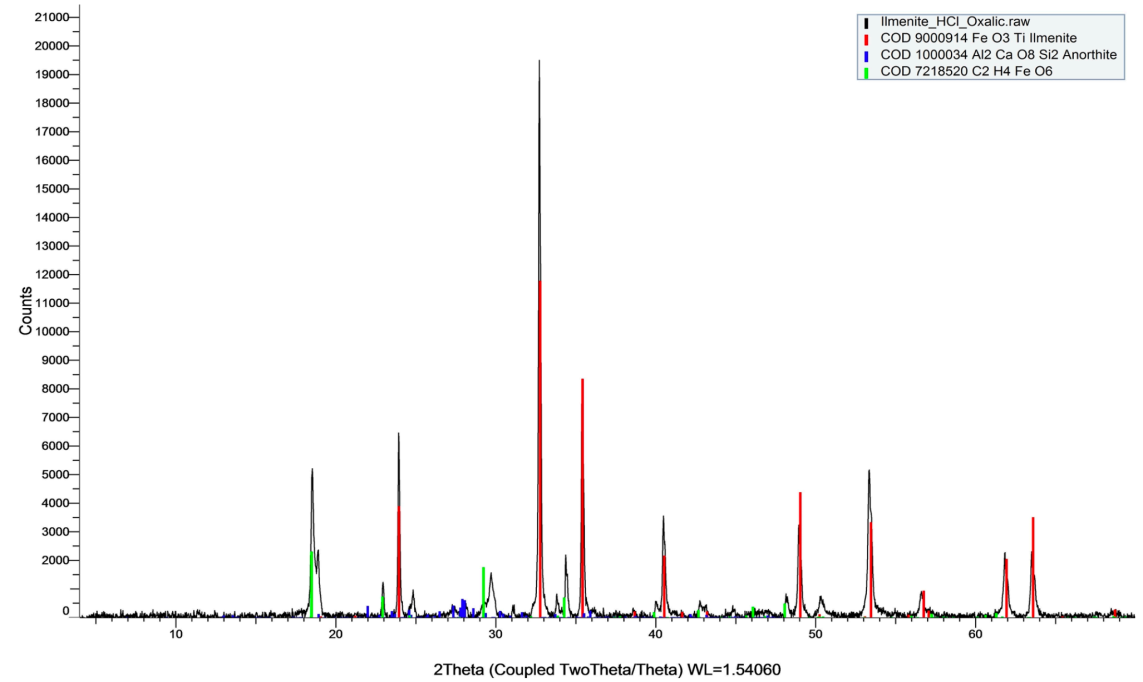

Figure IV-3 XRD analysis of a micronized ilmenite sample after exposure to a 7.5 wt% oxalic and 1 wt% HCl acid system for 24 hours.

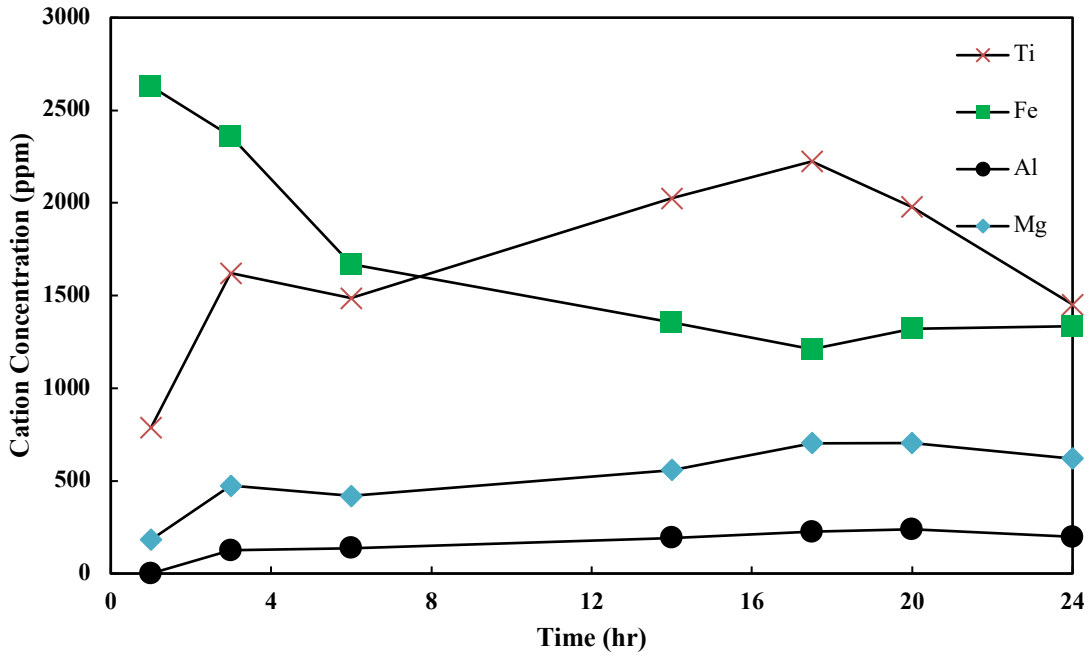

Figure IV-4 ICP analysis for effluent samples collected from ilmenite solubility testing with 7.5 wt% Oxalic + 1 wt% HCl acids.

7 wt% Glycolic + 1 wt% Hydrochloric Acid System

With the use of glycolic acid, the residual solids had a mass of 18.9 g, resulting in a solubility efficiency of 5.2%. XRD did not detect any minerals not previously present in the original ilmenite sample, indicating no precipitation of solids. ICP-OES results (**Figure IV-5**) indicated low solubility of titanium around 100 ppm that was constant throughout the duration of the test. Iron solubility, however, was much, and continuously increased to about 7500 ppm.

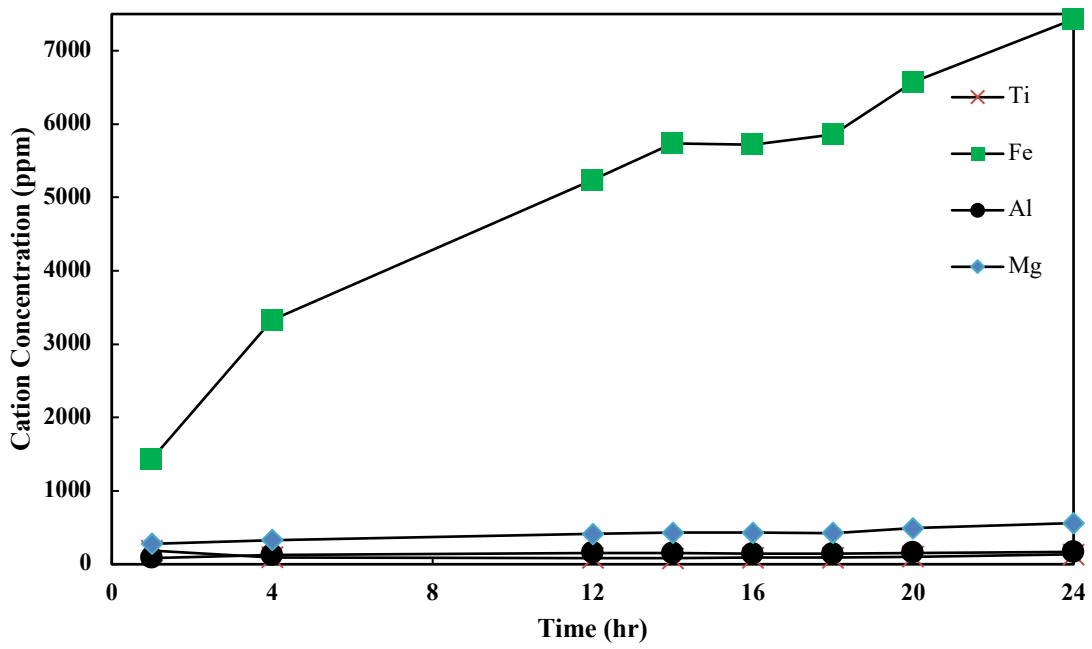

Figure IV-5 ICP analysis for effluent samples collected from ilmenite solubility testing with 7 wt% glycolic + 1 wt% HCl acids.

13 wt% Lactic + 1 wt% Hydrochloric Acid System

The lactic acid system further improved solubility to 9.8%, with residual micronized ilmenite solids weighing 18 g. Similar to the glycolic acid system, no solids precipitation was indicated by XRD testing, and the system was more effective at solubilizing iron relative to titanium, as is presented in **Figure IV-6**. Iron solubility reached a peak at approximately 20 hours.

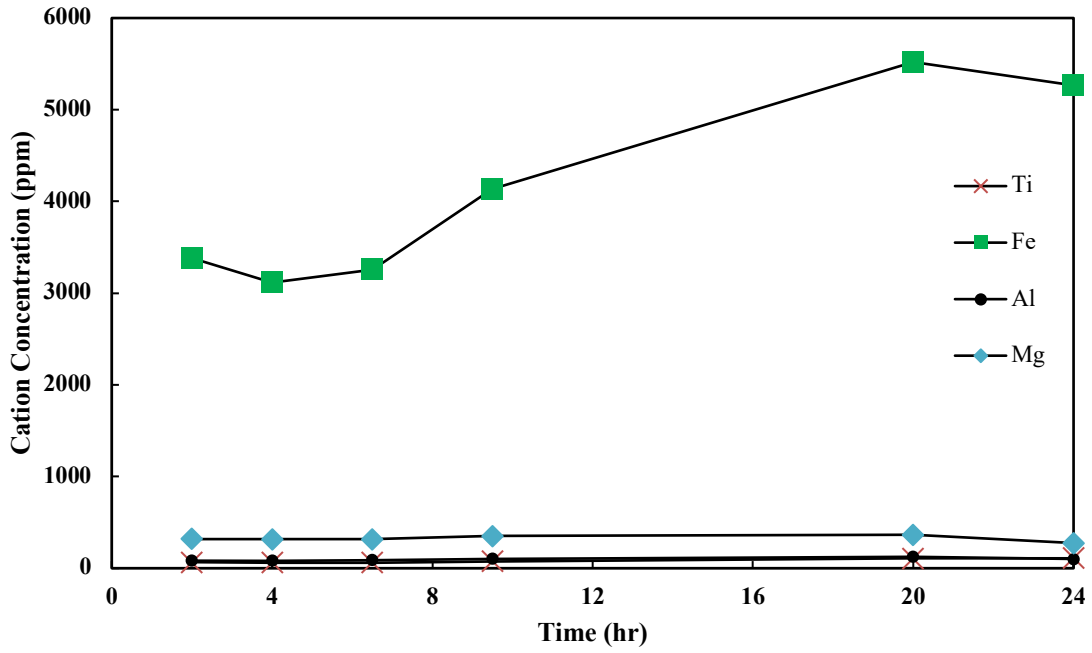

Figure IV-6 ICP analysis for effluent samples collected from ilmenite solubility testing with 13 wt% lactic + 1 wt% HCl acids.

11.6 wt% Citric + 1 wt% Hydrochloric Acid System

The solubility of micronized ilmenite increased incrementally with the use of a citric acid system. Residual solids weighing 17.7 g resulted in a solubility efficiency of 11.4%. No new minerals were detected by XRD testing; however, ICP-OES showed increased solubility of titanium, reaching upwards of 400 ppm, while maintaining high solubility of iron (**Figure IV-7**).

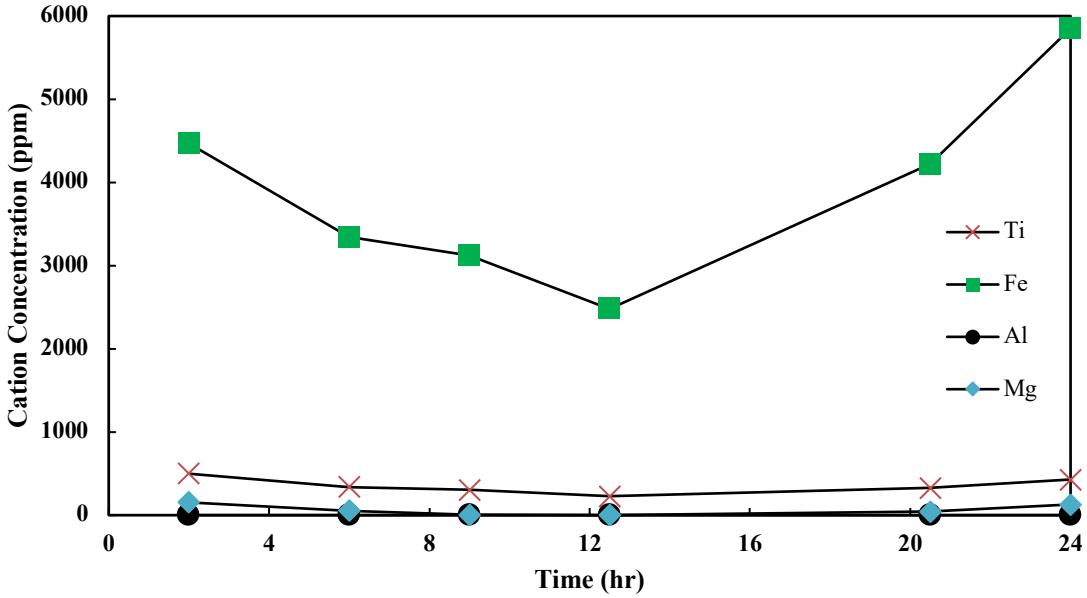

Figure IV-7 ICP analysis for effluent samples collected from ilmenite solubility testing with 11.6 wt% Citric + 1 wt% HCl acids.

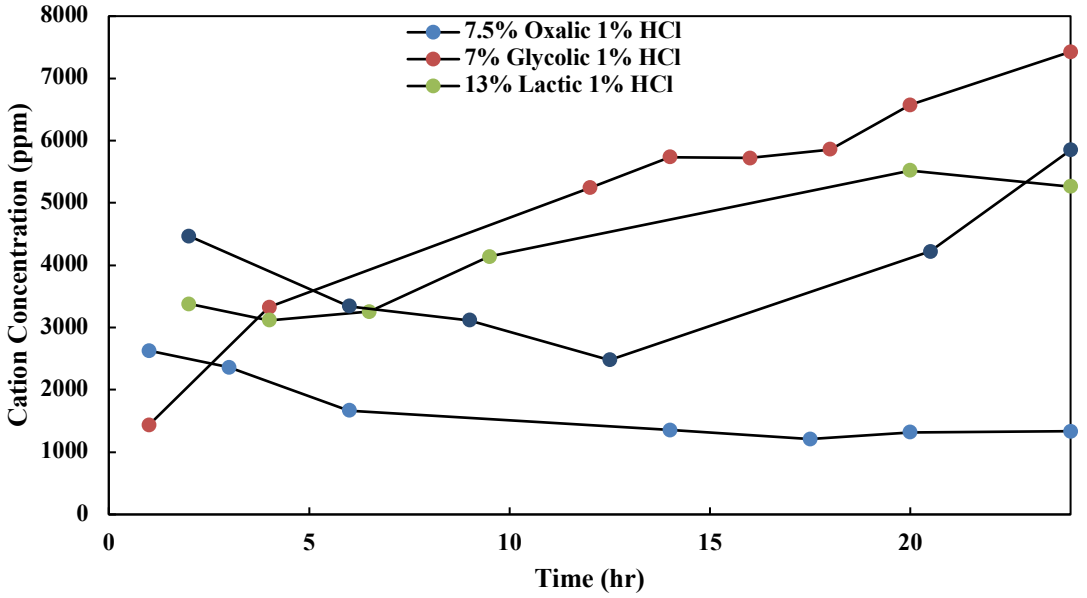

Figure IV-8 ICP analysis of iron concentrations in effluent samples collected from ilmenite solubility testing with organic acid systems.

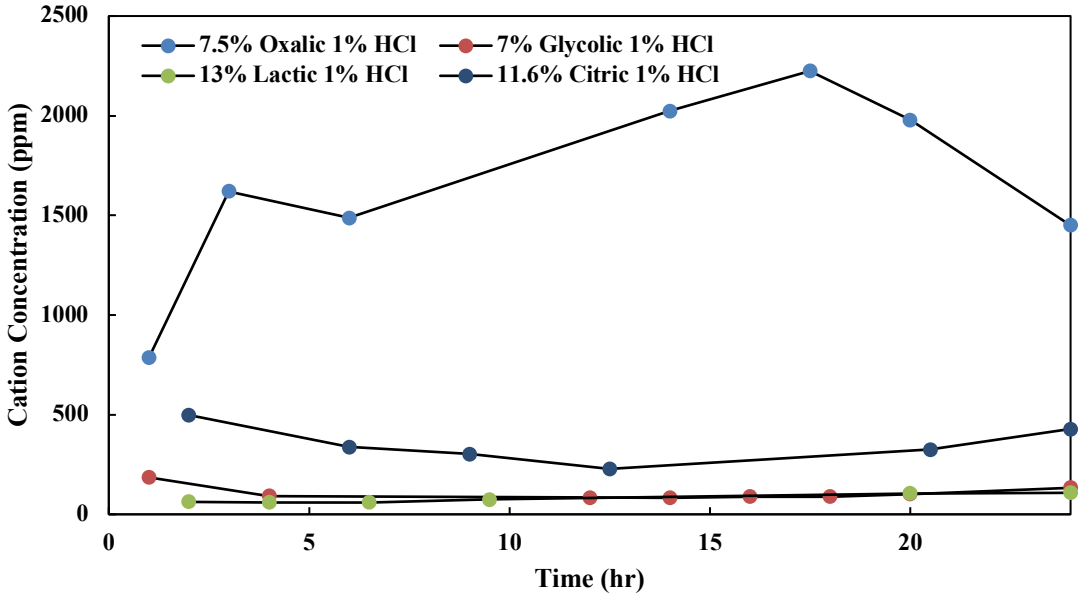

Figure IV-9 ICP analysis of titanium concentrations in effluent samples collected from ilmenite solubility testing with organic acid systems.

Figure IV-8 and **Figure IV-9** summarize the solubility of iron and titanium in the organic acid systems tested thus far as each reaction took place. The glycolic acid system was considerably more effective at solubilizing iron with time, while citric acid followed. As for titanium ions, they existed in solution in significantly higher concentrations when ilmenite reacted with the oxalic acid system. Citric acid, again, ranked second, with a larger difference in this case.

Solubility efficiencies of all organic acid systems tested as part of the initial study have been summarized in **Table IV-4** for reference.

ACID SYSTEM	INITIAL SAMPLE	RESIDUAL SOLIDS	SOLUBILITY EFFICIENCY
	g	*g*	*%*
7.5 wt% Oxalic + 1 wt% HCl	20	24.834	-24.2
7 wt% Glycolic + 1 wt% HCl	20	18.965	5.2
13 wt% Lactic + 1 wt% HCl	20	18.0317	9.8
11.6 wt% Citric + 1 wt% HCl	20	17.73	11.4

Table IV-4 A summary of solubility efficiencies for initial organic acid systems tested.

Following analysis of the results of the initial organic acid system solubility testing, it was decided to further examine the performance of oxalic acid, as it presented to be the most effective at solubilizing titanium. The concentration used was increased from 7.5 wt% to 20 wt%, and it was mixed with HCl and glycolic acids, both used to target the solubility of iron.

20 wt% Oxalic + 10 wt% Hydrochloric Acid System

The increased HCl concentration caused the concentration of iron in solution to jump from 2500 ppm to 25,000 ppm. The concentration of titanium in solution also increased tenfold with the larger oxalic acid concentration used during the first few hours (**Figure IV-10**). However, both concentrations dropped as the reaction continued. Residual solids showed a visible change in color from black to grey, as is shown in **Figure IV-11**. Multiple samples were collected and tested separately, leading to different mineralogical compositions (**Figure IV-12 and Figure IV-13**). XRD analysis explained the decrease as resulting from precipitation of both titanium oxide and ferrous oxide. An increase in the mass of the residual solids to 37.9 g further confirms this analysis.

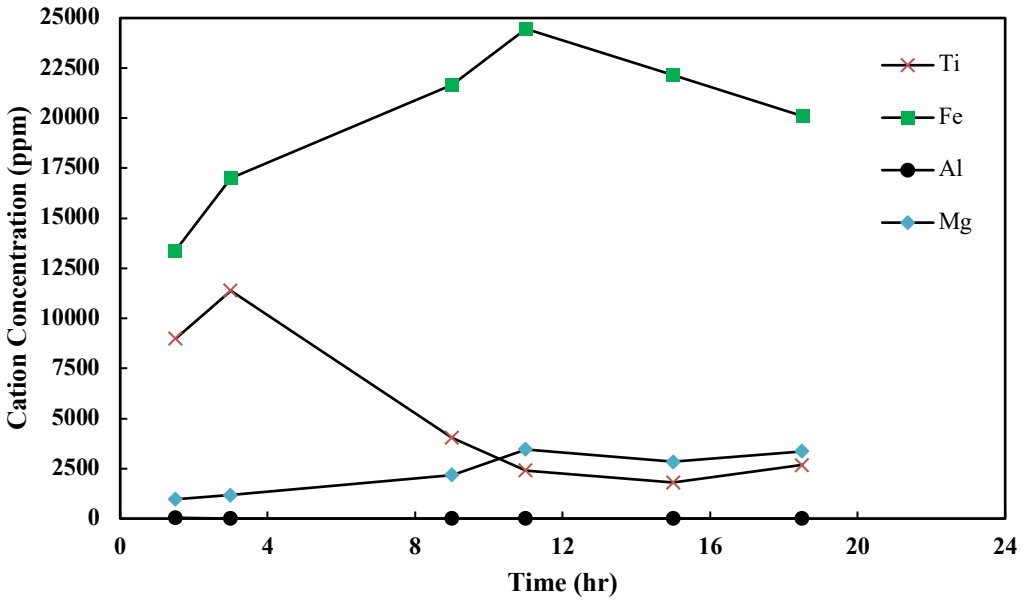

Figure IV-10 ICP analysis for effluent samples collected from ilmenite solubility testing with 20 wt% Oxalic + 10 wt% HCl acids.

Figure IV-11 Residual solids filtered and dried after exposure to 20 wt% Oxalic + 10 wt% HCl acids for 24 hours exhibited a color change due to solids precipitation.

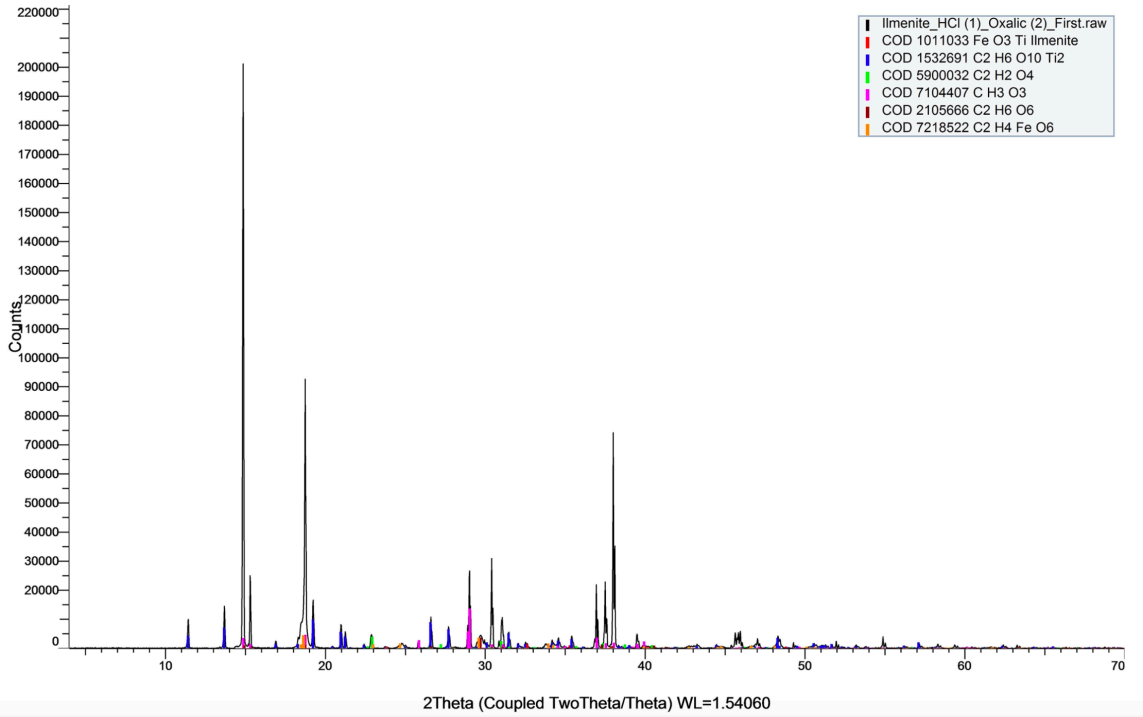

Figure IV-12 XRD analysis of the first micronized ilmenite sample after exposure to a 20 wt% oxalic and 10 wt% HCl acid system for 24 hours.

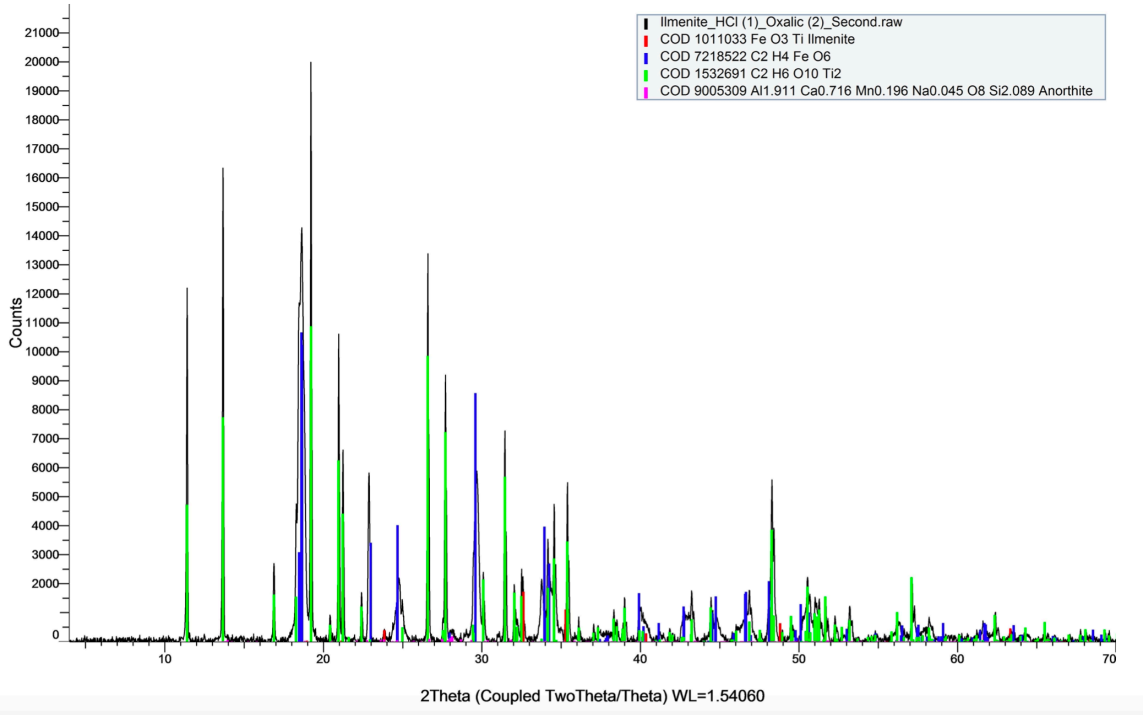

Figure IV-13 XRD analysis of the second micronized ilmenite sample after exposure to a 20 wt% oxalic and 10 wt% HCl acid system for 24 hours.

20 wt% Oxalic + 10 wt% Glycolic Acid System

Replacing HCl with glycolic acid resulted in a slightly more stable reaction, with a final concentration of 1955 and 11,575 ppm of iron and titanium in solution, respectively. ICP-OES results, plotted in **Figure IV-14**, showed a concentration increase in solution, which dropped as solids precipitated. XRD (**Figure IV-15**) showed that the hematite and part of the ilmenite minerals solubilized, causing solids precipitation of titanium and ferrous oxalates, with a residual solids mass increase of only 2.8 g, compared to 17.9 g when HCl was used.

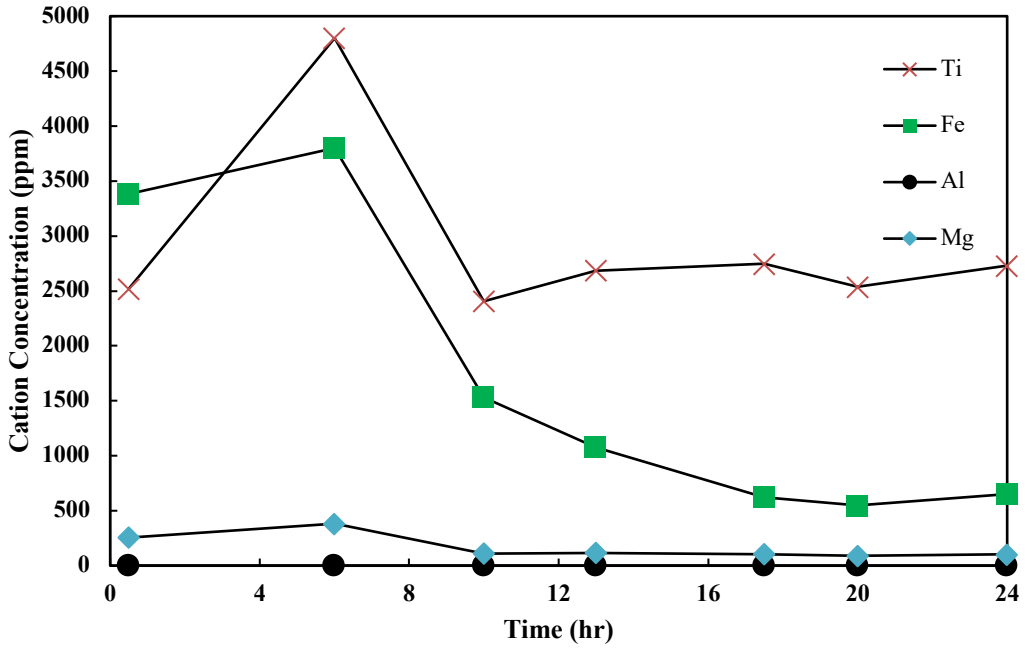

Figure IV-14 ICP analysis for effluent samples collected from ilmenite solubility testing with 20 wt% oxalic + 10 wt% glycolic acids.

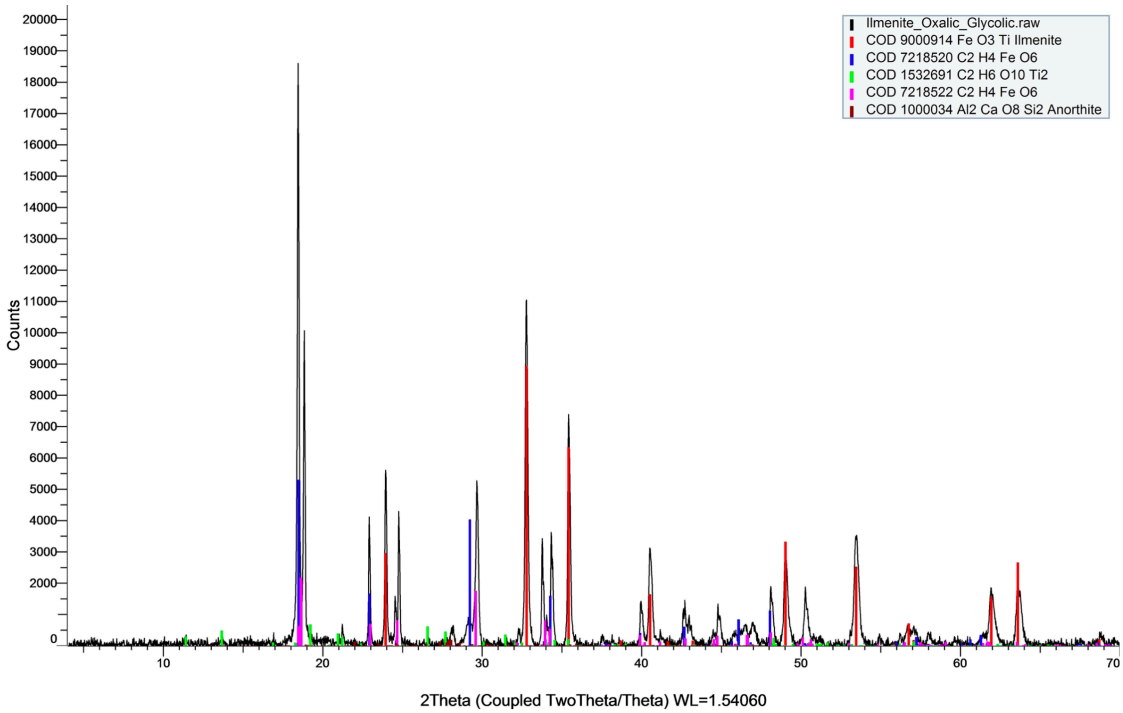

Figure IV-15 XRD analysis of a micronized ilmenite sample after exposure to a 20 wt% oxalic and 10 wt% glycolic acid system for 24 hours.

10 wt% Glycolic + 11.6 wt% Citric Acid System

With the solids precipitation issues related to the use of oxalic acid, the focus shifted towards combining glycolic acid with another that is able to solubilize titanium. From initial testing, this was identified as citric acid. The glycolic/citric acid system proved to perform better than those tested previously, as it exhibited a solubility efficiency of 23%. XRD did not detect any additional minerals, and concentrations of both titanium and iron in solution were at an acceptable range (**Figure IV-16**). Measured concentrations of iron and titanium in the filtered effluent spent acid sample were 9568 and 1104 ppm, respectively.

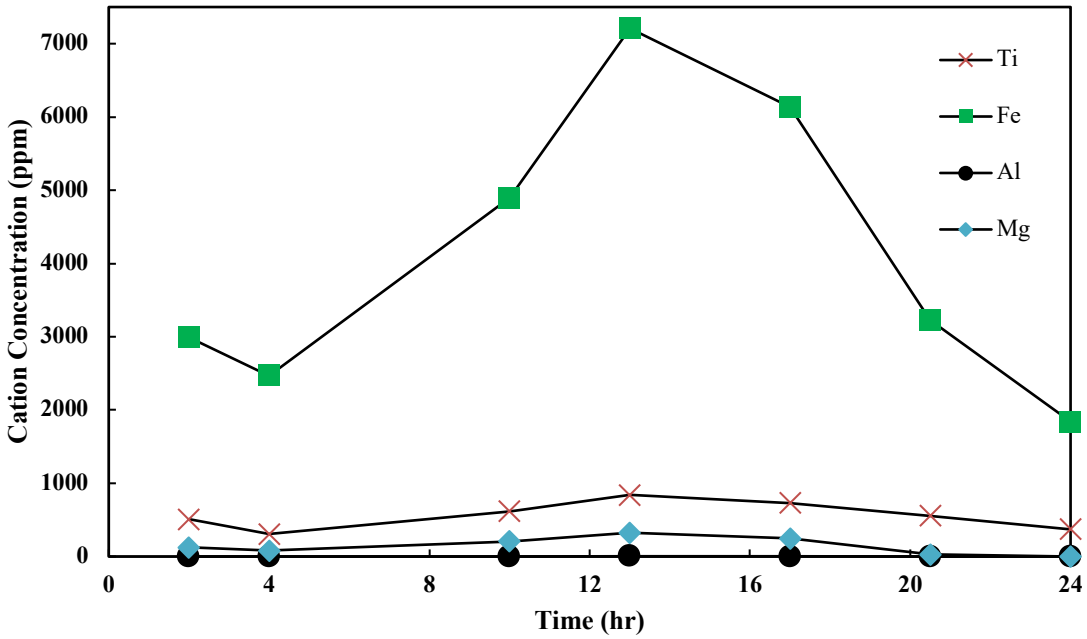

Figure IV-16 ICP analysis for effluent samples collected from ilmenite solubility testing with 10 wt% glycolic + 11.6 wt% citric acids.

ACID SYSTEM	INITIAL SAMPLE	RESIDUAL SOLIDS	SOLUBILITY EFFICIENCY
	g	*g*	*%*
20 wt% Oxalic + 10 wt% HCl	20	37.8765	-89.4
20 wt% Oxalic + 10 wt% Glycolic	20	22.7895	-13.9
10 wt% Glycolic + 11.6 wt% Citric	20	15.41	23.0

Table IV-5 A summary of solubility efficiencies for secondary organic acid systems tested.

Micronized Ilmenite-Based Drilling Fluid Filter Cake

The next step consists of evaluating the cleaning process for the filter cake created by HP/HT filtration of an oil-based drilling fluid system weighted with micronized

ilmenite. Again, solubility tests were conducted in an HP/HT reactor to examine the solubility of the created filter cake at 200˚F and 1,000 psi with an acid-to-solids weight ratio of 10:1.

Regular Mud Acid (12 wt% HCl 12+ 3 wt% HF) System

A solubility test was conducted using a regular mud acid system for 4 hours. **Figure IV-17** shows the scraped filter cake from the sandstone core after dynamic filtration. Mud acid was able to dissolve 87% of the created filter cake with some residue left on the medium-to-fine (5 µm) particle retention filter paper.

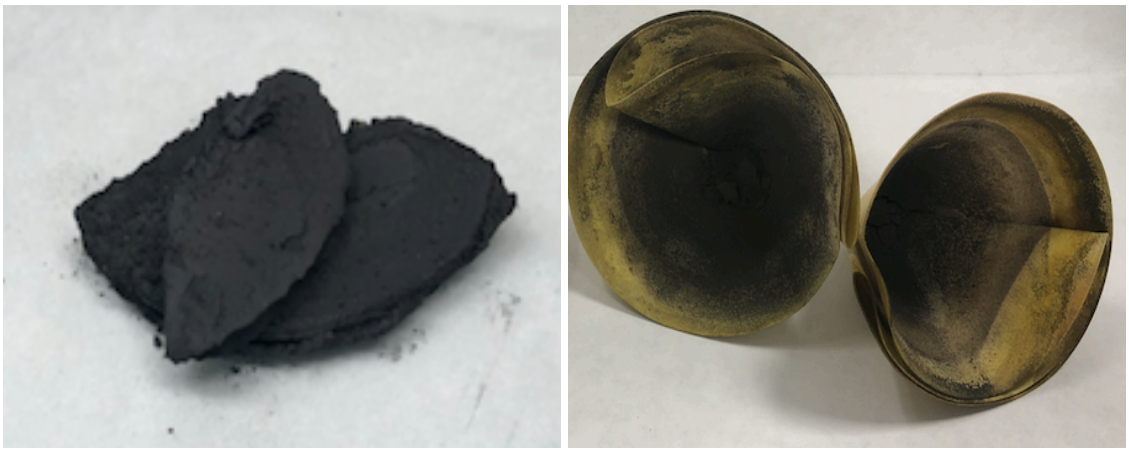

Figure IV-17 The filter cake used in the solubility test with regular mud acid (left) and the residue after the 4-hour solubility test collected on 5 µm filter paper (right). Reprinted with permission from (Ibrahim et al. 2020).

10 wt% Glycolic + 11.6 wt% Citric Acid System

After secondary organic acid system solubility testing, summarized in **Table IV-5**, the glycolic/citric organic acid system was able to better solubilize micronized ilmenite,

compared to other acid systems tested, it was selected for solubility testing on micronized ilmenite-weighted OBM filter cake. The filter cake was formed using a conventional filter press, and 20 g were used in solubility testing. **Figure IV-18** shows the filter cake used. After 24 hours of exposure to the citric/glycolic acid system, residual solids after filtering and drying weighed 14 g, resulting in a solubility efficiency of 29.9%, the highest achieved solubility in organic acid testing.

Figure IV-18 The filter cake used in the solubility test with the 10 wt% glycolic and 11.6 wt% citric acid system.

Although the solubility of the filter cake with this system is significantly lower than when using a regular mud acid, it is close to the solubility provided by a conventional 15 wt% HCl acid job used in the field. With all additional safety and transportation precautions required when dealing with stronger acids like HCl and HF, along with a decreased risk of corrosion, a system of organic acids with 30% solubility of micronized

ilmenite-weighted filter cake shows practical promise in reducing formation damage caused by micronized ilmenite.

CHAPTER V

CONCLUSIONS*

Field Cases

A drilling fluid system weighted with micronized ilmenite was used as a replacement for conventional OBM and water-based drilling fluids (WBM) to drill extended reach (ERD), horizontal drain holes through a cretaceous limestone reservoir. The field development plan was to maximize the horizontal lateral sections through the reservoir to 35,000 ft (1,067 m), in order to increase oil production by 50%. WBM and OBM were not able to reach the planned target due to increased ECD above the fracture initiation pressure, which induced significant drilling fluid losses. An inner phase of $CaBr_2$ was used in the OBM, with graded $CaCO_3$ as a bridging and weighting agent, to reduce ECD, but it still resulted in high drilling fluid losses, torque, and drag. The drilled wellbore length was less than 25,000 ft, indicating more wells will be needed to cover the target formation.

The micronized ilmenite fluid was prepared at a density of 1.29 SG and was used in the new wells. The plastic viscosity (PV) of the system, 15 cp, was half that of conventional, previously utilized fluid systems, causing the ECD (1.66 SG) to fall below equivalent mud weight (EMW) at fracture initiation condition (1.69 SG) at a pumping rate

---

* Part of this chapter is reprinted with permission from "Evaluation of Formation Damage of Oil-Based Drilling Fluids Weighted with Micronized Ilmenite or Micronized Barite" by Ibrahim, A. F., Al-Mujalhem, M. Q., Nasr-El-Din, H. A., and Al-Bagoury, M., 2020, *SPE Drilling & Completion*, Copyright 2020 by Society of Petroleum Engineers.

of 480 gpm. The high pumping rate (compared to 440 gpm in previous systems) increased the drilling rate by 25%. Additionally, the micronized ilmenite fluid had a lower friction factor of 0.10, compared to 0.2 in previous systems, which reduced torque and drag. The first well drilled with the micronized ilmenite fluid was able to reach a depth of 31,000 ft. Subsequent wells are now being drilled to 36,000 ft.

Performance Evaluation

Varied experimental work has been detailed in this study to evaluate formation damage resulting from the use of an ilmenite-weighted, oil-based drilling fluid system in comparison with micronized barite-weighted drilling fluid systems. The following are the main conclusions:

1. Micronized-weighted oil-based drilling fluids exhibit improved dynamic filtration capabilities compared to micronized-barite weighted fluids with the same average particle size.
2. Using micronized ilmenite as a weighing material instead of micronized barite enhanced the rheological properties of the fluid by decreasing viscosity at low and high shear rates, with low fluid leak-off fluid through the cores. More specifically, a decrease of up to 30% in viscosity parameters was observed.
3. The use of a mud loop/coreflood apparatus to evaluate filter cake buildup and removal during fluid circulation allows for the understanding of solid particle bridging and flowback capabilities, which more closely resemble field conditions.
4. No formation damage was observed when using micronized ilmenite-weighted drilling fluids in the case of both low and medium permeability sandstone.

Compared to micronized barite-weighted drilling fluids, testing showed an increase of up to 64% in permeability retention.

5. Computed tomography scanning confirmed no formation damage was created by micronized ilmenite-weighted fluids, while micronized barite-weighted fluids showed a depth of solids invasion of up to 2 inches.

Micronized ilmenite-based drilling fluids performed better than micronized barite-based drilling fluids, causing less formation damage while reducing torque and drag forces during drilling operations.

Damage Removal

Extensive experimental work was completed to evaluate the solubility of micronized ilmenite and micronized-ilmenite weighted OBM filter cake. Primary conclusions from this work include:

1. A regular mud acid system was the most promising in removal of micronized ilmenite and micronized ilmenite-based drilling fluids, with solubility efficiencies of 79% and 87%, respectively.
2. Lactic acid mixed with HF as organic mud acid showed better solubility performance, compared to lactic acid, at a solubility efficiency of 29.5% at 10 hours.
3. As hypothesized, organic acids did not perform as well in solubility testing, compared to only HCl or mud acid.

4. X-ray diffraction, used as a secondary method to analyze residual solids and determine precipitation occurrences, revealed the mineralogical composition of solid precipitates resulting from chemical reactions with the organic acids.
5. All solubility tests with acid systems containing oxalic acid precipitated a grey solid, identified by XRD as ferrous oxalate, resulting in a final mass of solids greater than initially added. As such, the weight method for solubility efficiency measurement is not entirely reliable.
6. The HCl/glycolic initial organic acid system was the most promising in terms of iron ion solubility, above 7400 ppm in 24 hours. Similarly, the HCl/citric system was the most promising in solubilizing titanium ions, with more than 400 ppm in solution.
7. Glycolic and citric acids were combined at concentrations identified as optimal in the literature. The solubility of ilmenite was highest in this organic acid system, with solubility efficiencies of 23% and 30%, respectively, in micronized ilmenite and micronized ilmenite-weighted OBM filter cake.

Recommendations

This work focused on providing a more extensive evaluation of micronized ilmenite as a weighting agent for invert emulsion drilling fluids. Performance parameters were compared to those of a fluid system weighted with micronized barite with s similar particle size distribution. Damage was investigated specifically in relation to filter cake formation on/in sandstone formations of varying permeabilities at a temperature of 250˚F.

A closely packed filter cake with low fluid loss resulted in little to no damage in the cores, suggesting that careful formulation of micronized ilmenite fluids will provide superior performance and decrease the need for damage removal following drilling. The case studies shared further reiterate the effectiveness and feasibility, economic and technical, of replacing current weighting materials with micronized ilmenite.

Furthermore, extensive solubility testing of micronized ilmenite provides a better idea of potential remediation techniques. Regular mud acid shows great promise as a clean-up fluid for micronized ilmenite fluids. Additionally, the study of micronized ilmenite solubility in organic acids provides a framework for more extensive testing.

Future work is recommended for further studies on the performance and efficacy of micronized ilmenite as a weighting material in invert emulsion drilling fluid systems, including:

1. Altering the specified testing conditions for solubility testing in organic acid systems, such as acid-to-ilmenite-solids ratio, reaction temperature, and/or stirring speed.
2. Considering additional acids and combinations of acid systems to solubilize iron and titanium ions.
3. Investigating reaction kinetics between micronized ilmenite and the various acid systems to better understand the process of mineral alteration and identify optimal acid concentrations and reaction times.

4. Modifying and expanding mudloop testing procedures to further simulate clean-up conditions by circulating effective acid systems after drilling fluid circulation and filter cake formation.

REFERENCES

Al Moajil, A., Nasr-El-Din, H. A., Al-Yami, A. et al. 2008. Removal of Filter Cake Formed by Manganese Tetraoxide Based-Drilling Fluids. Paper presented at the SPE International Symposium and Exhibition on Formation Damage Control, Lafayette, Louisiana, USA, 13-15 February. SPE-112450-MS. https://doi.org/10.2118/112450-MS.

Al Moajil, A. 2010. *Removal of Filter Cake Generated by Manganese Tetraoxide Water-Based Drilling Fluids.*MS Thesis, Texas A&M University, College Station, Texas (August 2010).

Al Moajil, A. and Nasr-El-Din, H. A. 2014. Removal of Manganese Tetraoxide Filter Cake Using a Combination of HCl and Organic Acid. *J Can Pet Technol* **53** (02): 122-130. https://doi.org/10.2118/165551-PA.

Al-Bagoury, M. and Steele, C. D. 2012. A New, Alternative Weight Material for Drilling Fluids. Paper presented at the IADC/SPE Drilling Conference and Exhibition, San Diego, California, USA, 6-8 March. SPE-151331-MS. https://doi.org/10.2118/151331-MS.

Al-Bagoury, M. 2014. Micronized Ilmenite – A Non-damaging & Non-sagging New Weight Material for Drilling Fluids. Paper presented at the SPE Bergen One Day Seminar, Bergen, Norway, 2 April. SPE-169182-MS. https://doi.org/10.2118/169182-MS.

Al-Harbi, B. G., Al-Dahlan, M. N., Al-Khaldi, M. H. et al. 2013. Evaluation of Organic-Hydrofluoric Acid Mixtures for Sandstone Acidizing. Paper presented at the International Petroleum Technology Conference, Beijing, China, 26-28 March. IPTC-16967-MS. https://doi.org/10.2523/IPTC-16967-MS.

Al-Yami, A. S., Nasr-El-Din, H. A., Al-Shafei, M. et al. 2010. Impact of Water-Based Drilling-In Fluids on Solids Invasion and Damage Characteristics. *SPE Prod & Oper* **25** (01): 40-49. https://doi.org/10.2118/117162-PA.

Aldea, C., Growcock, F. B., Lee, L. J. et al. 2001. Prevention of Dynamic Sag in Deepwater Invert Emulsion Fluids. Paper presented at the AADE National Drilling Conference, Houston, TX, USA, 27-29 March. AADE-01-NC-HO-51.

Alkhalaf, S., Alawami, M., Wagle, V. et al. 2019. Less Damaging Drilling Fluids: Development and Lab Testing. Paper presented at the International Petroleum Technology Conference, Beijing, China, 26-28 March. IPTC-19205-MS. https://doi.org/10.2523/IPTC-19205-MS.

Amaefule, J. O., Kersey, D. G., Norman, D. L. et al. 1988. Advances in Formation Damage Assessment and Control Strategies. Paper presented at the Annual Technical Meeting of the Petroleum Society of CIM, Calgary, Alberta, Canada, 12-16 June. PETSOC-88-39-65. https://doi.org/10.2118/88-39-65.

Amanullah, M. and Tan, C. P. 2000. A Non-Destructive Method of Cake Thickness Measurement. Paper presented at the SPE Asia Pacific Oil and Gas Conference and Exhibition, Brisbane, Australia, 16-18 October. SPE-64517-MS. https://doi.org/10.2118/64517-MS.

Bageri, B. S., Mahmoud, M. A., Shawabkeh, R. A. et al. 2017. Evaluation of Barium Sulfate (Barium) Solubility Using Different Chelating Agents at a High Temperature. *Pet Sci Technol* **7** (01): 42-56. https://doi.org/10.22078/JPST.2017.707.

Bennet, R. B. 1984. New Drilling Fluid Technology - Mineral Oil Mud. *J Pet Technol* **36** (06): 975-981. https://doi.org/10.2118/11355-PA.

Bennion, B. 1999. Formation Damage - The Impairment of the Invisible, By the Inevitable And Uncontrollable, Resulting In an Indeterminate Reduction of the Unquantifiable! *J Can Pet Technol* **38** (02): 11-17. https://doi.org/10.2118/99-02-DA.

Bennion, D. B. and Thomas, F. B. 1994. Underbalanced Drilling of Horizontal Wells: Does It Really Eliminate Formation Damage? Paper presented at the SPE Formation Damage Control Symposium, Lafayette, Louisiana, USA, 7-10 February. SPE-27352-MS. https://doi.org/10.2118/27352-MS.

Bishop, S. R. 1997. The Experimental Investigation of Formation Damage Due to the Induced Flocculation of Clays Within a Sandstone Pore Structure by a High Salinity Brine. Paper presented at the SPE European Formation Damage Conference. The Hague, Netherlands, 2-3 June. SPE-38156-MS. https://doi.org/10.2118/38156-MS.

Blattel, S. R. and Rupert, J. P. 1982. The Effect of Weight Material Type on Rate of Penetration Using Dispersed and Non-Dispersed Water-Base Muds. Paper presented at the SPE Annual Technical Conference and Exhibition, New Orleans,

Louisiana, USA, 26-29 September. SPE-10961-MS. https://doi.org/10.2118/10961-MS.

Bleier, R. 1990. Selecting a Drilling Fluid. *J Pet Technol* **42** (07): 832-834. https://doi.org/10.2118/20986-PA.

Blomberg, N. E. and Melberg, B. 1984. Evaluation of Ilmenite as Weight Material in Drilling Fluids. *J Pet Technol* **36** (06): 969-974. https://doi.org/10.2118/11085-PA.

Bruton, J. R., Bacho, J. P., and Newcaster, J. 2006. The Future of Drilling-Grade Barite Weight Material - A Case for a Substitute Specification. Paper presented at the SPE Annual Technical Conference and Exhibition, San Antonio, Texas, USA, 24-27 September. SPE-103135-MS. https://doi.org/10.2118/103135-MS.

Calçada, L. A., Scheid, C. M., de Araújo, C. A. O. et al. 2011. Analysis of Dynamic and Static Filtration and Determination of Mud Cake Parameters. *Brazilian Journal of Petroleum and Gas* **5**(03): 159-170. https://doi.org/10.5419/bjpg2011-0016.

Dill, R. W. and Keeney, B. R. 1978. Optimizing HCl-Formic Acid Mixtures for High Temperature Stimulation. Paper presented at the SPE Annual Fall Technical Conference and Exhibition, Houston, Texas, USA, 1-3 October. SPE7567-MS. https://doi.org/10.2118/7567-MS.

Elkatatny, S., Mahmoud, M. A., and Nasr-El-Din, H. A. 2012a. Characterization of Filter Cake Generated by Water-Based Drilling Fluids Using CT Scan. *SPE Drill & Compl* **27** (02): 282-293. https://doi.org/10.2118/144098-PA.

Elkatatny, S. M., Nasr-El-Din, H. A., and Al-Bagoury, M. 2012b. Evaluation of Ilmenite as Weighting Material in Water-Based Drilling Fluids for HP/HT Applications. Paper presented at the SPE Kuwait International Petroleum Conference and Exhibition, Kuwait City, Kuwait, 10-12 December. SPE-163377-MS. https://doi.org/10.2118/163377-MS.

Elkatatny, S. M., Nasr-El-Din, H. A., and Al-Bagoury, M. 2013a. Properties of Ilmenite Water-Based Drilling Fluids for HPHT Applications. Paper presented at the International Petroleum Technology Conference, Beijing, China, 26-28 March. IPTC-16983-MS. https://doi.org/10.2523/IPTC-16983-MS.

Elkatatny, S. M., Nasr-El-Din, H. A., and Al-Bagoury, M. 2013b. Using Hydrochloric Acid to Remove Ilmenite Water-Based Filter Cake in HPHT Applications. Paper presented at the SPE European Formation Damage Conference and Exhibition, Noordwijk, The Netherlands, 5-7 June. SPE-165181-MS. https://doi.org/10.2118/165181-MS.

Elkatatny, S. M., Al Moajil, A. M., and Nasr-El-Din, H. A. 2013c. Filter Cake Cleanup Using HCl/Glycolic Acid System. Paper presented at the SPE Middle East Oil and Gas Show and Conference, Manama, Bahrain, 10-13 March. SPE-164452-MS. https://doi.org/10.2118/164452-MS.

Fattah, K. A. and Lashin, A. 2016. Investigation of Mud Density and Weighting Materials Effect on Drilling Fluid Filter Cake Properties and Formation Damage. *Journal of African Earth Sciences* **117** (01): 345-357. https://doi.org/10.1016/j.jafrearsci.2016.02.003.

Fisk, J. V. and Jamison, D. E. 1989. Physical Properties of Drilling Fluids at High Temperatures and Pressures. *SPE Drill Eng* **4** (04): 341-346. https://doi.org/10.2118/17200-PA.

Fleming, N., Moldrhein, E., Teigland, E. et al. 2020. Systematic Approach to Well Productivity Evaluation to Determine the Significance of Formation Damage for Walls Drilled in a Depleted Reservoir Without Bridging Particles: Oseberg Main Case History. *SPE Prod & Oper* **35** (03): 681-690. https://doi.org/10.2118/199266-PA.

Fouda, M. F. R., Amin, R. S., Saleh, H. I. et al. 2010. Preparation and Characterization of Nanosized Titania Prepared from Beach Black Sands Broad on the Mediterranean Sea Coast in Egypt via Reaction with Acids. *Aust. J. Basic Appl. Sci.* **4** (10): 4540-4553.

Fjogstad, A., Saasen, A., Hagen, R. et al. 2000. Field Trial of Alternative Weight Material with Improved Occupational Hygiene and Environmental Performance. Paper presented at the SPE International Conference on Health, Safety and Environment in Oil and Gas Exploration and Production, Stavanger, Norway, 26-28 Jun. SPE-61042-MS. https://doi.org/10.2118/61042-MS.

Fjogstad, A., Tanche-Larsen, P., Løkken, M. et al. 2002. It's Not Your Grandfather's Ilmenite. Paper presented at the AADE Technology Conference "Drilling & Completion Fluids and Waste Management", Houston, Texas, USA, 2-3 April. AADE-02-DFWM-HO-40.

Haaland, E., Pettersen, G., and Tuntland, O. B. 1976. Testing of Iron Oxides as Weight Materials for Drilling Fluids. SPE-6218-MS. https://doi.org/10.2118/6218-MS.

Han, K. N., Rubcumintara, T., and Fuerstenau, M. C. 1987. Leaching Behavior of Ilmenite with Sulfuric Acid. *Metall Mater Trans B*. **18**: 325-330. https://doi.org/10.1007/BF02656150.

Hanson, P. M., Trigg Jr., T. K., Rachal, G. et al. 1990. Investigation of Barite "Sag" in eighted Drilling Fluids in Highly Deviated Well. Paper presented at the SPE Annual Technical Conference and Exhibition, New Orleans, Louisiana, USA, 23-26 September. SPE-20423-MS. https://doi.org/10.2118/20423-MS.

Herzig, J. P, Leclerc, D. M., and Goff, P. Le. 1970. Flow of Suspensions Through Porous Media – Application to Deep Filtration. *Ind. Eng. Chem.* **62** (05): 8-35. https://doi.org/10.1021/ie50725a003.

Hoberock, L. L. and Bratcher, G. J. 1998. Dynamic Differential Pressure Effects on Drilling of Permeable Formations. *ASME J. Energy Resour. Technol.* **120** (02): 118-123. https://doi.org/10.1115/1.2795021.

Ibrahim, A. F., Nasr-El-Din, H. A., Rabie, A. et al. 2018. A New Friction-Reducing Agent for Slickwater-Fracturing Treatments. *SPE Prod & Oper* **33** (03): 583–595. https://doi.org/10.2118/180245-PA.

Ibrahim, A. F., Al-Mujalhem, M. Q., Nasr-El-Din, H. A. et al. 2020. Evaluation of Formation Damage of Oil-Based Drilling Fluids Weighted with Micronized Ilmenite or Micronized Barite. *SPE Drill & Compl* **35** (03): 402-413. https://doi.org/10.2118/200482-PA.

Ismail, A. R., Peden, J. M., and Arshad, A. M. 1994. The Effect of Solids Concentration and Formation Characteristics on Formation Damage and Permeability Recovery. Paper presented at the SPE Asia Pacific Oil and Gas Conference, Melbourne, Australia, 7-10 November. SPE-28762-MS. https://doi.org/10.2118/28762-MS.

Ismail, I. and Murugesu, T. S. 2005. A Study of Formation Damage Caused by Oil-Based Mud in Dynamic Condition. *Jurnal Teknologi* **43** (F): 85-94. https://doi.org/10.11113/jt.v43.788.

Ivan, C., Al Katheeri, Y. S., Reichle, M. et al. 2018. The Evolution of the Non-Damaging Fluids Design and Implementation Offshore Abu Dhabi. Paper presented at the Abu Dhabi International Petroleum Exhibition and Conference, Abu Dhabi, United Arab Emirates, 12-15 November. SPE-192735-MS. https://doi.org/10.2118/192735-MS.

Jonglertjunya, W. and Rubcumintara, T. 2012. Titanium and Iron Dissolutions from Ilmenite by Acid Leaching and Microbiological Oxidation Techniques. *Asia-Pac J Chem Eng* **8**: 323-330. https://doi.org/10.1002/apj.1663.

Khodja, M., Khodja-Saber, M., Canselier, J. P. et al. 2010. Drilling Fluid Technology: Performances and Environmental Considerations. In *Products and Services; from R&D to final Solution*, ed. I. Fuerstner, Chap. 13, 227-256. Rijeka: InTech.

Lakatos, I., Lakatos-Szabo, J., and Kosztin, B. 2002. Optimization of Barite Dissolvers by Organic Acids and pH Regulation. Paper presented at the SPE International Symposium on Oilfield Scale, Aberdeen, United Kingdom, 30-31 January. SPE-74667-MS. https://doi.org/10.2118/74667-MS.

Liu, X. and Civan, F. 1995. Formation Damage by Fines Migration Including Effects of Filter Cake, Pore Compressibility, and Non-Darcy Flow – A Modeling Approach to Scaling from Core to Field. Paper presented at the SPE International Symposium on Oilfield Chemistry, San Antonio, Texas, USA, 14-17 February. SPE-28980-MS. https://doi.org/10.2118/28980-MS.

Liu, X. and Civan, F. 1996. Formation Damage and Filter Cake Buildup in Laboratory Core Tests: Modeling and Model-Assisted Analysis. *SPE Form Eval* **11** (01): 26-30. https://doi.org/10.2118/25215-PA.

Mahmoud, O. and Nasr-El-Din, H. 2018. Formation Damage Assessment and Filter Cake Characterization of NPs/Ca-Bentonite Fluids for Drilling Harsh Environments Using Computed-Tomography Scan. Paper presented at the SPE Trinidad and Tobago Section Energy Resources Conference, Port of Spain, Trinidad and Tobago, 25-26 June. SPE-191155-MS. https://doi.org/10.2118/191155-MS.

Massam, J., Popplestone, A., and Burn, A. 2004. A Unique Technical Solution to Barite Sag in Drilling Fluids. Paper presented at the AADE Drilling Fluids Conference, Houston, Texas, USA, 6-7 April. AADE-04-DF-HO-21.

Mohamed, A. K., Elkatatny, M. A., Mahmoud, M. A. et al. 2017. The Evaluation of Micronized Barite As a Weighting Material for Completing HPHT Wells. Paper presented at the SPE Middle East Oil and Gas Show and Conference, Manama, Bahrain, 6-9 March. SPE-183768-MS. https://doi.org/10.2118/183768-MS.

Mohamed, R. S., Rabie, A. I., and Nasr-El-Din, H. A. 2015. A New Technique to Increase the Performance of Organic Acids to Stimulate Carbonate Reservoirs at

High Acid Concentrations. Paper presented at the SPE Kuwait Oil and Gas Show and Conference, Mishref, Kuwait, 11-14 October. SPE-175192-MS. https://doi.org/10.2118/175192-MS.

Nabivanets, B. I. and Kudritskaya, L. N. 1967. A Study of the Polymerisation of Titanium(IV) in Hydrochloric Acid Solutions. *Russ J Inorg* **12** (05): 616.

Nasr-El-Din, H. A., Al-Mutairi, S. H., Al-Hajji, H. H. et al. 2004. Evaluation of a New Barite Dissolver: Lab Studies. Paper presented at the SPE International Symposium and Exhibition on Formation Damage Control, Lafayette, Louisiana, USA, 18-20 February. SPE-86501-MS. https://doi.org/10.2118/86501-MS.

Olanipekun, E. O. 1999. A Kinetic Study of the Leaching of a Nigerian Ilmenite Ore by Hydrochloric Acid. *Hydrometallurgy* **53** (01): 1-10. https://doi.org/10.1016/S0304-386X(99)00028-6.

Omidi, M. H., Nuri, O. S., and Tavakoli, H. 2018. Optimization of Ilmenite Dissolution by Synergistic Effect of Oxalic Acid and Hydrochloric Acid for Preparing Synthetic Rutile. *International Journal of Nonferrous Metallurgy* **7** (03): 25-38. https://doi.org/10.4236/ijnm.2018.73003.

Patton, J. T. and Phelan, P. F. 1985 Well Damage Hazards Associated with Conventional Completion Fluids. Paper presented at the SPE Production Operations Symposium, Oklahoma City, Oklahoma, USA, 10-12 March. SPE-13800-MS. http://doi.org/10.2118/13800-MS.

Putnis, A., Putnis, C. V., and Paul, J. M. 1995. The Efficiency of a DTPA-Based Solvent in the Dissolution of Barium Sulfate Scale Deposits. Paper presented at the SPE

International Symposium on Oilfield Chemistry, San Antonio, Texas, USA, 14-17 February. SPE-29094-MS. https://doi.org/10.2118/29094-MS.

Rae, P., Di Lullo, G., and bte Ahmad, A. 2001. Towards Environmentally-Friendly Additives for Well Completion and Stimulation Operations. Paper presented at the SPE Asia Pacific Oil and Gas Conference, Jakarta, Indonesia, 17-19 April. SPE-68651-MS. https://doi.org/10.2118/68651-MS.

Reed, M. G. 1989. Formation Damage Prevention During Drilling and Completion. Paper presented at the SPE Centennial Symposium at New Mexico Tech, Socorro, New Mexico, 16-19 October. SPE-20149-MS. https://doi.org/10.2118/20149-MS.

Saasen, A., Hoset, H., Rostad, E. J. et al. 2001. Application of Ilmenite as Weight Material in Water Based and Oil Based Drilling Fluids. Paper presented at the SPE Annual Technical Conference and Exhibition, New Orleans, Louisiana, USA, 30 September – 3 October. SPE-71401-MS. https://doi.org/10.2118/71401-MS.

Salehi, S., Ghalambor, A., Saleh, F. K. et al. Study of Filtrate and Mud Cake Characterization in HPHT: Implications for Formation Damage Control. Paper presented at the SPE European Formation Damage Conference and Exhibition, Budapest, Hungary, 3-5 June. SPE-174273-MS. http://doi.org/10.2118/174273-MS.

Scheid, C. M., Calcada, L. A., Araujo, C. A. O., Waldmann, A. T. A. et al. 2010. A Theoretical and Experimental Analysis of Dynamic Filtration in Drilling Operations. Paper presented at the SPE International Symposium and Exhibition

on Formation Damage Control, Lafayette, Louisiana, USA, 10-12 February. SPE-128035-MS. https://doi.org/10.2118/128035-MS.

Sinha, H. N. 1984. Hydrochloric Acid Leaching of Ilmenite. *Proc*., Australasian Intsitute of Mining and Metallurgy Symposium on Extractive Metallurgy, Melbourne, Australia, November, 163-168.

Smith, C. F. and Hendrickson, A. R. 1965. Hydrofluoric Acid Stimulation of Sandstone Reservoirs. *J Pet Technol* **17** (02): 215-222. https://doi.org/10.2118/980-PA.

Su, J. 2016. *Characterization and Removal of Filter Cake Generated By Ilmenite Water-Based Drilling Fluids*. MS Thesis, Texas A&M University, College Station, Texas (August 2016).

Taugbøl, K., Fimreite, G., Prebensen, O. I. et al. 2005. Development and Field Testing of a Unique High-Temperature/High-Pressure (HTHP) Oil-Based Drilling Fluid with Minimum Rheology and Maximum Sag Stability. Paper presented at the SPE Offshore Europe Oil and Gas Exhibition and Conference, Aberdeen, United Kingdom, 6-9 September. SPE-96285-MS. https://doi.org/10.2118/96285-MS.

Tehrani, A., Cliffe, A., Hodder, M. H. et al. 2014. Alternative Drilling Fluid Weighting Agents: A Comprehensive Study on Ilmenite and Hematite. Paper presented at the IADC/SPE Drilling Conference and Exhibition, Fort Worth, Texas, USA, 4-6 March. IADC/SPE-167937-MS. https://doi.org/10.2118/167937-MS.

Van Dyk, J. P., Vegter, N. M., and Pistorius, P.C. 2002. Kinetics of Ilmenite Dissolution in Hydrochloric Acid. *Hydrometallurgy* **65** (01): 31-36. https://doi.org/10.1016/S0304-386X(02)00063-4.

Wagle, V. Al-Yami, A., Al-Bahrani, H. et al. 2017. Development and Field Trial of New Acid Soluble Drilling Fluids. Paper presented at the SPE Kuwait Oil and Gas Show, Kuwait City, Kuwait, 15-18 October. SPE-187652-MS. https://doi.org/10.2118/187652-MS.

Xiao, J., Nasr-El-Din, H. A., and Al-Bagoury, M. 2013. Evaluation of Micronized Ilmenite as a Weighting Material in Oil-Based Drilling Fluids for HPHT Applications. Paper presented at the SPE European Formation Damage Conference and Exhibition, Noordwijk, The Netherlands, 5-7 June. SPE-165184-MS. https://doi.org/10.2118/165184-MS.

Xiao, J., Nasr-El-Din, H. A., and Al-Bagoury, M. 2015. Removal of Ilmenite Oil-Based Filter Cake Under HP/HT Conditions Using Hydrochloric Acid. Paper presented at the SPE North Africa Technical Conference and Exhibition, Cairo, Egypt, 14-16 September. SPE-175728-MS. https://doi.org/10.2118/175728-MS.

Supplemental Sources Consulted

API RP 13B-2, Recommended Practice for Field Testing Oil-Based Drilling Fluids, fifth edition. 2014. Washington, DC: API.

API RP 40, Recommended Practices for Core Analysis, second edition. 1998. Washington, DC: API.

Baker Hughes Drilling Fluids. 2004. Fluid Facts Engineering Handbook. Houston, Texas: Baker Hughes Incorporated.

Baker Hughes Drilling Fluids. 2006. Drilling Fluids Reference Manual. Houston, Texas: Baker Hughes Incorporated.

Caenn, R., Darley, H. C. H., and Gray, G. R. 2017. *Composition and Properties of Drilling and Completion Fluids*, seventh edition. Cambridge, Massachusetts: Gulf Professional Publishing/Elsevier.

Civan, F. 2016. *Reservoir Formation Damage – Fundamentals, Modeling, Assessment, and Mitigation*, third edition. Waltham, Massachusetts: Gulf Professional Publishing/Elsevier.

Fink, J. K. 2012. *Petroleum Engineer's Guide to Oil Field Chemicals and Fluids*, first edition. Waltham, Massachusetts: Gulf Professional Publishing/Elsevier.

APPENDIX A

CORE PERMEABILITY MEASUREMENTS

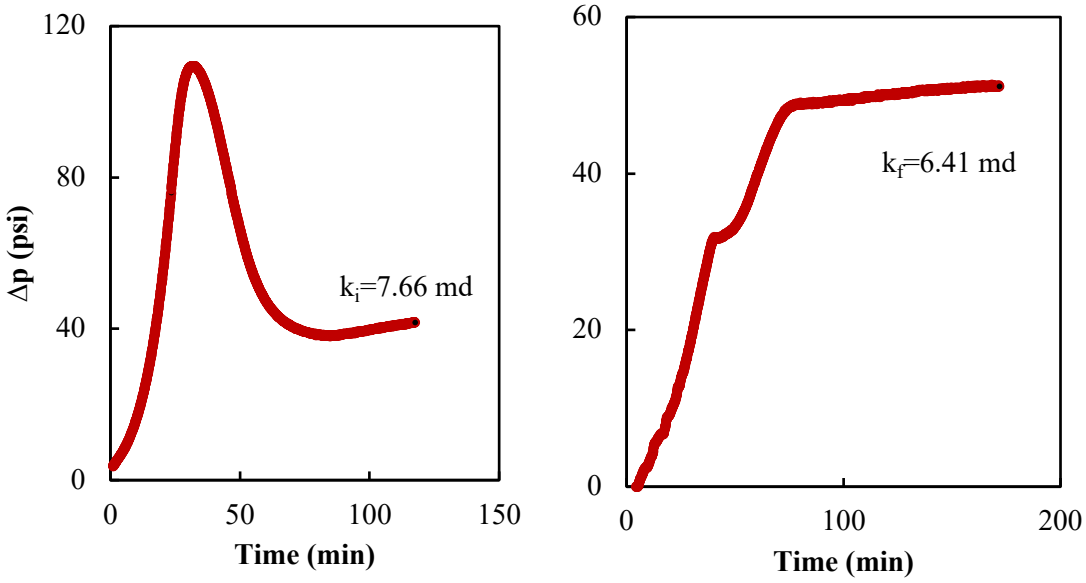

Figure A-1 Pressure drop across the core for Experiment 1 at an injection rate of 1 cm^3/min at 250˚F.

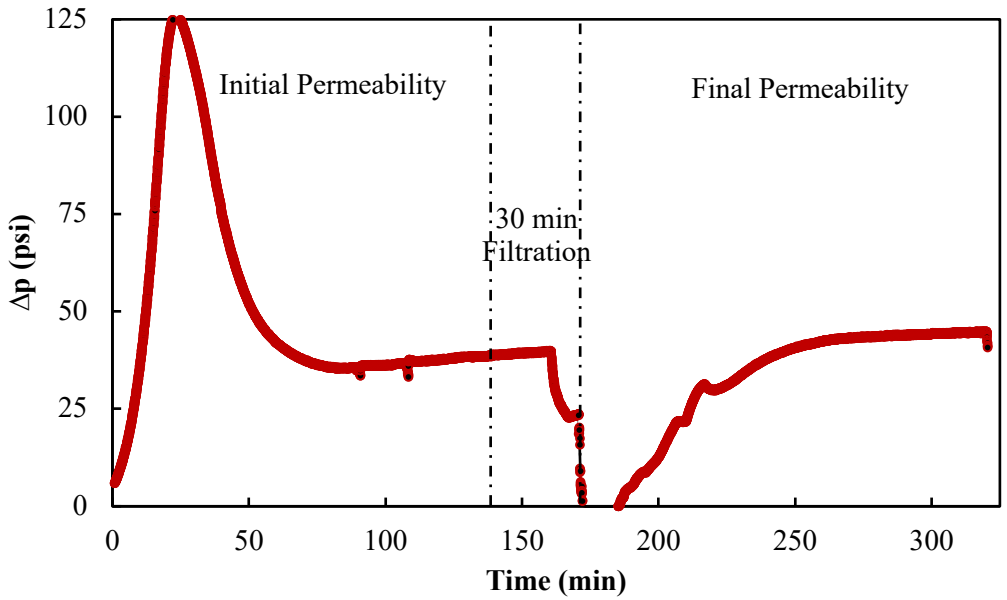

Figure A-2 Pressure drop across the core for Experiment 2 at an injection rate of 1 cm^3/min at 250˚F.

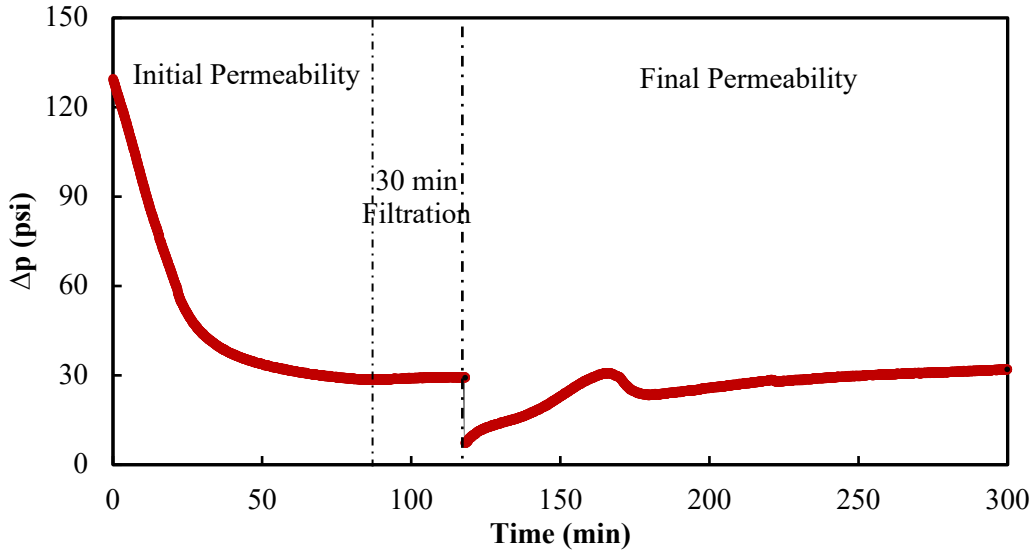

Figure A-3 Pressure drop across the core for Experiment 3 at an injection rate of 1 cm^3/min at 250˚F.

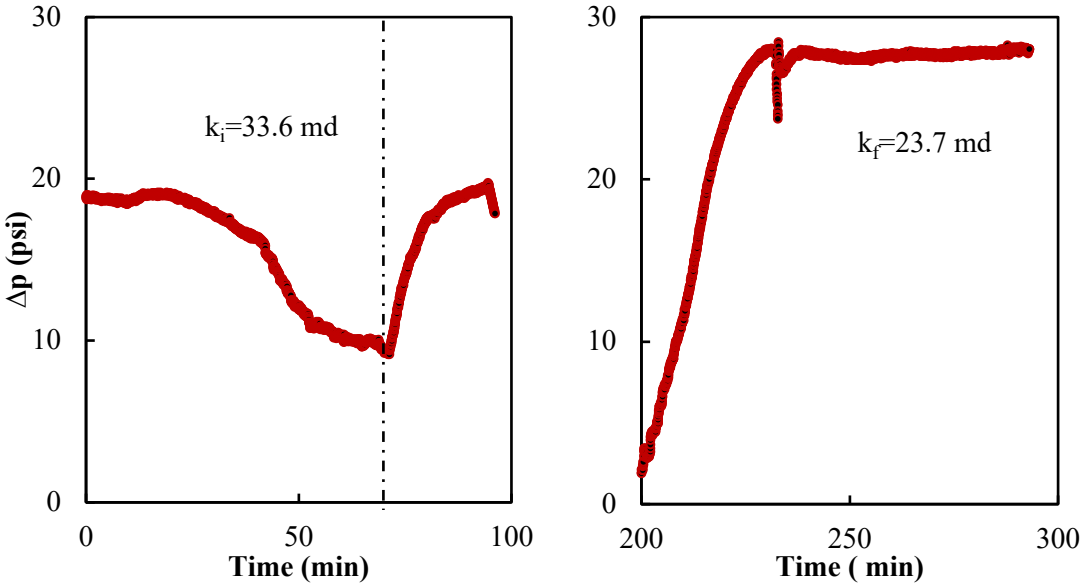

Figure A-4 Pressure drop across the core for Experiment 4 at an injection rate of 0.5 cm^3/min (initial) and 2 cm^3/min (both) at 250˚F.

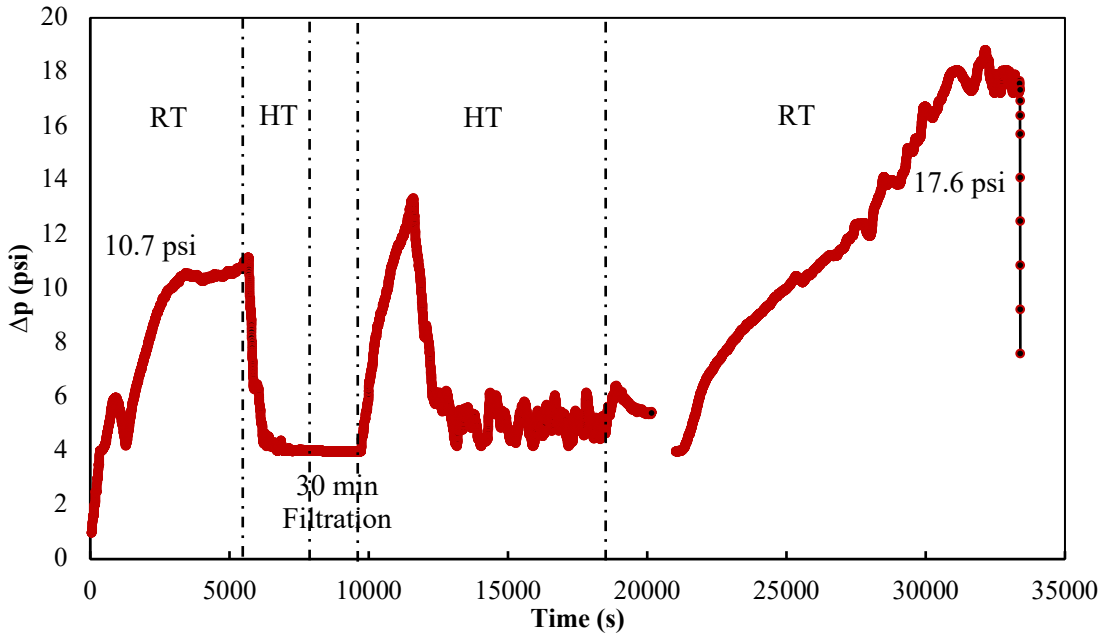

Figure A-5 Pressure drop across the core for Experiment 5 at an injection rate of 0.5 cm^3/min at room temperature (RT) and 250˚F (HT).

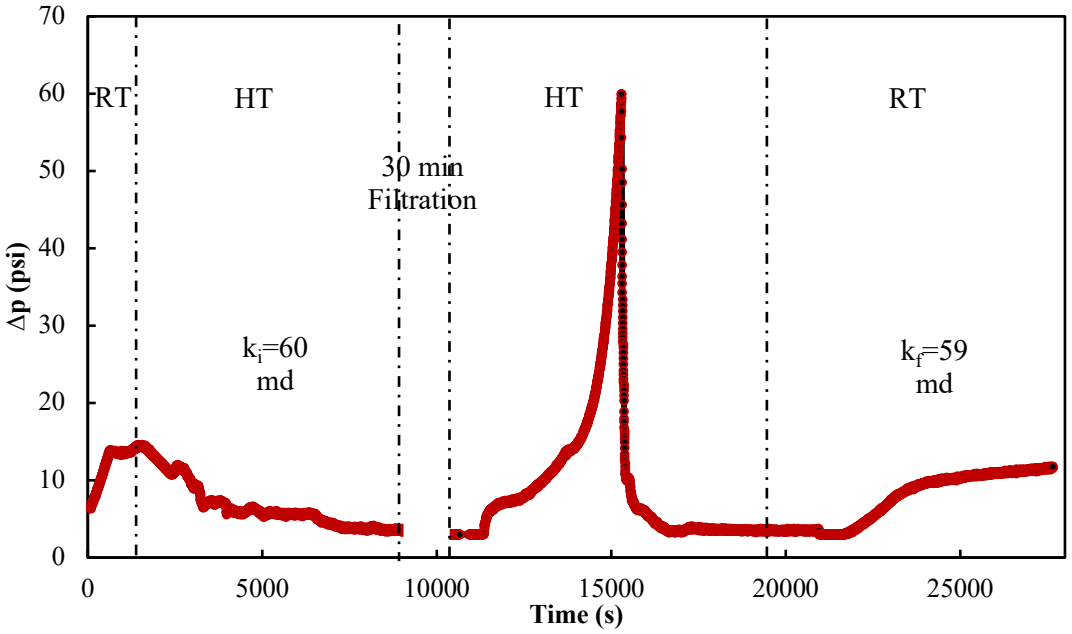

Figure A-6 Pressure drop across the core for Experiment 6 at an injection rate of 0.5 cm^3/min at room temperature (RT) and 250˚F (HT).

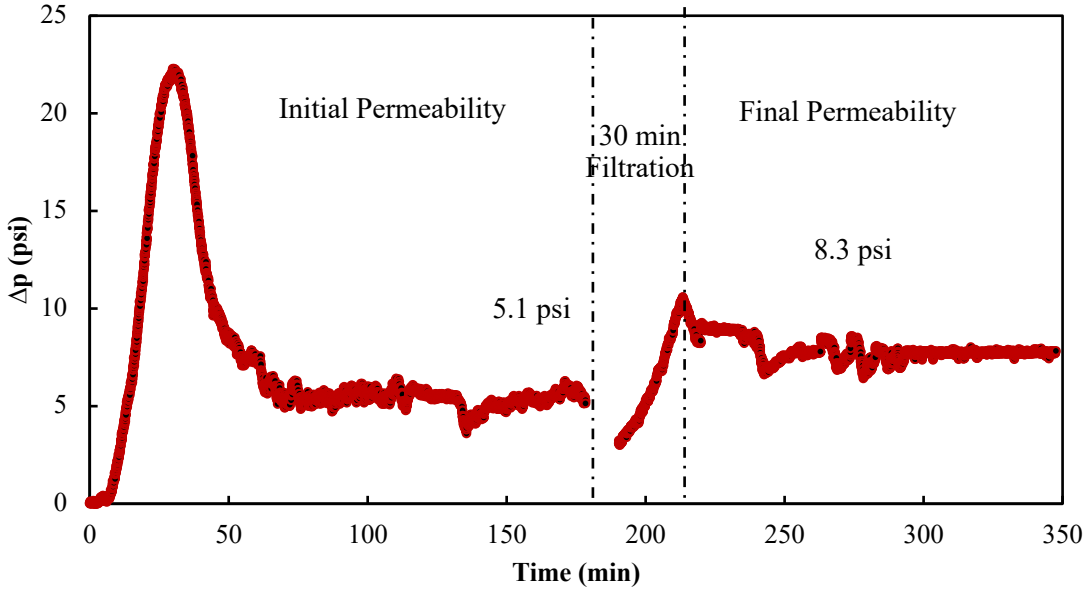

Figure A-7 Pressure drop across the core for Experiment 7 at 250˚F.

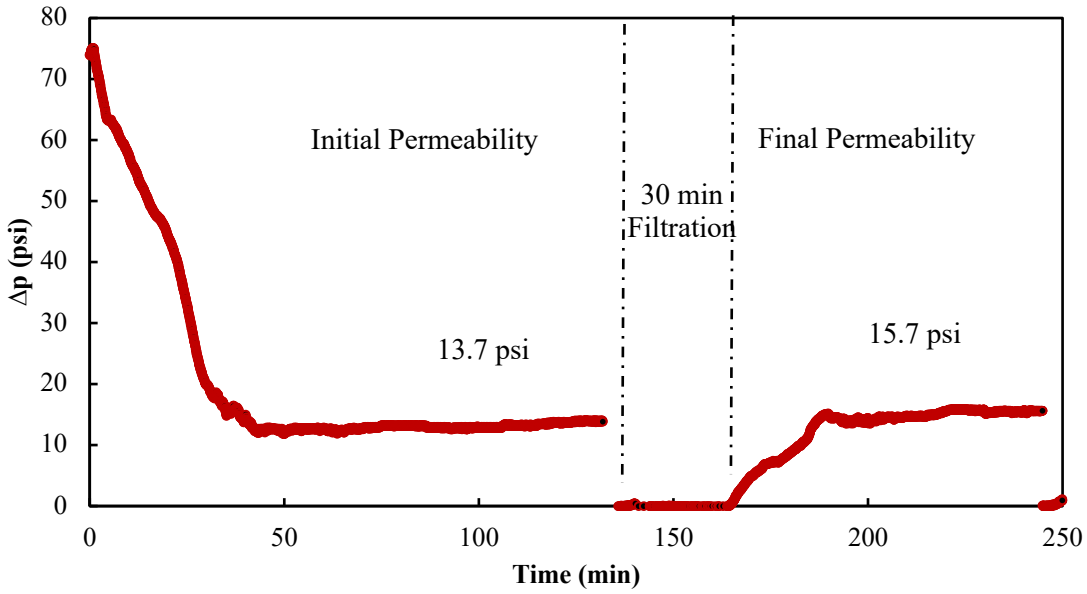

Figure A-8 Pressure drop across the core for Experiment 8 at an injection rate of 1 cm^3/min at 250˚F.

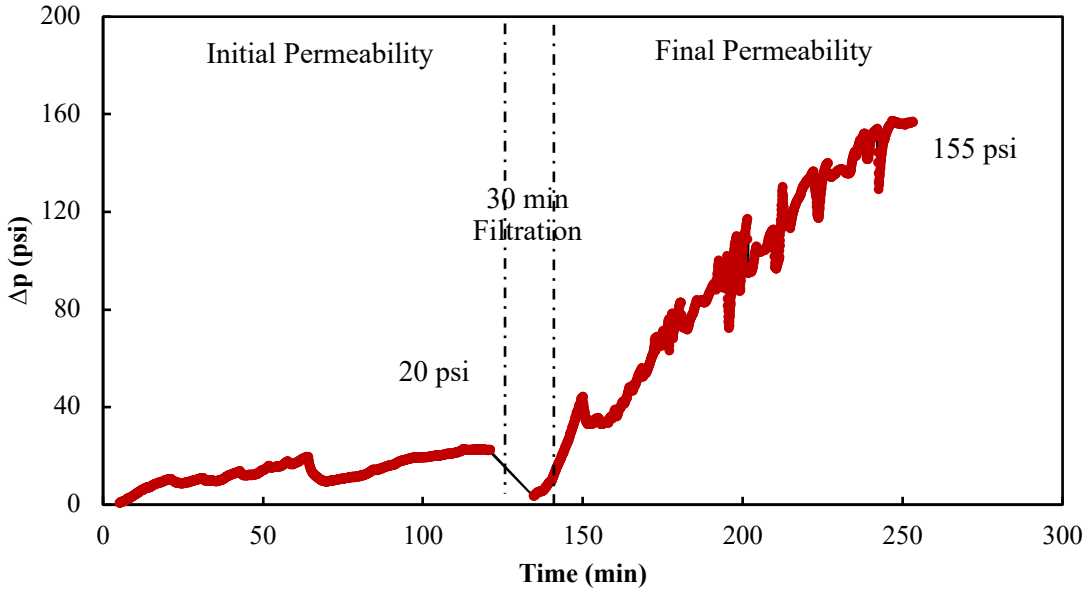

Figure A-9 Pressure drop across the core for Experiment 9 at an injection rate of 5 cm^3/min at 250˚F.

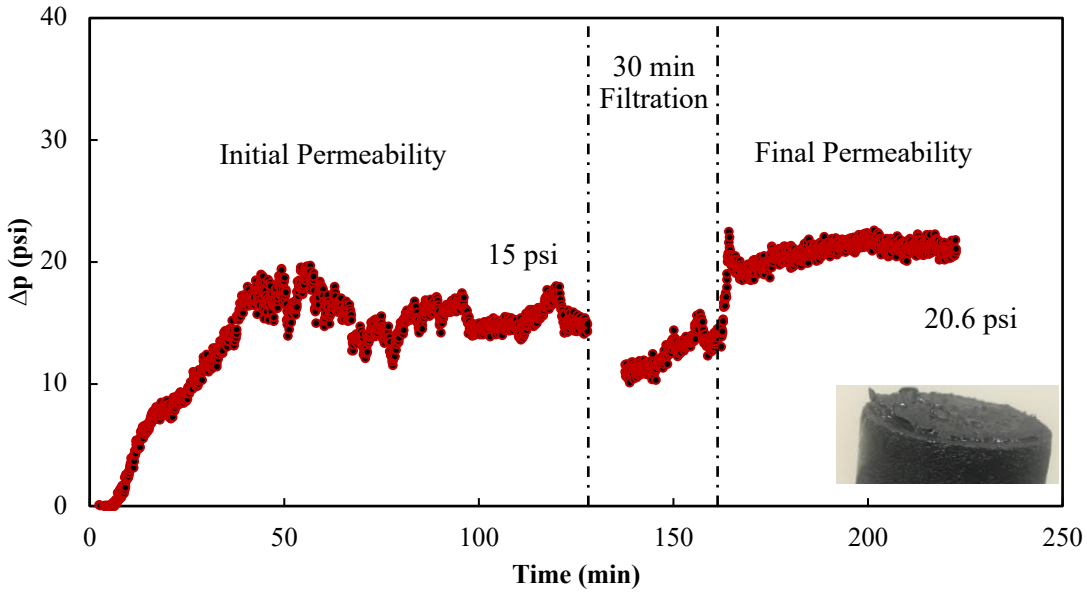

Figure A-10 Pressure drop across the core for Experiment 10 at an injection rate of 5 cm^3/min at 250˚F.

APPENDIX B

ADDITIONAL SOLUBILITY DATA

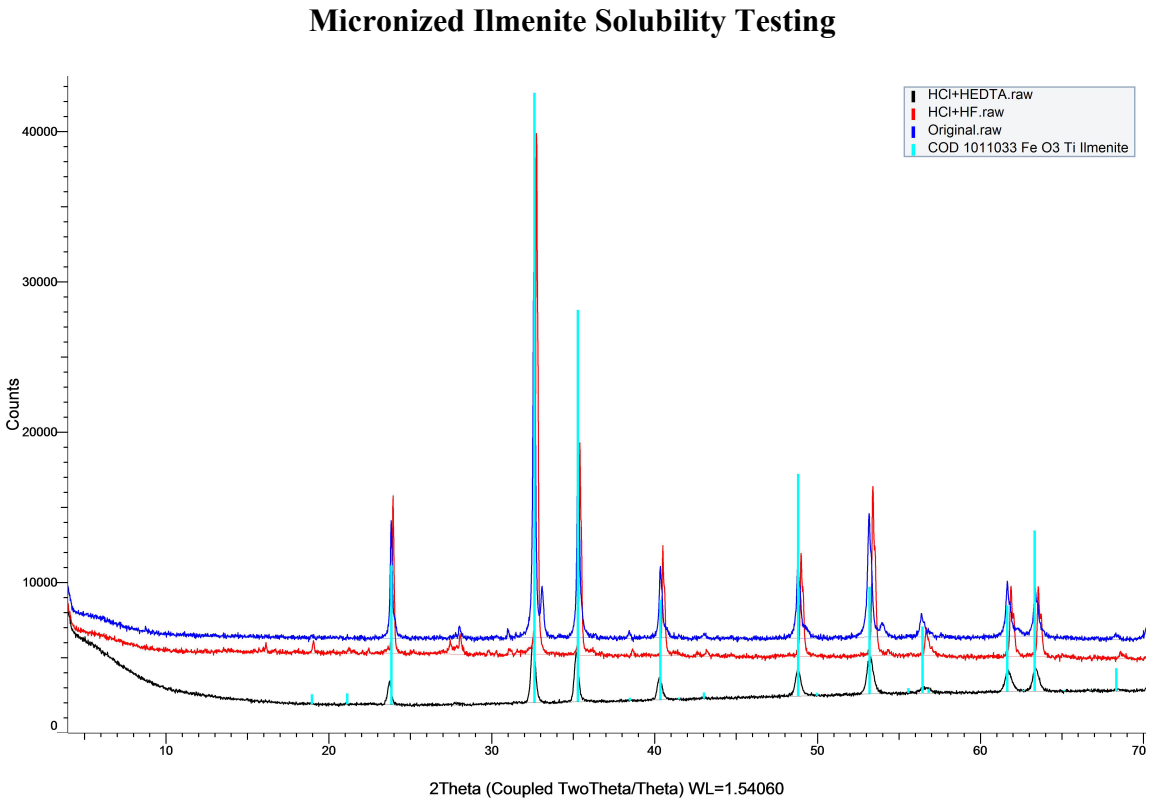

Figure B-1 XRD analysis of three ilmenite samples (original, after regular mud acid, and after HCl + HEDTA).

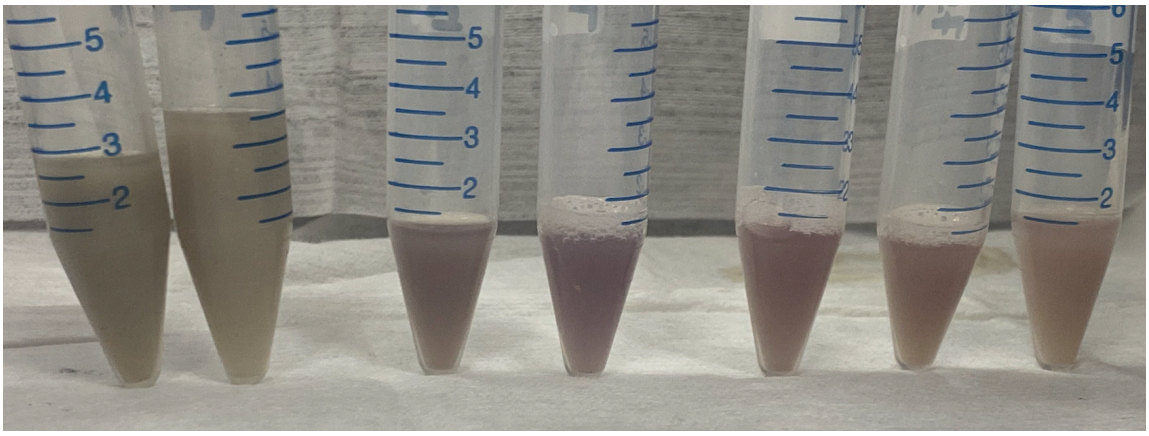

Figure B-2 Effluent samples collected from solubility testing of micronized ilmenite with a 7.5 wt% oxalic and 1 wt% HCl acid system at (left to right) 1, 3, 6, 14, 17.5, 20, and 24 hours.

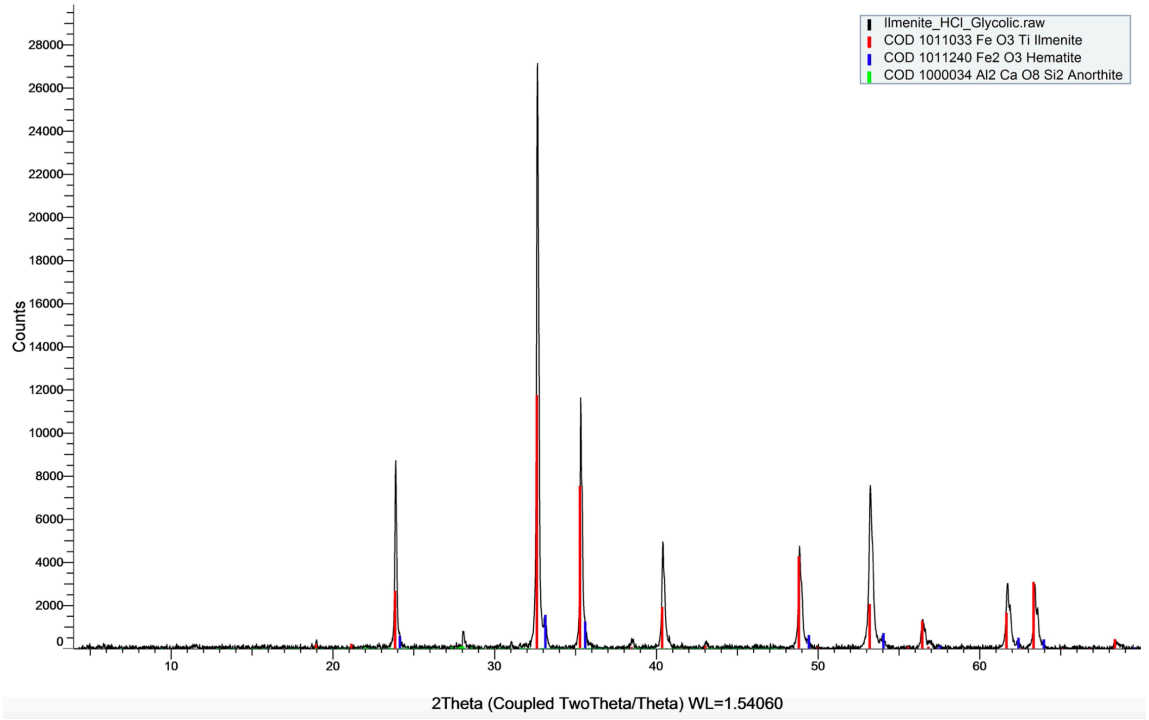

Figure B-3 XRD analysis of a micronized ilmenite sample after exposure to a 7 wt% glycolic and 1 wt% HCl acid system for 24 hours.

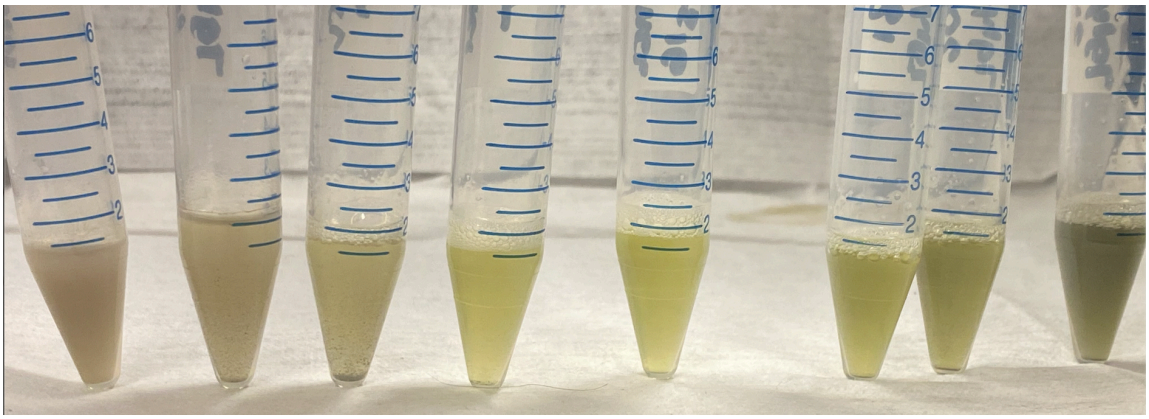

Figure B-4 Effluent samples collected from solubility testing of micronized ilmenite with a 7 wt% glycolic and 1 wt% HCl acid system at (left to right) 1, 4, 12, 14, 16, 18, 20, and 24 hours.

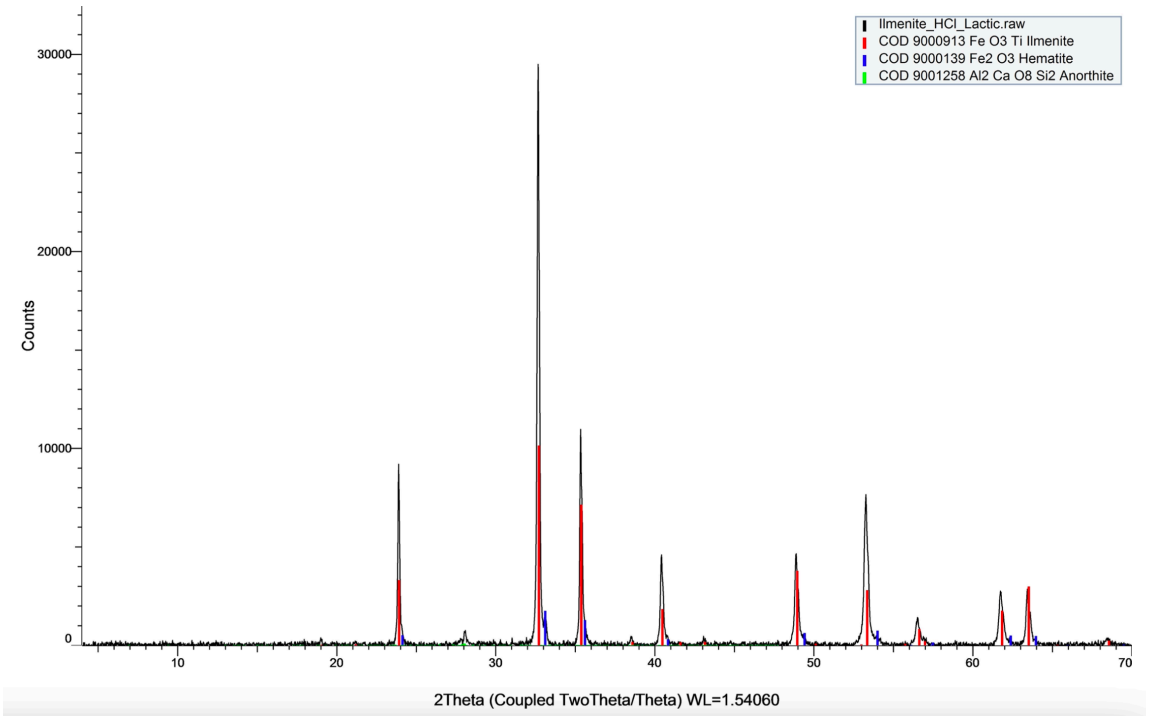

Figure B-5 XRD analysis of a micronized ilmenite sample after exposure to a 13 wt% lactic and 1 wt% HCl acid system for 24 hours.

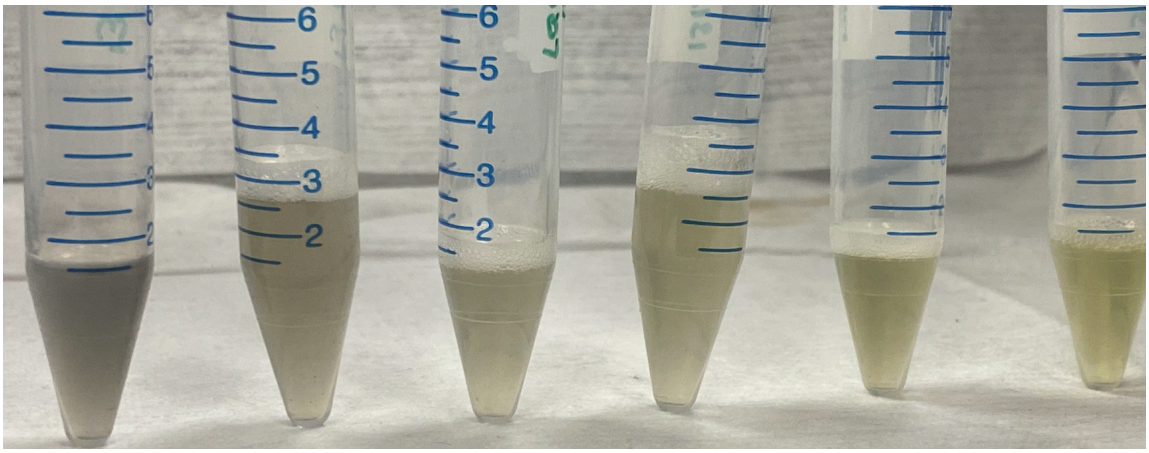

Figure B-6 Effluent samples collected from solubility testing of micronized ilmenite with a 13 wt% lactic and 1 wt% HCl acid system at (left to right) 2, 4, 6.5, 9.5, 20, and 24 hours.

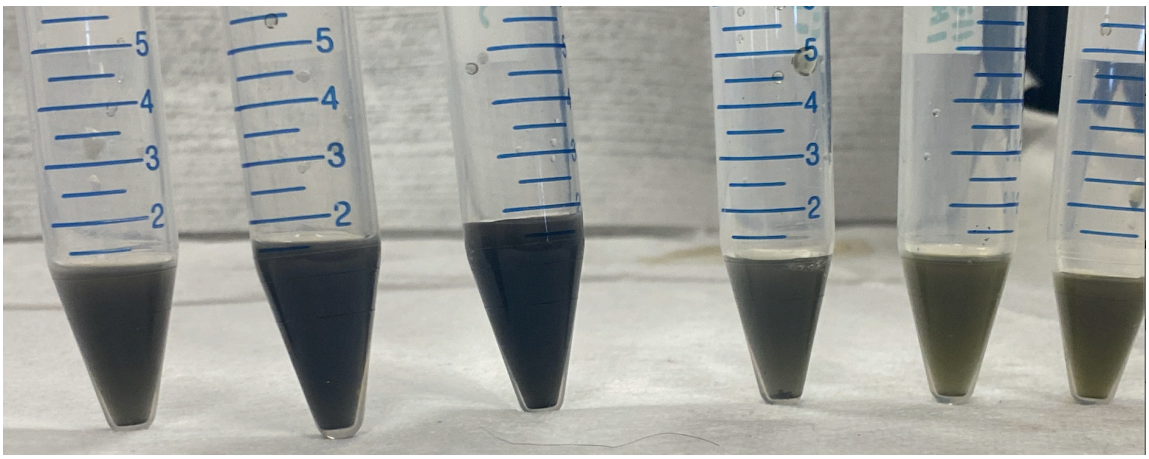

Figure B-7 Effluent samples collected from solubility testing of micronized ilmenite with a 11.6 wt% citric and 1 wt% HCl acid system at (left to right) 2, 6, 9, 12.5, 20.5, and 24 hours.

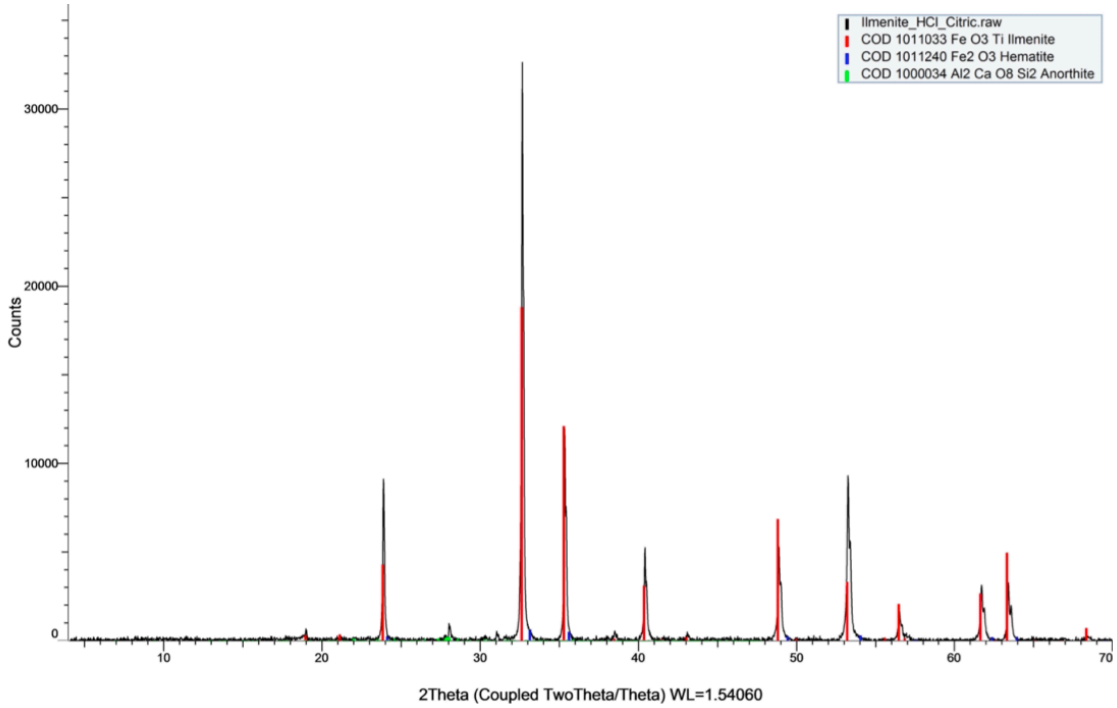

Figure B-8 XRD analysis of a micronized ilmenite sample after exposure to a 11.6 wt% citric and 1 wt% HCl acid system for 24 hours.

XRD	**Original Sample**	**After Solubility**			
	Ilmenite	**Oxalic/HCl**	**Glycolic/HCl**	**Lactic/HCl**	**Citric/HCl**
Mineral	*Concentration (%)*				
Ilmenite	88.12	58.02	84.93	83.91	91.88
Hematite	9.42	0.00	10.98	12.47	2.83
Anorthite	2.46	18.11	4.09	3.61	5.29
Ferrous Oxalate	-	23.88	-	-	-

Table B-1 Summary of XRD results for residual solids after exposure to initial organic acid systems.

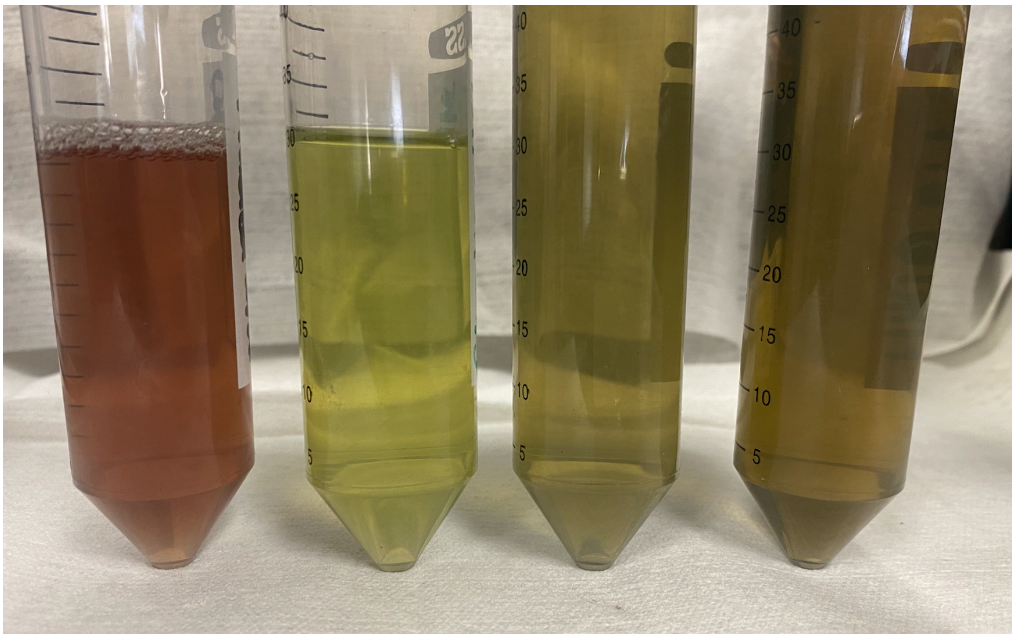

Figure B-9 Effluent spent acid samples collected after initial organic acid solubility tests. The samples from left to right are oxalic, glycolic, lactic, and citric.

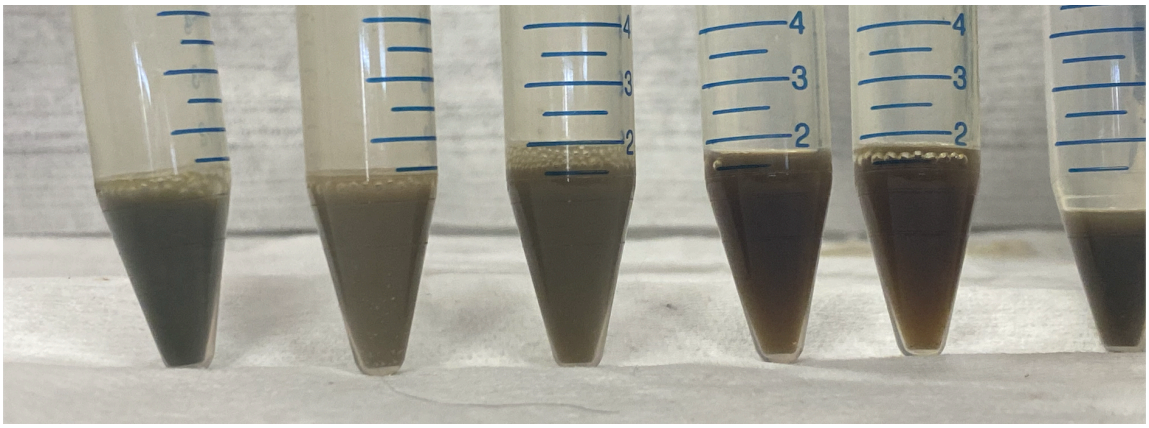

Figure B-10 Effluent samples collected from solubility testing of micronized ilmenite with a 20 wt% oxalic and 10 wt% HCl acid system at (left to right) 1.5, 3, 9, 11, 15, and 18.5 hours.

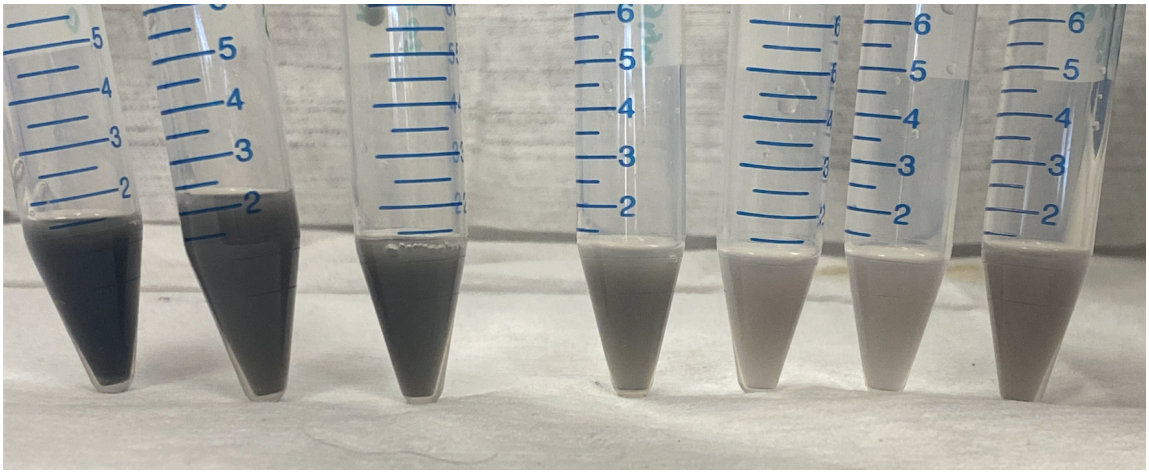

Figure B-11 Effluent samples collected from solubility testing of micronized ilmenite with a 20 wt% oxalic and 10 wt% glycolic acid system at (left to right) 0.5, 6, 10, 13, 17, 20.5, and 24 hours.

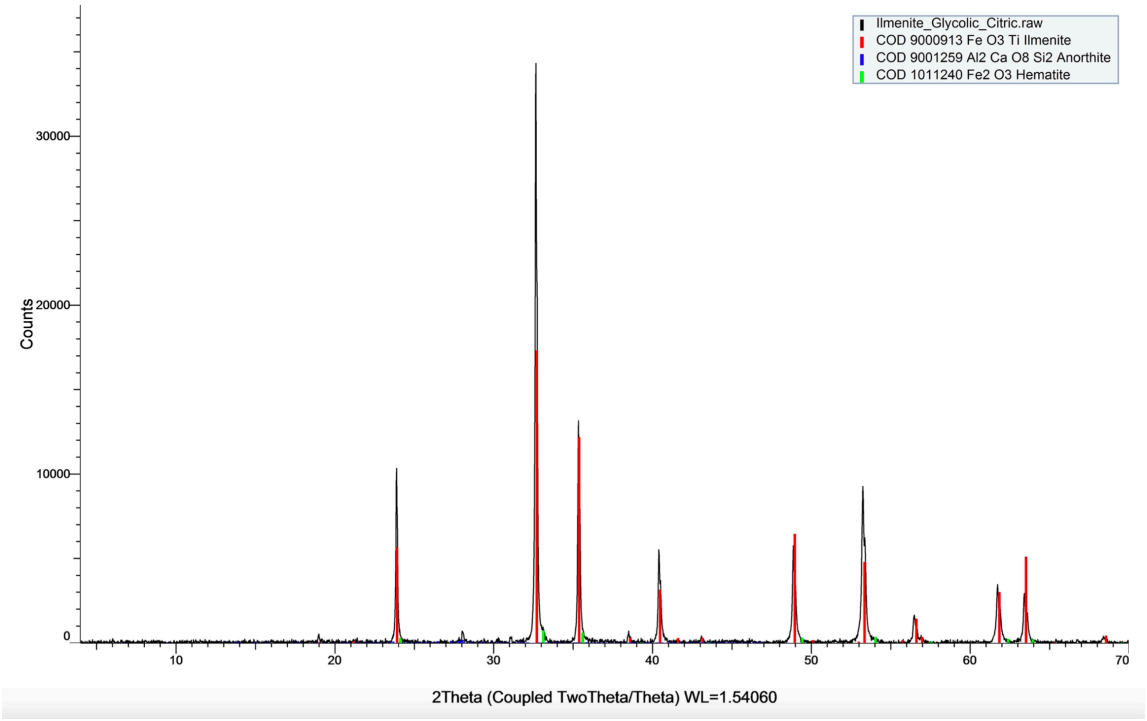

Figure B-12 XRD analysis of a micronized ilmenite sample after exposure to a 10% glycolic and 11.6 wt% citric acid system for 24 hours.

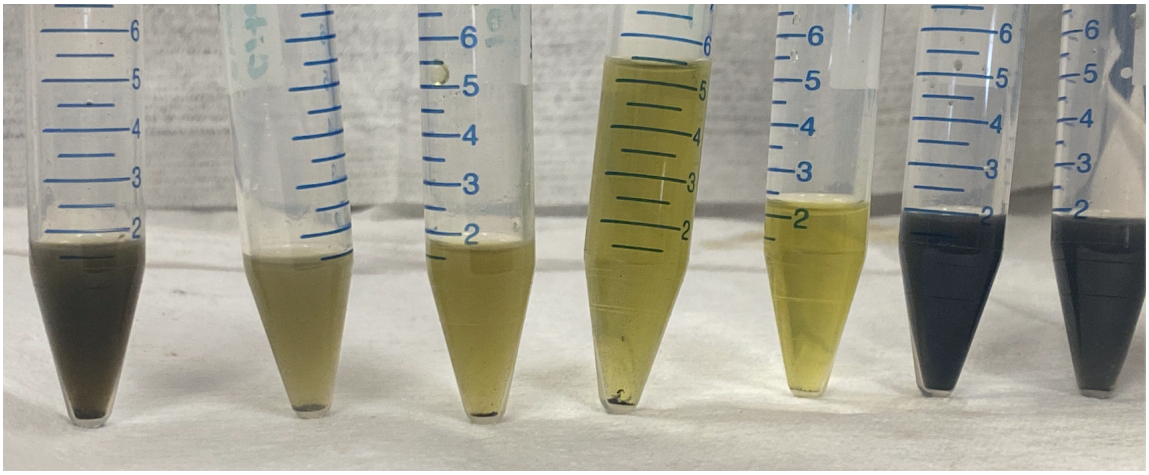

Figure B-13 Effluent samples collected from solubility testing of micronized ilmenite with a 10 wt% glycolic and 11.6 wt% citric acid system at (left to right) 2, 4, 10, 13, 17, 20.5, and 24 hours.

XRD	Original Sample	After Solubility		
	Ilmenite	**Oxalic/HCl**	**Oxalic/Glycolic**	**Citric/Glycolic**
Mineral	*Concentration (%)*			
Ilmenite	88.12	1.31	31.63	91.50
Hematite	9.42	0.00	0.00	3.60
Anorthite	2.46	0.00	4.02	4.90
Titanium Oxalate	-	32.20	8.37	-
Ferrous Oxalate	-	8.88	55.98	-
Oxalic Acid	-	10.24	-	-
Hydroperoxyoxymethyl	-	37.47	-	-
Oxalic Acid Dihydrate	-	9.90	-	-

Table B-2 Summary of XRD results for residual solids after exposure to secondary organic acid systems.

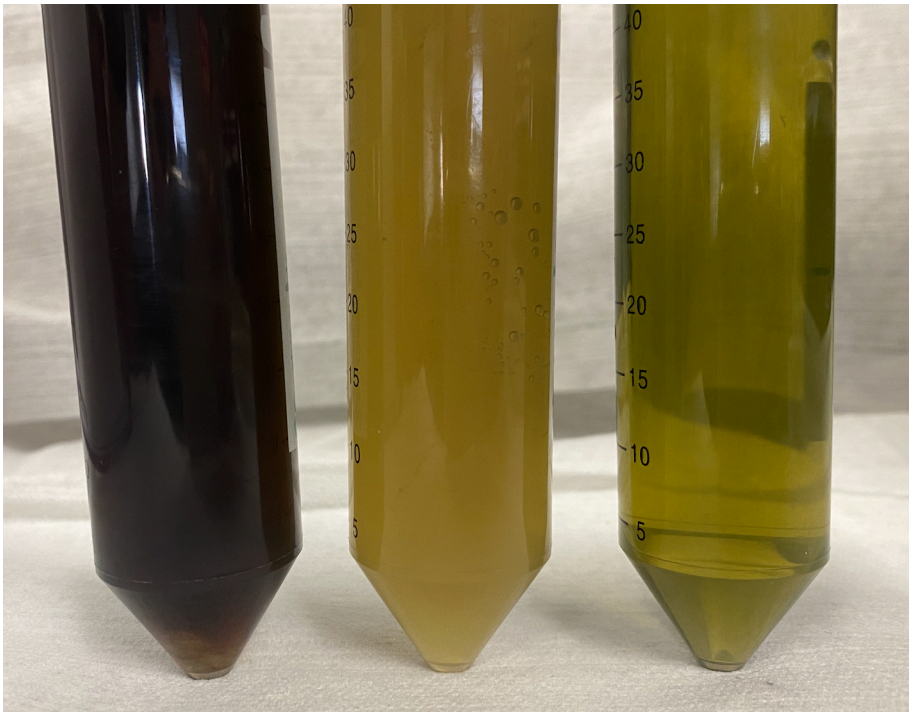

Figure B-14 Effluent spent acid samples collected after secondary organic acid solubility tests. The samples from left to right are oxalic/HCl, oxalic/glycolic, and citric/glycolic.

ACID SYSTEM		pH	
		BEFORE	AFTER
7.5 wt% Oxalic + 1 wt% HCl		0	0.82
7 wt% Glycolic + 1 wt% HCl		0	1.78
13 wt% Lactic + 1 wt% HCl		0	1.66
11.6 wt% Citric + 1 wt% HCl		1.07	2.00
20 wt% Oxalic + 10 wt% HCl		0	0
20 wt% Oxalic + 10 wt% Glycolic		0.92	0.8
10 wt% Glycolic + 11.6 wt% Citric	Ilmenite	1.7	2.33
	Filter Cake	1.7	2.02

Table B-3 Measured pH values for organic acid systems before and after solubility testing.

Micronized Ilmenite-Weighted Filter Cake Solubility Testing

MATERIAL	MIXING TIME	MASS ADDED
	min	*g*
Base Oil	-	129.04
Primary Emulsifier	1	2.00
Secondary Emulsifier	1	12.00
Lime	1	4.00
Fluid Loss Additive (Polymer)	1	2.00
$CaCl_2$ Brine (25 wt%)	10	86.81
Organophilic Clay	15	2.50
Micronized Ilmenite	10	410.32
Rheology Modifier	5	2.00
Simulated Drill Solids	5	10.00
Wetting Agent	5	2.00
		662.67

Table B-4 Composition of the 1.9 SG micronized ilmenite-weighted oil-based drilling fluid system used to create the filter cake for solubility tests.

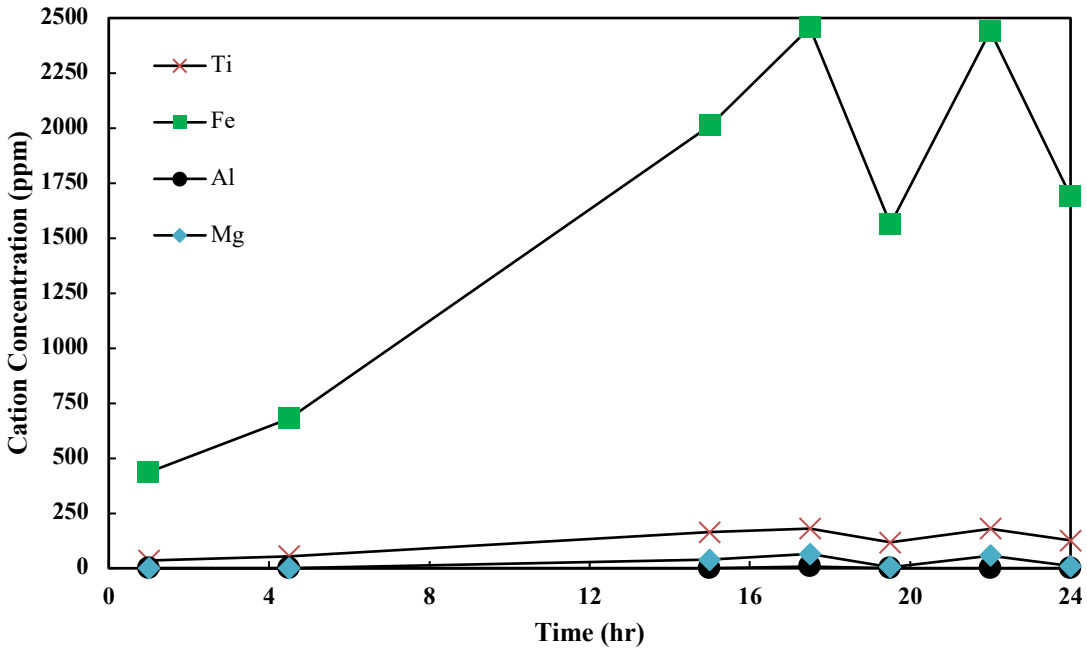

Figure B-15 ICP analysis for effluent samples collected from filter cake solubility testing with 10 wt% glycolic + 11.6 wt% citric acids.

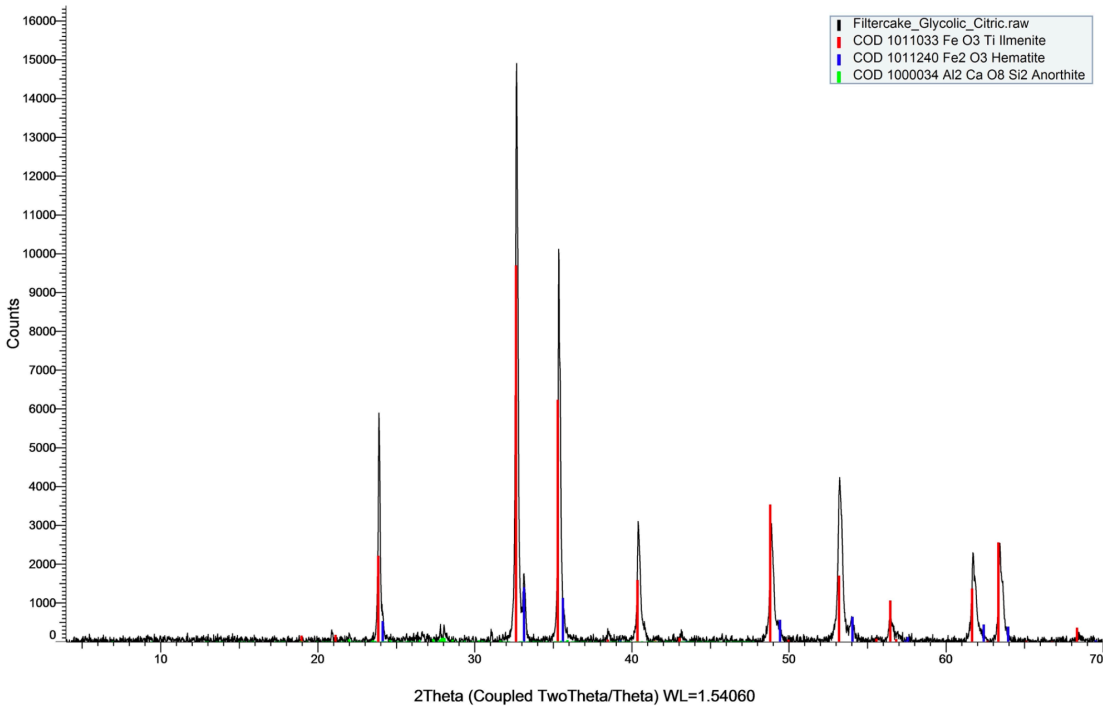

Figure B-16 XRD analysis of a micronized ilmenite-weighted drilling fluid filter cake after exposure to a 10% glycolic and 11.6 wt% citric acid system for 24 hours.

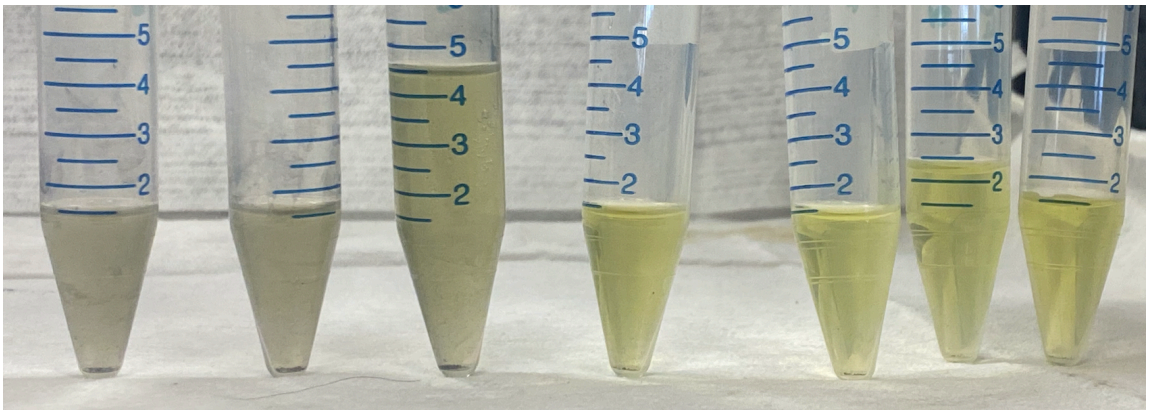

Figure B-17 Effluent samples collected from solubility testing of micronized ilmenite-weighted drilling fluid filter cake with a 10 wt% glycolic and 11.6 wt% citric acid system at (left to right) 1, 4.5, 15, 17.5, 19.5, 22, and 24 hours.

XRD	Original Sample	After Solubility
	Ilmenite	**Citric/Glycolic**
Mineral	*Concentration (%)*	
Ilmenite	88.12	83.07
Hematite	9.42	11.69
Anorthite	2.46	5.24

Table B-5 XRD results for filter cake residual solids after exposure to a 10% glycolic and 11.6 wt% citric acid system for 24 hours.